Interactive discussion on *Chemical composition of nanoparticles from α-pinene nucleation and the influence of isoprene and relative humidity at low temperature* by Caudillo et al., Atmos. Chem. Phys. Discuss., https://doi.org/10.5194/acp-2021-512

We thank the referees for their positive and constructive feedback. We greatly appreciate their time investment for carefully reviewing our manuscript. We have given different font colors for facilitating the discussion. The specific and technical comments addressed by the referees are in black, while our answers are in blue. Any changes made to the manuscript can be found in red.

Anonymous Referee #1

Caudillo and co-authors present and discuss the gas and particle phase composition of pure biogenic nucleation events measured with a nitrate chemical ionization atmospheric pressure interface time of flight mass spectrometer (coupled with a thermal desorption differential mobility analyzer for the particle phase) in the CLOUD chamber at a range of conditions representing free tropospheric conditions. Specifically, alpha-pinene and a mix of alpha-pinene and isoprene were oxidized at -30 deg C and - 50 deg C, and at 20 % or 60 - 100 % relative humidity. The authors find C8-10 monomers and C18-20 dimers as major compounds, and C5 and C15 compounds contributing to particle growth when isoprene is present in the system. I very much appreciate the systematic analysis. The manuscript is well-written and the experimental results are thoroughly discussed. In my opinion, this is an original and valuable contribution to the field. Therefore, it should be published in ACP after minor revisions.

Specific comments:

In the abstract, the last sentence ("Besides the chemical information...", lines 64-66) was confusing to me. After reading section 3.4.1, I suggest to be more specific in the abstract, e.g., "Compared with previous studies, we found lower nucleation rates measured at 1.7 nm, very likely due to higher alpha-pinene and ozone mixing ratios used in the present study."

The sentences have been modified as suggested:

For the experiments reported here, most likely isoprene oxidation products enhance the growth of particles larger than 15 nm. Additionally, we report on the nucleation rates measured at 1.7 nm ($J_{1.7nm}$) and compared with previous studies, we found lower $J_{1.7nm}$ values, very likely due to the higher α-pinene and ozone mixing ratios used in the present study.

In section 2.1, there is no information about GCR conditions during the experiments, please add.

The requested information about GCR conditions has been added accordingly in Section 2.1.

In order to promote particle production from ions, Galactic Cosmic Rays conditions (GCR) can be achieved by turning off the high voltage field (30 kV m^{-1}). The equilibrium ion-pair concentration in the chamber due to GCR is around 700 cm^{-3} (Kirkby et al., 2016).

The experiments relevant for this work were done under GCR conditions and in a flow-through mode with continuous addition of the reactants, performed at -50 °C and -30 °C, at low and high relative humidity to simulate pure biogenic new particle formation at a range of free tropospheric conditions.

In section 2.2, please add some more information about the heating procedure of the filament. Is the temperature slowly ramped up, or do you apply high temperature directly to instantaneously vaporize the sample? This is also relevant for the discussion of potential thermal decomposition of molecules in section 3.2.2.

The information regarding the heating produce of the filament was added in the Section 2.2.

For the experiments that are reported in this work, a filament of platinum/rhodium (90:10) was used, and an integral, non-size selective mode of operation was chosen in order to maximize the mass of collected particles. For desorbing the sample, an electric current was applied to the filament and ramped linearly over a duration of approximately 1 minute. Due to the very low experimental temperatures, cold sheath flows and isolated inlet lines were installed in order to avoid drastic temperature changes between the CLOUD chamber and the instrument. Evaporation of particulate material before the active heating should therefore not be substantial.

Regarding the non-size selective mode of operation of the TD-DMA, it would be helpful to get an idea about the contribution of freshly nucleated particles vs. grown particles to the sampled mass. From the measured particle size distributions and the PSM and CPC total number concentrations, could you calculate a rough estimate of the volume/mass fraction of particles < 15 nm in the samples collected in the periods shown in Figure 1 as shaded areas? Please add this information to Table 1.

The calculation was done accordingly and the requested information has been added to Table 1.

For calculating the mass fraction of particles collected on the filament during the TD-DMA collection time we used only SMPS size distributions, in a range from 9 nm to 834 nm. We estimated that the mass of particles with sizes smaller than 9 nm is negligible (by comparing to nanoSMPS data in a size range from 2 to 63 nm). Thus, the mass fraction reported in Table 1 takes only into account SMPS measurements. From these data we derived the mass fractions for the collected particles with a diameter smaller than 15 nm (Mass $_{< 15\ nm}$) and for a diameter larger than 15 nm (Mass $_{> 15\ nm}$).

This calculation is an ideal estimate, it does not take into account uncertainties due to charging efficiency, collection efficiency and transmission efficiency in the TD-DMA as reported in detail by Wagner et al. (2018) for the size-selective mode.

Table 1. Summary of the main parameters for four pure biogenic new particle formation experiments.

Experiment	Isoprene [ppb]	α-pinene [ppb]	Isoprene-to-monoterpene carbon ratio (*R*)	Ozone [ppb]	T [°C]	RH [%]	HOM total* [molec. cm^{-3}]	$J_{1.7}$* [cm^{-3} s^{-1}]	Growth rate 3.2-8 nm [nm h^{-1}]	Growth rate 5-15 nm [nm h^{-1}]	Mass $_{< 15\ nm}$ /Mass $_{> 15\ nm}$** [%]
αIP-30,20	13.71 31.38	0.95 5.12	14.4 6.1	98.58 101.56	-30 -30	20 20	1.50e8 3.04e8	7.29 10.10	18.0 NA	22.8 39.0	0.29 / 99.7
α-30,20	~ 0	3.35	NA	102.10	-30	20	2.20e8	23.76	76.9	77.1	0.11 / 99.9
α-50,20	~ 0	3.04	NA	100.55	-50	20	6.72e7	51.24	41.1	42.0	0.26 / 99.7
α-50,60	~ 0	7.72	NA	110.20	-50	60	8.00e7	79.17	63.4	78.4	0.09 / 99.9

* Run-to-run experimental uncertainties of HOMs is ± 20 % and for $J_{1.7}$ is ± 30 %. NA, Not Applicable. **Mass fraction of particles collected on the filament during the TD-DMA collection time, calculation based on SMPS mass distributions.

In Figure 3f, to me it is not obvious that specifically C4-5 and C13-16 compounds are enhanced as stated in lines 237/238. Please clarify.

Many thanks for pointing this out. Regarding the isoprene effect, we do observe an increase in the intensity for several species in the particle phase, not only for C_5 and C_{15} compounds. We believe that this might be related to the method we apply for evaporating the particles (thermal desorption), possibly fragmentation and chemical reactions are occurring. We are further investigating this phenomenon in a forthcoming study.

We clarified in Section 3.2.1 that C_5 and C_{15} compounds correspond to $C_5H_{10}O_{5\text{-}7}$ and $C_{15}H_{24}O_{5\text{-}10}$ which are observed in both gas and particle phase.

Fig. 3f shows the intensity difference in the particle phase. In contrast with what is observed in the gas phase, the particle phase effects seem more diverse. There is an increase in the intensity difference for several species in the system with isoprene (*αIP-30,20*), such as $C_{4\text{-}5}$, $C_{13\text{-}16}$ and some $C_{17\text{-}19}$ (see Fig. S1 in the supplement). Especially, a distinct group of C_{15} compounds $C_{15}H_{24}O_{5\text{-}10}$ and $C_5H_{10}O_{5\text{-}7}$ can be identified in the particle and in the gas phase. A previous study has shown that isoprene can enhance particle growth rates despite its negative effect on nucleation (Heinritzi et al., 2020). The identification of C_{15} dimers in nanometer-sized particles in the present study confirms this with a direct measurement. The suppressing effect of isoprene on nucleation will further be discussed in Section 3.4.2. However, isoprene can still contribute to the growth of particles by C_5 or by C_{15} compounds. Additionally, these species can be an important fingerprint to identify SOA formation from a mixture of biogenic vapors containing isoprene.

In section 3.3, looking at Figures 5 and S4 I agree with the statement that mainly LVOC and ELVOC compounds were detected in the particle phase, however, the ULVOC compounds appear to be a minor fraction.

We agree as well that ULVOC do not represent the highest fraction. We have calculated the volatility bin fractions and reported these values in Table 2.

Table 2. Bin volatility fractions for the different experiments.

Experiment	T [ºC]	RH [%]	ULVOC [%]	ELVOC [%]	LVOC [%]	SVOC [%]	IVOC [%]
αIP-30,20	-30	20	8.6	28.3	59.1	3.8	0.2
α-30,20	-30	20	5.9	44.1	48.1	1.9	0
α-50,20	-50	20	16.5	36.4	46.1	1.0	0
α-50,60	-50	60	13.8	50.6	34.8	0.8	0

In Section 3.3, we have mentioned that LVOC and ELVOC represents the major fractions, and ULVOC only a minor fraction.

We classified the volatility bins according to the regimes proposed by Donahue et al. (2012) and Schervish and Donahue (2020), and calculated the corresponding fractions (Table 2). Overall, the particle phase detected compounds correspond mainly to Low Volatility Organic Compounds (LVOC) and Extremely Low Volatility Compounds (ELVOC) by explaining more than 80 % of the signals, while Ultralow Volatility Organic Compounds (ULVOC) represent only a small fraction (between 6 and 17 %). With this parametrization we are able to approximate the saturation mass concentration for the particle phase

compounds measured using the TD-DMA in the CLOUD chamber. For this parametrization we assume that the elemental composition is one of the main parameters to take into account.

Section 3.4.2: Regarding the discussion of isoprene suppression of new particle formation, please consider adding a reference to Lee et al. (2016), doi:10.1002/2016JD024844.

The reference has been added accordingly in Section 3.4.2.

For instance, in a plant chamber experiment R = 19.5 resulted in no significant new particle formation (Kiendler-Scharr et al., 2009). Additionally, in the Michigan forest with R = 26.4, NPF events did not occur frequently (Kanawade et al., 2011). Lee et al. (2016) reported observations of NPF suppression in a rural forest in Alabama where R = 2.0. However, one has to consider that the suppression effect at a given value of *R* likely decreases as temperature decreases and so does the saturation vapor pressure of the oxidation products.

In Figures 6 and 8, please explain the meaning of "1α run-to-run uncertainty".

1σ run-to-run uncertainty refers to the experimental errors calculated based on run-to-run repeatability in the CLOUD chamber (experiments under identical conditions). Detailed information about this calculation has been previously published in Kirkby et al. (2016), Lehtipalo et al. (2018) and, Dada et al. (2020).

We have changed “1α run-to-run uncertainty” for “1σ run-to-run experimental uncertainty” in the caption for Figures 6 and 8.

Figure 6. Pure biogenic nucleation rates of pure α-pinene at 1.7 nm diameter against total HOM concentration at different temperatures. HOM total is defined as the sum of C_5, C_{10}, C_{15} and C_{20} carbon classes. Triangles represent Galactic Cosmic Rays (GCR) conditions and circles represent Neutral conditions. Data points at -50 °C, -25 °C, -10 °C, +5 °C and +25 °C are from Simon et al. (2020). The points with orange marker on the background are the contribution of this study (experiments α-30,20, α-50,20 and α-50,60). Solid and dashed lines represent power-law fits to GCR and Neutral conditions. Bars indicate 1 σ run-to-run experimental uncertainty. The overall systematic scale uncertainty of HOM of +78 % and -68 % is not shown.

Figure 8. Pure biogenic nucleation rates at 1.7 nm diameter against total HOM concentration at different temperatures for α-pinene and α-pinene + isoprene systems. HOM total is defined as the sum of C_5, C_{10}, C_{15} and C_{20} carbon classes. Triangles represent Galactic Cosmic Rays (GCR) conditions. Data points at +5 °C and +25 °C are from Kirkby et al. (2016) and Heinritzi et al., (2020). Data points at -25 °C are from Simon et al., (2020). The value of isoprene-to-monoterpene carbon ratio (R) varies from 1.5 to 6.5 for Heinritzi et al., (2020), and R equals to 14.4 and 6.1 for this study. The points with orange marker on the background indicate the contribution of this work. Solid lines represent power-law fits to GCR conditions of the systems with α-pinene only and dashed lines are the power-law fits of the systems with isoprene added. Bars indicate 1 σ run-to-run experimental uncertainty. The overall systematic scale uncertainty of HOM of +78 % and -68 % is not shown.

Technical comments:

lines 225, 301, 322: Make sure that there is no line break between sign and number in "-30" and "- 50".

We have attended this comment accordingly.

line 226: "While the gas..." is not a full sentence.

We have modified the sentence.

Figure 3 shows mass defect plots of gas and particle phase and the intensity difference between each phase at -30 °C. Figure 3a and Fig. 3d display the gas and particle composition of *α-30,20*, while the gas and particle composition of *αIP-30,20* are shown in Fig. 3b and Fig. 3e, respectively. As both phases were measured with the same instrument, they can be directly inter-compared.

Section 3.2, first paragraph: When presenting and discussing Figure 2, add a reference to supplementary material Figures S1 and S2 for other systems.

We have added this information as requested.

Figure 2 shows the carbon distribution as an overview of the compounds detected in gas and particle phase for a system where only α-pinene was oxidized (*α-30,20*). $C_{8\text{-}10}$ monomers (Fig. 2a) and $C_{18\text{-}20}$ (Fig. 2b) dimers are observed in the gas as well as in the particle phase. For instance, some of the signals with the highest intensity correspond to $C_{10}H_{16}O_{3\text{-}9}$, and $C_{20}H_{32}O_{5\text{-}13}$, especially $C_{10}H_{16}O_6$ and $C_{10}H_{16}O_7$ have an important presence in both phases. Overall, most of the compounds that are present in the gas phase are detected as well in the particle phase, although their relative contribution to the total signal can differ between the phases. The corresponding carbon distribution for the other systems can be found in Figures S1 and S2 in the supplement.

Line 248: "While GR..." is not a full sentence.

We have modified the sentence.

This is a factor of ~ 4 difference, while $GR_{5\text{-}15}$ nm represents a factor of 2 to 3 difference between *αIP-30,20* compared to *α-30,20*.

line 285: Change "autooxidation" to "autoxidation" to be consistent throughout the manuscript.

We have attended this comment accordingly.

lines 204, 312, 336, 375: Here, "new particle formation rate" is used, while J_1.7nm is introduced as "nucleation rate" in the manuscript. For consistency, I recommend using "nucleation rate" throughout the manuscript.

We have attended this comment accordingly.

In Figures 6 and 8: "GRC" should read "GCR" in the figure legend. Also, in the last sentence of the figure caption, remove "and" before "is not shown".

We have attended this comment accordingly.

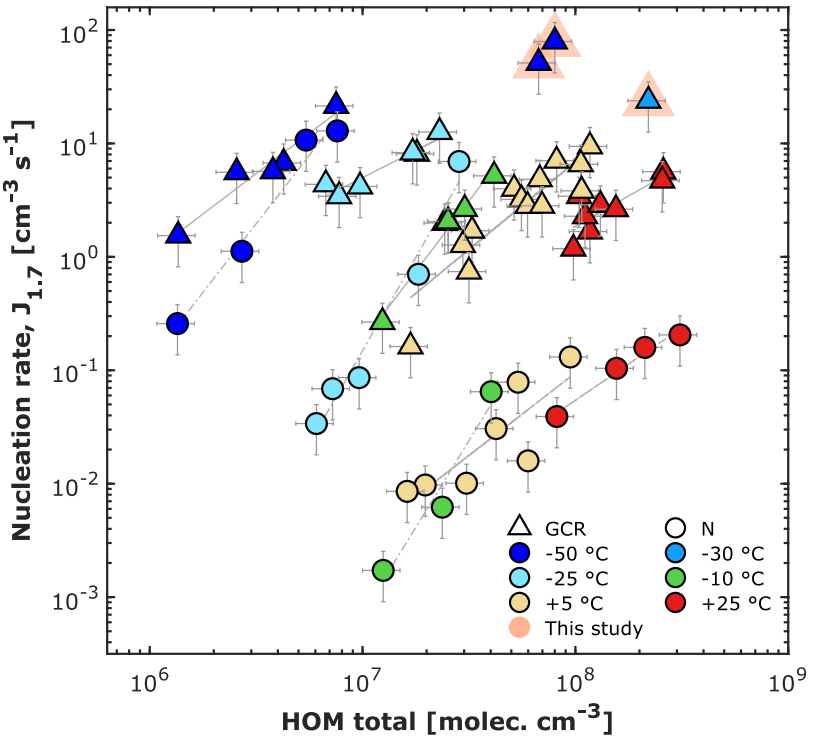

Figure 6. Pure biogenic nucleation rates of pure α-pinene at 1.7 nm diameter against total HOM concentration at different temperatures. HOM total is defined as the sum of C_5, C_{10}, C_{15} and C_{20} carbon classes. Triangles represent Galactic Cosmic Rays (GCR) conditions and circles represent Neutral conditions. Data points at -50 °C, -25 °C, -10 °C, +5 °C and +25 °C are from Simon et al. (2020). The points with orange marker on the background are the contribution of this study (experiments α-30,20, α-50,20 and α-50,60). Solid and dashed lines represent power-law fits to GCR and Neutral conditions. Bars indicate 1 σ run-to-run experimental uncertainty. The overall systematic scale uncertainty of HOM of +78 % and -68 % is not shown.

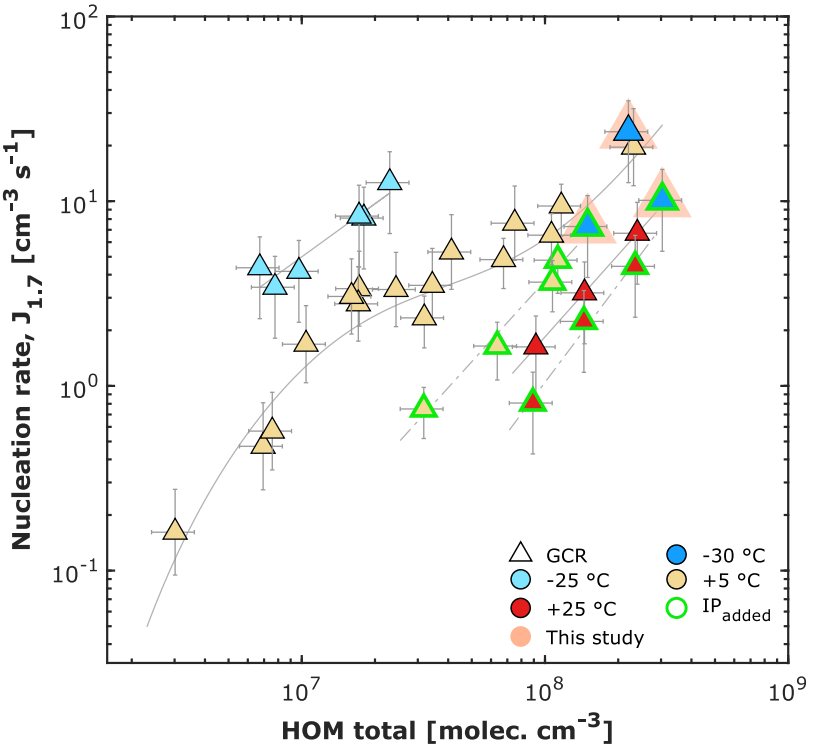

Figure 8. Pure biogenic nucleation rates at 1.7 nm diameter against total HOM concentration at different temperatures for α-pinene and α-pinene + isoprene systems. HOM total is defined as the sum of C_5, C_{10}, C_{15} and C_{20} carbon classes. Triangles represent Galactic Cosmic Rays (GCR) conditions. Data points at +5 °C and +25 °C are from Kirkby et al. (2016) and Heinritzi et al., (2020). Data points at -25 °C are from Simon et al., (2020). The value of isoprene-to-monoterpene carbon ratio (R) varies from 1.5 to 6.5 for Heinritzi et al., (2020), and R equals to 14.4 and 6.1 for this study. The points with orange marker on the background indicate the contribution of this work. Solid lines represent power-law fits to GCR conditions of the systems with α-pinene only and dashed lines are the power-law fits of the systems with isoprene added. Bars indicate 1 σ run-to-run experimental uncertainty. The overall systematic scale uncertainty of HOM of +78 % and -68 % is not shown.

Anonymous Referee #2

General comments

Caudillo et al. present chamber measurements of new-particle formation from α-pinene (AP) oxidation products at low temperatures, and study the effects of added isoprene (IP) and increased relative humidity (RH). The main focus is on the chemical composition of gas-phase species and (non-size-resolved) ultrafine particles, determined with a nitrate chemical ionization mass spectrometer and a thermal desorption-differential mobility analyzer, and in addition also nucleation rates are reported. Isoprene is observed to affect the chemical composition through an increase in e.g. C5 and C15 compounds, and to suppress new-particle formation as also reported in other studies.

Simultaneous measurements of gas- and particle-phase composition are essential for improving the understanding of biogenic secondary aerosol formation. The manuscript is generally well written and the results are clearly presented. I can recommend the work to be published in ACP after the authors have addressed the following comments:

Specific comments

1. Regarding the discussion on the effects of isoprene on the elemental composition, especially C_5 and C_{15} compounds are stated to be increased in intensity. This seems clearer in the case of gas phase, whereas for particle phase the effects seem more diverse and e.g. Figure 3 shows similar increases in the signal intensity for various compounds with carbon content of up to ca. C_{18}, C_{19}. I cannot clearly distinguish a stronger increase specifically at C_{15} in Figs. 3 or S1; can this be further clarified?

Many thanks for pointing this out. Regarding the isoprene effect, we do observe an increase in the intensity for several species in the particle phase, not only for C_5 and C_{15} compounds. We believe that this might be related to the method we apply for evaporating the particles (thermal desorption), possibly fragmentation and chemical reactions are occurring. We are further investigating this phenomenon in a forthcoming study.

We clarified in Section 3.2.1 that C_5 and C_{15} compounds correspond to $C_5H_{10}O_{5\text{-}7}$ and $C_{15}H_{24}O_{5\text{-}10}$ which are observed in both gas and particle phase.

Fig. 3f shows the intensity difference in the particle phase. In contrast with what is observed in the gas phase, the particle phase effects seem more diverse. There is an increase in the intensity difference for several species in the system with isoprene (*αIP-30,20*), such as $C_{4\text{-}5}$, $C_{13\text{-}16}$ and some $C_{17\text{-}19}$ (see Fig. S1 in the supplement). Especially, a distinct group of C_{15} compounds $C_{15}H_{24}O_{5\text{-}10}$ and $C_5H_{10}O_{5\text{-}7}$ can be identified in the particle and in the gas phase. A previous study has shown that isoprene can enhance particle growth rates despite its negative effect on nucleation (Heinritzi et al., 2020). The identification of C_{15} dimers in nanometer-sized particles in the present study confirms this with a direct measurement. The suppressing effect of isoprene on nucleation will further be discussed in Section 3.4.2. However, isoprene can still contribute to the growth of particles by C_5 or by C_{15} compounds. Additionally, these species can be an important fingerprint to identify SOA formation from a mixture of biogenic vapors containing isoprene.

2. It may not be obvious that higher particle growth rates (GR) at larger particle sizes are due to isoprene (Section 3.2.1, last paragraph: "Reaching the same mass with a lower number of particles for the experiment with isoprene (αIP-30,20) compared to α-30,20, means that the growth rates at larger sizes (> 15 nm) are higher in the presence of isoprene").

Particle GRs can generally be higher at lower particle number concentrations, as the amount of available condensable vapor per particle is higher. Can it be concluded that the enhanced growth at larger sizes is specifically related to isoprene, and not to such dynamic effects?

Yes, we think that the enhanced growth at sizes larger than 15 nm for the experiment *αIP-30,20* is related to isoprene. The mentioned dynamic effects can be ruled out in our opinion as the HOM concentrations are not affected by the presence of the particles. This means that the particle number concentration does not influence the degree of supersaturation. Or in other words, there is not depletion of HOM total (as is shown in Figure 1, fourth panel) as there is a continuous replenishment of the gases in the CLOUD chamber.

Additionally, several studies have reported that some oxidation products from isoprene play an important role in SOA formation (different from new particle formation). We mentioned some studies in Section 1.

Isoprene (C_5H_8) is the biogenic vapor with the highest global emission rate. Its estimated emissions are between 500 to 600 Tg per year (Guenther et al., 2006; Sindelarova et al., 2014) and there are many studies that indicate the global importance of isoprene in terms of SOA formation (Surratt et al., 2006; Surratt et al., 2007; Surratt et al., 2010; Paulot et al., 2009; Lin et al., 2012; Riva et al., 2016).

3. Effect of RH (Section 3.2.2): the particle mass concentration is observed to increase at elevated RH at otherwise similar conditions. However, Fig. S3 shows that the α-pinene level is somewhat higher for the experiments with higher RH. Can the higher AP level contribute to the increased particle mass?

Effectively the α-pinene level in *α-50,60* is a factor of ~ 2 higher than *α-50,20* in the steady-state (as shown in Table 1). In the same way, the mass concentration also shows an increase by a factor of 2. In this sense, the α-pinene level might influence the number of new particles that are formed and in some proportion the mass. Nevertheless, the very small particles do not contribute significantly to the mass. Additionally, the total HOM concentration and nucleation rates in the gas phase are similar (see Figure 6).

We think that the α-pinene level probably influences the system, but very likely the bigger effect is due to the change in the relative humidity from 20 to 60 %.

Also, the RH range of 60-100% for the high-RH experiments is rather broad. What is the reasoning for lumping together these different RH values, and is it possible that the RH effects vary within this 60-100% range?

The RH for the experiment classified as high RH, was ~ 60 % and did not vary between 60 and 100 % during the particle collection period. In order to clarify this, we included the RH times series in the fifth panel of Figure S3 and we changed the notation accordingly from *α-50,60-100* to *α-50,60* throughout the whole manuscript.

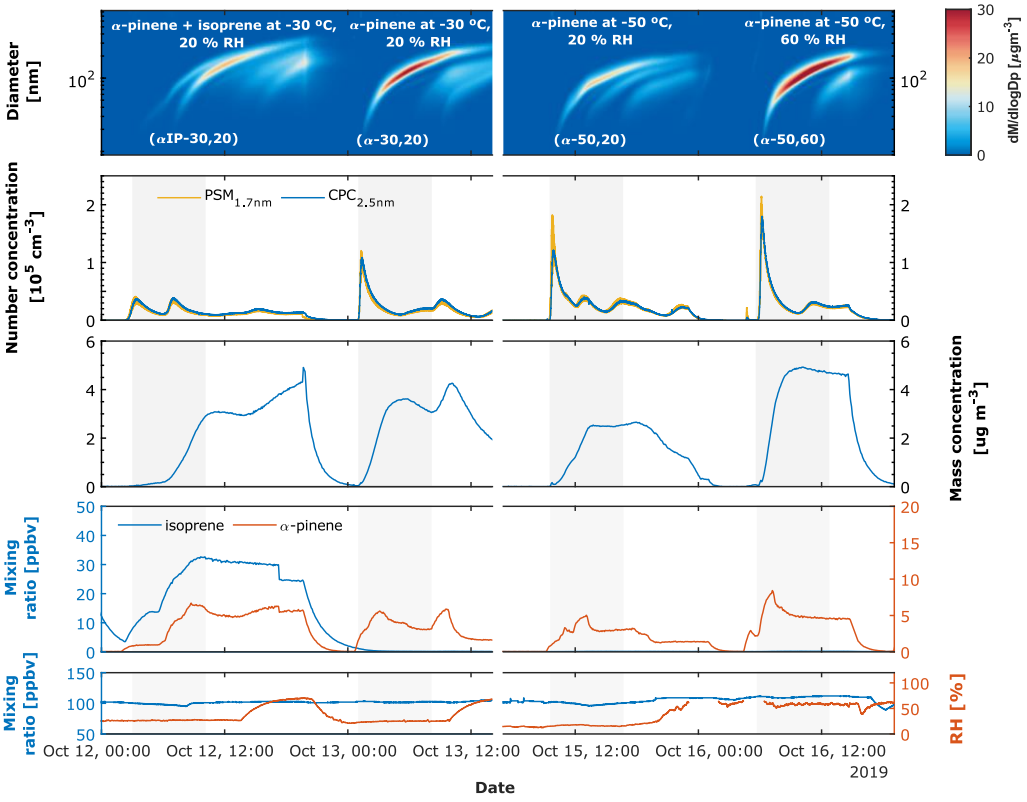

Figure S3. Experimental overview for pure biogenic new particle formation. First panel: particle size distribution for four different experiments: α-pinene + isoprene at -30 °C and 20 % RH (αIP-30,20); α-pinene at -30 °C and 20 % RH (α-30,20); α-pinene at -50 °C and 20 % RH (α-50,20) and α-pinene at -50 °C and 60% RH (α-50,60). The color scale represents the normalized mass concentration in μg m^{-3}. Second panel: Particle number concentration in cm^{-3} measured by the PSM with a cut-off diameter of 1.7 nm and CPC with a cut-off diameter of 2.5 nm. Third panel: Mass concentration in μg m^{-3} (obtained by integrating the normalized mass concentration from the SMPS). Fourth panel: Mixing ratio in ppbv for the biogenic precursor gases, isoprene and α-pinene. Fifth panel: Ozone mixing ratio in ppbv and relative humidity in %. The shaded areas refer to the time where the particles were collected using the TD-DMA.

4. Similarly to the RH experiments, it seems that the AP level during the particle formation event and sample collection of the isoprene experiment is not exactly similar to the experiments without IP; it seems to be lower for the AP-IP set-up (Figure 1, third row). Can this affect the AP vs. AP-IP comparison?

It is correct that the α-pinene levels in the experiments with (*αIP-30,20*) and without (*α-30,20*) isoprene are not identical. In fact, since the precursor gases are continuously added into the chamber, reaching identical levels is challenging. Therefore, for the experiments reported in this work, we normalized the mass spectrum, this means that for each experiment, we divided every signal by the total signal, in this sense we are comparing fractions rather than absolute values.

We think that the data analysis treatment together with the fact that all the other parameters (RH, O_3, time collection, temperature) are as similar as reasonably achievable, allows a comparison of the different experiments.

5. Section 3.3: It would be helpful to list the actual fractions of the different VBS bins instead of only stating that the particle-phase species are mainly LVOC, ELVOC and ULVOC (it also seems that ULVOC is only a minor fraction). This could be a table with the bin fractions given for the different experiments.

We agree as well that ULVOC do not represent the highest fraction. We have calculated the volatility bin fractions and reported these values in Table 2.

Table 2. Bin volatility fractions for the different experiments.

Experiment	T [ºC]	RH [%]	ULVOC [%]	ELVOC [%]	LVOC [%]	SVOC [%]	IVOC [%]
αIP-30,20	-30	20	8.6	28.3	59.1	3.8	0.2
α-30,20	-30	20	5.9	44.1	48.1	1.9	0
α-50,20	-50	20	16.5	36.4	46.1	1.0	0
α-50,60	-50	60	13.8	50.6	34.8	0.8	0

In Section 3.3, we have mentioned that LVOC and ELVOC represents the major fractions, and ULVOC only a minor fraction.

We classified the volatility bins according to the regimes proposed by Donahue et al. (2012) and Schervish and Donahue (2020), and calculated the corresponding fractions (Table 2). Overall, the particle phase detected compounds correspond mainly to Low Volatility Organic Compounds (LVOC) and Extremely Low Volatility Compounds (ELVOC) by explaining more than 80 % of the signals, while Ultralow Volatility Organic Compounds (ULVOC) represent only a small fraction (between 6 and 17 %). With this parametrization we are able to approximate the saturation mass concentration for the particle phase compounds measured using the TD-DMA in the CLOUD chamber. For this parametrization we assume that the elemental composition is one of the main parameters to take into account.

6. The O_3 level of 100 ppbv seems rather high. How does it compare with typical tropospheric values? This is relevant considering the discussion on the effects of mixing ratios on the composition and nucleation of HOM (Section 3.4.1).

The ozone levels along the vertical profile might vary depending on the latitude and longitude. Nevertheless, we can state that in the upper troposphere, approximately between 8 and 12 km, the O_3 level of 100 ppbv falls in the upper limit of the observed range (Oltmans et al., 1996; Crutzen et al., 1999; Staehelin, 2003).

However, the ozone and α-pinene mixing ratios used in this study (O_3 = 100 ppbv and α-pinene = 1 - 8 ppbv) are considerable higher than the levels reported in Simon et al. (2020), ~ 30 - 50 ppbv O_3 and 0.2 - 1 ppbv α-pinene.

In Section 3.4.1, we discuss the possible effects that high levels of precursor gases might have on the composition and nucleation of HOM.

In order to investigate a possible reason for this finding, we have chosen two representative experiments at -10 °C and 80 to 90 % RH with different levels of α-pinene and ozone. Fig. 7 shows the mass defect plots for the gas phase chemical composition of the oxidation products. In one experiment (Fig. 7a) α-pinene and the ozone mixing ratio were between 0.2 to 0.8 ppbv and 40 to 50 ppbv, respectively, while for the second

experiment (Fig. 7b) the mixing ratios were 2 to 3 ppbv and 100 ppbv, respectively. From Fig. 7c it can be concluded that the formation of HOM with low oxygen content is favored when the α-pinene and ozone mixing ratio are higher (relative to the system at low levels of precursor gases). An explanation for this is that the high concentration of RO_2 enhances the terminating reactions before the autoxidation can lead to high oxygen content for the products. As the compounds with low oxygen content tend to have higher saturation vapor pressures, they do not contribute efficiently to new particle formation. For this reason, a given total HOM concentration is not unambiguously tied to a new particle formation rate (even at constant temperature). The magnitude of the precursor gas mixing ratio (more specifically the full volatility distribution of the products and not just the simple measure of total HOM) also needs to be taken into account (see Fig.S6 in the supplement). In summary, the lower $J_{1.7nm}$ values compared with previous studies are very likely due to the higher α-pinene and ozone mixing ratios used in the present study. There are several compounds with low oxygen content that contribute to the total HOM concentration in the gas phase while these do not contribute to the formation of new particles.

7. On P5L149-150, it is stated that particle evaporation before analysis should not be substantial; can this be assessed in a quantitative manner? Are there other uncertainty sources such as different charging efficiencies or transmission of the compounds?

Yes, charging and transmission efficiencies are important sources of uncertainties.

Regarding the charging efficiency, the nitrate CI-APi-TOF mass spectrometer uses nitrate reagent ions $(HNO3)_n$ NO_3^- with n = 0-2 for detecting HOM. This ionization scheme favors the detection of organic compounds with high O:C ratio (Hyttinen et al., 2017; Ehn et al., 2017), specifically Simon et al. (2020) reported an O:C ratio > 0.6. In this sense, we might underestimate compounds with lower O:C ratio.

On the other hand, the transmission efficiency of the nitrate CI-APi-TOF has been well characterized. Heinritzi et al. (2016) developed a method that makes the HOM quantification more reliable. We applied this method and corrected particle and gas phase mass spectra regarding the mass dependent transmission efficiency.

We have mentioned it briefly in Section 2.3.

Here the nitrate CI-APi-TOF mass spectrometer data for gas and particle phase have been corrected for background signals and the mass-dependent transmission efficiency in the mass classifier (Heinritzi et al., 2016). The data analysis and processing were performed using IGOR Pro 7 (WaveMetrics, Inc., USA), Tofware (Version 3.2, Aerodyne Inc., USA) and MATLAB R2019b (MathWorks, Inc., USA).

I also agree with Referee #1 that an assessment of the relative contributions of the smallest and the larger particles to the particle-phase mass samples would be very useful.

The calculation was done accordingly and the requested information has been added to Table 1.

For calculating the mass fraction of particles collected on the filament during the TD-DMA collection time we used only SMPS size distributions, in a range from 9 nm to 834 nm. We estimated that the mass of particles with sizes smaller than 9 nm is negligible (by comparing to nanoSMPS data in a size range from 2 to 63 nm). Thus, the mass fraction reported in Table 1 takes only into account SMPS measurements. From these data we derived the mass fractions for the collected particles with a diameter smaller than 15 nm ($Mass_{< 15\ nm}$) and for a diameter larger than 15 nm ($Mass_{> 15\ nm}$).

This calculation is an ideal estimate, it does not take into account uncertainties due to charging efficiency, collection efficiency and transmission efficiency in the TD-DMA as reported in detail by Wagner et al. (2018) for the size-selective mode.

Table 1. Summary of the main parameters for four pure biogenic new particle formation experiments.

Experiment	Isoprene [ppb]	α-pinene [ppb]	Isoprene-to-monoterpene carbon ratio (*R*)	Ozone [ppb]	T [°C]	RH [%]	HOM total* [molec. cm^{-3}]	$J_{1.7}$* [cm^{-3} s^{-1}]	Growth rate 3.2-8 nm [nm h^{-1}]	Growth rate 5-15 nm [nm h^{-1}]	Mass $_{< 15\ nm}$ /Mass $_{> 15\ nm}$** [%]
αIP-30,20	13.71 31.38	0.95 5.12	14.4 6.1	98.58 101.56	-30 -30	20 20	1.50e8 3.04e8	7.29 10.10	18.0 NA	22.8 39.0	0.29 / 99.7
α-30,20	~ 0	3.35	NA	102.10	-30	20	2.20e8	23.76	76.9	77.1	0.11 / 99.9
α-50,20	~ 0	3.04	NA	100.55	-50	20	6.72e7	51.24	41.1	42.0	0.26 / 99.7
α-50,60	~ 0	7.72	NA	110.20	-50	60	8.00e7	79.17	63.4	78.4	0.09 / 99.9

* Run-to-run experimental uncertainties of HOMs is ± 20 % and for $J_{1.7}$ is ± 30 %. NA, Not Applicable. **Mass fraction of particles collected on the filament during the TD-DMA collection time, calculation based on SMPS mass distributions.

8. P11L350: The meaning of "GCR conditions" is not explained; please clarify.

The requested information about GCR conditions has been added accordingly in Section 2.1.

In order to promote particle production from ions, Galactic Cosmic Rays conditions (GCR) can be achieved by turning off the high voltage field (30 kV m^{-1}). The equilibrium ion-pair concentration in the chamber due to GCR is around 700 cm^{-3} (Kirkby et al., 2016).

The experiments relevant for this work were done under GCR conditions and in a flow-through mode with continuous addition of the reactants, performed at -50 °C and -30 °C, at low and high relative humidity to simulate pure biogenic new particle formation at a range of free tropospheric conditions.

Technical corrections

P6L174: The particle formation rate is said to be defined as the flux of particles of a certain size as a function of time, but presumably the reported rates are not actually time dependent; "as a function of time" should thus be removed, for clarity.

We have removed "as a function of time" as suggested.

The nucleation rate (J_{dp}), which is defined as the flux of particles of a certain size, is calculated using the method proposed by Dada et al. (2020), see equation (9) therein.

P6L202: It may be more appropriate to write "this is in line with the results of Kiendler-Scharr et al…." instead of "this confirms the results of …"

We have modified the sentence as suggested.

This is in line with the results of Kiendler-Scharr et al. (2009), who first reported the decrease in particle number of the nucleated particles.

P7L226-227: Please reformulate the expression “the gas and particle of α-pinene” and similar occurrences.

We have modified the sentence.

Figure 3 shows mass defect plots of gas and particle phase and the intensity difference between each phase at -30 °C. Figure 3a and Fig. 3d display the gas and particle composition of *α-30,20*, while the gas and particle composition of *αIP-30,20* are shown in Fig. 3b and Fig. 3e, respectively. As both phases were measured with the same instrument, they can be directly inter-compared.

P8L245: Please change “nSEMS” to “nSMPS” (?).

For determining the growth rates, we used the nano-Scanning Electrical Mobility Spectrometer (nSEMS) as indicated not the nSMPS.

P8L254: Change “growth at higher sizes” to “growth at larger sizes”.

We have modified the sentence as suggested.

Most likely, isoprene might enhance growth at larger sizes (> 15 nm) in the present study.

P9L268: The term “mass distribution” (here referring to particle mass size distribution?) may be a bit misleading as it might be confused with elemental composition or volatility distribution; please reformulate.

We have changed “mass distribution” to “particle mass size distribution”.

This observation can likely be attributed to a change in the particle mass size distribution (see Fig. S3 in the supplement), which indicates that at similar α-pinene and ozone mixing ratio, and the same temperature, the particle mass concentration increases possibly due to the effect of the relative humidity in the system.

Figure 2 and similar plots: also the particle-phase fractions should preferably be written as positive instead of negative numbers (even if they are presented on the “negative” axis).

For Figures 2, S1 and S2, we have modified the negative axis to positive numbers as suggested.

Caption of Figure 2: For clarity, “each system” could be changed to “each system and phase”.

We have modified the sentence as suggested, in the captions of Figure 2, S1 and S2.

Caption of Figure 3 and similar occurrences: the expression “mass defect plots of gas and particle phase and the intensity difference between them” is misleading; this sounds like the intensity difference between the gas and particle phases instead of the difference between the experiments. Please reformulate.

We have changed “mass defect plots of gas and particle phase and the intensity difference between them” to “mass defect plots of gas and particle phase and the intensity difference between each phase”, in Figures 3 and 4.

Legend of Figure 6 and similar occurrences: Please change “GRC” to “GCR”.

We have attended this comment accordingly.

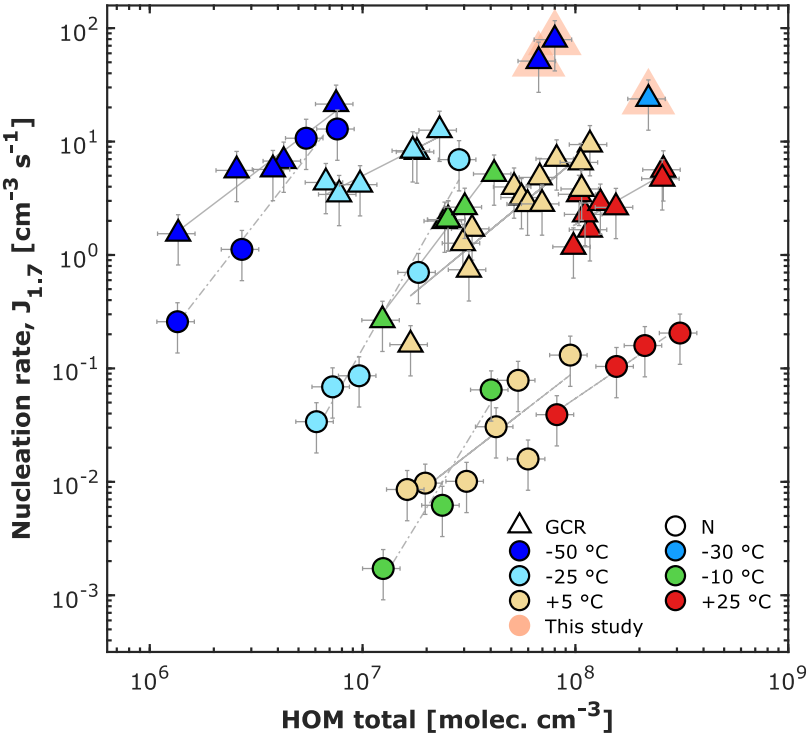

Figure 6. Pure biogenic nucleation rates of pure α-pinene at 1.7 nm diameter against total HOM concentration at different temperatures. HOM total is defined as the sum of C_5, C_{10}, C_{15} and C_{20} carbon classes. Triangles represent Galactic Cosmic Rays (GCR) conditions and circles represent Neutral conditions. Data points at -50 °C, -25 °C, -10 °C, +5 °C and +25 °C are from Simon et al. (2020). The points with orange marker on the background are the contribution of this study (experiments α-30,20, α-50,20 and α-50,60). Solid and dashed lines represent power-law fits to GCR and Neutral conditions. Bars indicate 1 σ run-to-run experimental uncertainty. The overall systematic scale uncertainty of HOM of +78 % and -68 % is not shown.

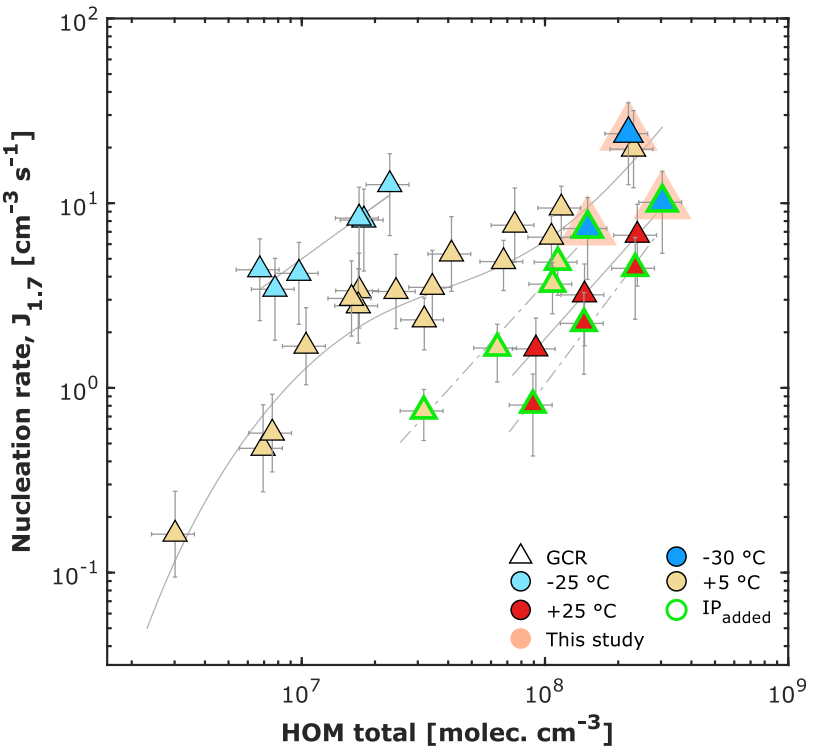

Figure 8. Pure biogenic nucleation rates at 1.7 nm diameter against total HOM concentration at different temperatures for α-pinene and α-pinene + isoprene systems. HOM total is defined as the sum of C_5, C_{10}, C_{15} and C_{20} carbon classes. Triangles represent Galactic Cosmic Rays (GCR) conditions. Data points at +5 °C and +25 °C are from Kirkby et al. (2016) and Heinritzi et al., (2020). Data points at -25 °C are from Simon et al., (2020). The value of isoprene-to-monoterpene carbon ratio (R) varies from 1.5 to 6.5 for Heinritzi et al., (2020), and R equals to 14.4 and 6.1 for this study. The points with orange marker on the background indicate the contribution of this work. Solid lines represent power-law fits to GCR conditions of the systems with α-pinene only and dashed lines are the power-law fits of the systems with isoprene added. Bars indicate 1 σ run-to-run experimental uncertainty. The overall systematic scale uncertainty of HOM of +78 % and -68 % is not shown.

Caption of Figure 8 and similar occurrences: Please change “galactic comic rays” to “galactic cosmic rays”. :-)

We have attended this comment accordingly.

Figure 8. Pure biogenic nucleation rates at 1.7 nm diameter against total HOM concentration at different temperatures for α-pinene and α-pinene + isoprene systems. HOM total is defined as the sum of C_5, C_{10}, C_{15} and C_{20} carbon classes. Triangles represent Galactic Cosmic Rays (GCR) conditions. Data points at +5 °C and +25 °C are from Kirkby et al. (2016) and Heinritzi et al., (2020). Data points at -25 °C are from Simon et al., (2020). The value of isoprene-to-monoterpene carbon ratio (R) varies from 1.5 to 6.5 for Heinritzi et al., (2020), and R equals to 14.4 and 6.1 for this study. The points with orange marker on the background indicate the contribution of this work. Solid lines represent power-law fits to GCR conditions of the systems with α-pinene only and dashed lines are the power-law fits of the systems with isoprene added. Bars indicate 1 σ run-to-run experimental uncertainty. The overall systematic scale uncertainty of HOM of +78 % and -68 % is not shown.

Caption of Figure S4: Please state that this is Figure 5 in linear scale.

We added this information as suggested

Figure S4. TD-DMA Volatility distribution of the measured oxidation products in the particle phase for four different experiments (Figure 5 in linear scale): (a) α-pinene at -30 °C and 20 % RH (α-30,20); (b) α-pinene + isoprene at -30 °C and 20 % RH (αIP-30,20); (c) α-pinene at -50 °C and 20 % RH (α-50,20) and (d) α-pinene at -50 °C and 60-100 % RH (α-50,60-100). Every individual volatility bin includes the sum of the intensity for the oxidation products normalized by the total signal in each system. Every individual volatility bin is defined at 300 K, shifted, and widened according to their corresponding temperature. The color bands in the background indicate the volatility regimes as in Donahue et al. (2012) and in Schervish and Donahue (2020). The normalized intensity is dimensionless. Nevertheless, it should be noted that the particle phase signal is given in normalized counts per second integrated over the evaporation time [ncps. s].

Figure S5: Why are the orange shades triangle-shaped?

The orange shades indicate the new results reported in this work. Since Figure S5 shows the data points with circle markers, we changed as well to circles for consistency.

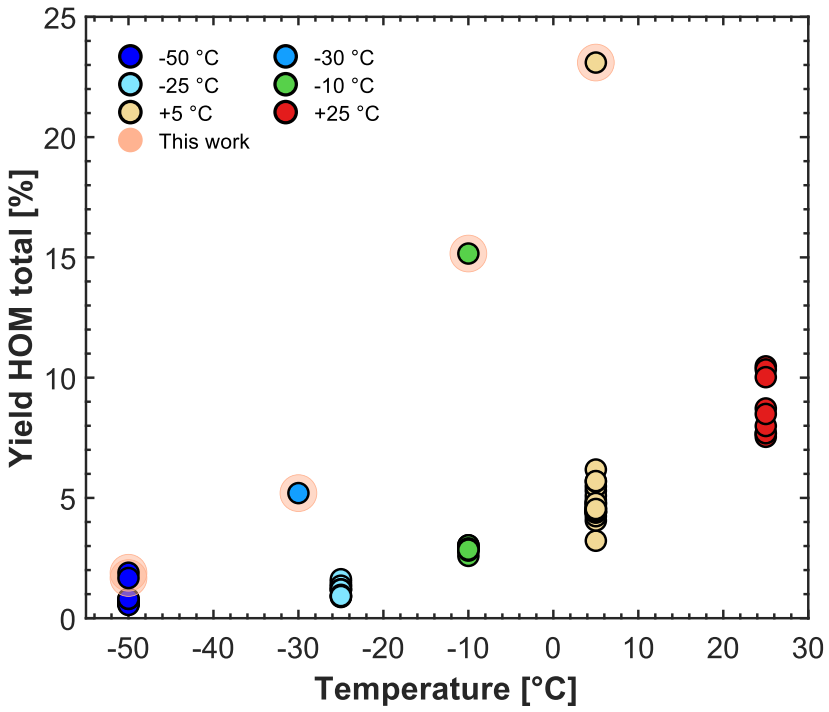

Figure S5. Yield of total HOM as a function of temperature for pure α-pinene systems. Data points at -50 °C, -25 °C, -10 °C, +5 °C and +25 °C are from Simon et al. (2020) and the data points with the orange shadows are the contribution of this study (α-30,20, α-50,20 and α-50,60 and complementary pure α-pinene experiments at +5 °C and at -10 °C). The level of precursor gases from Simon et al., (2020) were 0.2 to 0.8 ppbv for α-pinene and 40 to 50 ppbv for ozone, while for experiments reported here (shown with orange shadows), the mixing ratios were 1 to 8 ppbv for α-pinene and 100 ppbv for ozone.

Caption of Figure S6: Please explain the meaning of "overflow bin" and why the values of the first bin are both negative and positive.

The overflow bin contains the volatility bins with a saturation concentration lower than -11 ug m^{-3}.

Figure S6. Volatility distribution of gas phase for two different systems and the normalized difference between them. Gas phase is measured with a Nitrate CI-APi-TOF Mass Spectrometer. Every individual volatility bin includes the normalized intensity difference (high-low)/low, which is calculated based on intensity of the system at high level of precursor gases (α-pinene was 2 - 3 ppbv and Ozone ~ 100 ppbv) and on the system at low level of precursor gases (α-pinene was 0.2 - 0.8 ppbv and Ozone ~ 40 - 50 ppbv). Every individual volatility bin is defined at 300 K, shifted, and widened according to their corresponding temperature. The lowest bin is an overflow bin (which contains the volatility bins with saturation concentration < -11 ug m^{-3}.). The color bands in the background indicate the volatility regimes as in Donahue et al. (2012) and in Schervish and Donahue (2020).

All the positive and negative bins with saturation values < -11 ug m^{-3} have been summed up and represented in the volatility bin overflow at - 11 ug m^{-3}.

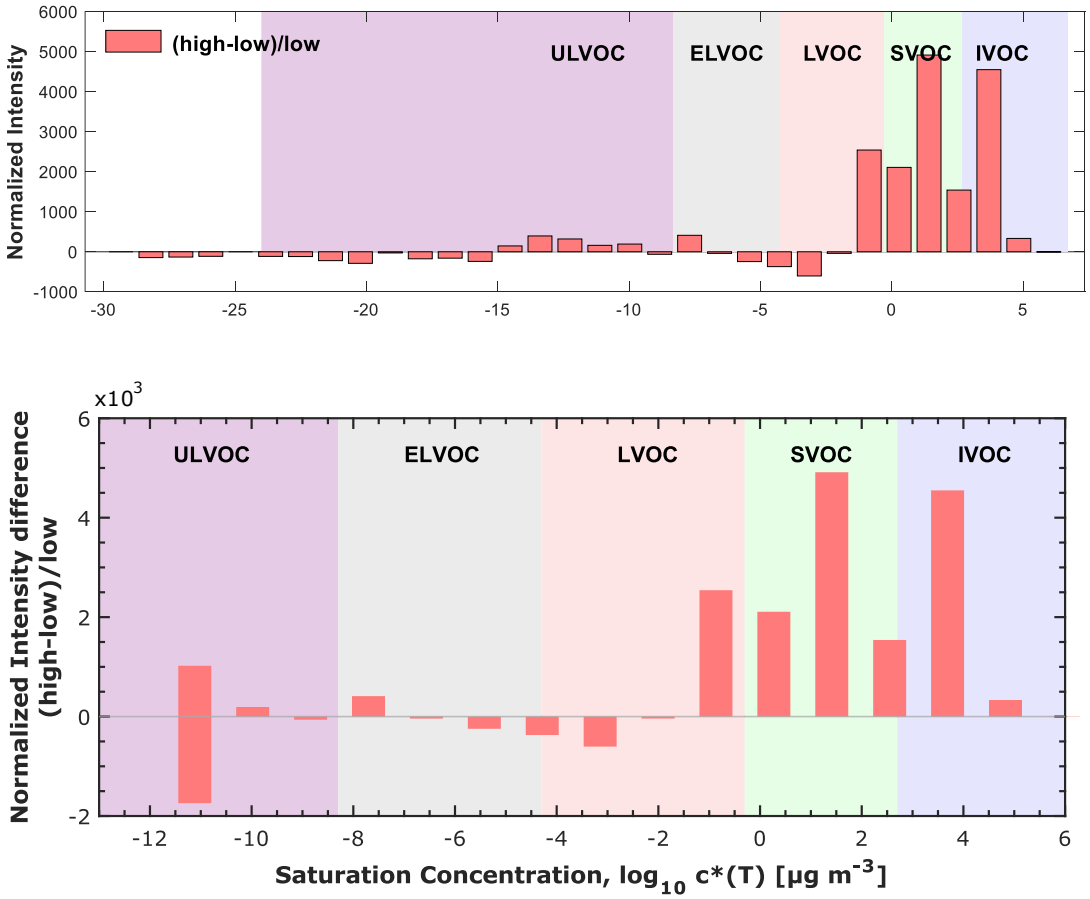

References

Crutzen, P. J., Lawrence, M. G., and Pöschl, U.: On the background photochemistry of tropospheric ozone, Tellus B: Chemical and Physical Meteorology, 51, 123-146, 10.3402/tellusb.v51i1.16264, 1999.

Dada, L., Lehtipalo, K., Kontkanen, J., Nieminen, T., Baalbaki, R., Ahonen, L., Duplissy, J., Yan, C., Chu, B., Petäjä, T., Lehtinen, K., Kerminen, V.-M., Kulmala, M., and Kangasluoma, J.: Formation and growth of sub-3-nm aerosol particles in experimental chambers, Nature Protocols, 15, 1013-1040, 10.1038/s41596-019-0274-z, 2020.

Ehn, M., Berndt, T., Wildt, J., and Mentel, T.: Highly Oxygenated Molecules from Atmospheric Autoxidation of Hydrocarbons: A Prominent Challenge for Chemical Kinetics Studies, International Journal of Chemical Kinetics, 49, 821-831, 2017.

Heinritzi, M., Simon, M., Steiner, G., Wagner, A. C., Kürten, A., Hansel, A., and Curtius, J.: Characterization of the mass-dependent transmission efficiency of a CIMS, Atmos. Meas. Tech., 9, 1449-1460, 10.5194/amt-9-1449-2016, 2016.

Hyttinen, N., Rissanen, M. P., and Kurtén, T.: Computational Comparison of Acetate and Nitrate Chemical Ionization of Highly Oxidized Cyclohexene Ozonolysis Intermediates and Products, The Journal of Physical Chemistry A, 121, 2172-2179, 10.1021/acs.jpca.6b12654, 2017.

Kirkby, J., Duplissy, J., Sengupta, K., Frege, C., Gordon, H., Williamson, C., Heinritzi, M., Simon, M., Yan, C., Almeida, J., Tröstl, J., Nieminen, T., Ortega, I. K., Wagner, R., Adamov, A., Amorim, A., Bernhammer, A.-K., Bianchi, F., Breitenlechner, M., Brilke, S., Chen, X., Craven, J., Dias, A., Ehrhart, S., Flagan, R. C., Franchin, A., Fuchs, C., Guida, R., Hakala, J., Hoyle, C. R., Jokinen, T., Junninen, H., Kangasluoma, J., Kim, J., Krapf, M., Kürten, A., Laaksonen, A., Lehtipalo, K., Makhmutov, V., Mathot, S., Molteni, U., Onnela, A., Peräkylä, O., Piel, F., Petäjä, T., Praplan, A. P., Pringle, K., Rap, A., Richards, N. A. D., Riipinen, I., Rissanen, M. P., Rondo, L., Sarnela, N., Schobesberger, S., Scott, C. E., Seinfeld, J. H., Sipilä, M., Steiner, G., Stozhkov, Y., Stratmann, F., Tomé, A., Virtanen, A., Vogel, A. L., Wagner, A. C., Wagner, P. E., Weingartner, E., Wimmer, D., Winkler, P. M., Ye, P., Zhang, X., Hansel, A., Dommen, J., Donahue, N. M., Worsnop, D. R., Baltensperger, U., Kulmala, M., Carslaw, K. S., and Curtius, J.: Ion-induced nucleation of pure biogenic particles, Nature, 533, 521-526, 10.1038/nature17953, 2016.

Lehtipalo, K., Yan, C., Dada, L., Bianchi, F., Xiao, M., Wagner, R., Stolzenburg, D., Ahonen, L. R., Amorim, A., Baccarini, A., Bauer, P. S., Baumgartner, B., Bergen, A., Bernhammer, A.-K., Breitenlechner, M., Brilke, S., Buchholz, A., Mazon, S. B., Chen, D., Chen, X., Dias, A., Dommen, J., Draper, D. C., Duplissy, J., Ehn, M., Finkenzeller, H., Fischer, L., Frege, C., Fuchs, C., Garmash, O., Gordon, H., Hakala, J., He, X., Heikkinen, L., Heinritzi, M., Helm, J. C., Hofbauer, V., Hoyle, C. R., Jokinen, T., Kangasluoma, J., Kerminen, V.-M., Kim, C., Kirkby, J., Kontkanen, J., Kürten, A., Lawler, M. J., Mai, H., Mathot, S., Mauldin, R. L., Molteni, U., Nichman, L., Nie, W., Nieminen, T., Ojdanic, A., Onnela, A., Passananti, M., Petäjä, T., Piel, F., Pospisilova, V., Quéléver, L. L. J., Rissanen, M. P., Rose, C., Sarnela, N., Schallhart, S., Schuchmann, S., Sengupta, K., Simon, M., Sipilä, M., Tauber, C., Tomé, A., Tröstl, J., Väisänen, O., Vogel, A. L., Volkamer, R., Wagner, A. C., Wang, M., Weitz, L., Wimmer, D., Ye, P., Ylisirniö, A., Zha, Q., Carslaw, K. S., Curtius, J., Donahue, N. M., Flagan, R. C., Hansel, A., Riipinen, I., Virtanen, A., Winkler, P. M., Baltensperger, U., Kulmala, M., and Worsnop, D. R.: Multicomponent new particle

formation from sulfuric acid, ammonia, and biogenic vapors, Science Advances, 4, eaau5363, 10.1126/sciadv.aau5363, 2018.

Oltmans, S. J., Levy II, H., Harris, J. M., Merrill, J. T., Moody, J. L., Lathrop, J. A., Cuevas, E., Trainer, M., O′Neill, M. S., Prospero, J. M., Vömel, H., and Johnson, B. J.: Summer and spring ozone profiles over the North Atlantic from ozonesonde measurements, Journal of Geophysical Research: Atmospheres, 101, 29179-29200, https://doi.org/10.1029/96JD01713, 1996.

Simon, M., Dada, L., Heinritzi, M., Scholz, W., Stolzenburg, D., Fischer, L., Wagner, A. C., Kürten, A., Rörup, B., He, X. C., Almeida, J., Baalbaki, R., Baccarini, A., Bauer, P. S., Beck, L., Bergen, A., Bianchi, F., Bräkling, S., Brilke, S., Caudillo, L., Chen, D., Chu, B., Dias, A., Draper, D. C., Duplissy, J., El-Haddad, I., Finkenzeller, H., Frege, C., Gonzalez-Carracedo, L., Gordon, H., Granzin, M., Hakala, J., Hofbauer, V., Hoyle, C. R., Kim, C., Kong, W., Lamkaddam, H., Lee, C. P., Lehtipalo, K., Leiminger, M., Mai, H., Manninen, H. E., Marie, G., Marten, R., Mentler, B., Molteni, U., Nichman, L., Nie, W., Ojdanic, A., Onnela, A., Partoll, E., Petäjä, T., Pfeifer, J., Philippov, M., Quéléver, L. L. J., Ranjithkumar, A., Rissanen, M. P., Schallhart, S., Schobesberger, S., Schuchmann, S., Shen, J., Sipilä, M., Steiner, G., Stozhkov, Y., Tauber, C., Tham, Y. J., Tomé, A. R., Vazquez-Pufleau, M., Vogel, A. L., Wagner, R., Wang, M., Wang, D. S., Wang, Y., Weber, S. K., Wu, Y., Xiao, M., Yan, C., Ye, P., Ye, Q., Zauner-Wieczorek, M., Zhou, X., Baltensperger, U., Dommen, J., Flagan, R. C., Hansel, A., Kulmala, M., Volkamer, R., Winkler, P. M., Worsnop, D. R., Donahue, N. M., Kirkby, J., and Curtius, J.: Molecular understanding of new-particle formation from α-pinene between −50 and +25 °C, Atmos. Chem. Phys., 20, 9183-9207, 10.5194/acp-20-9183-2020, 2020.

Staehelin, J.: Ozone Measurements and Trends (Troposphere), in: Encyclopedia of Physical Science and Technology (Third Edition), edited by: Meyers, R. A., Academic Press, New York, 539-561, 2003.

Wagner, A. C., Bergen, A., Brilke, S., Fuchs, C., Ernst, M., Hoker, J., Heinritzi, M., Simon, M., Bühner, B., and Curtius, J.: Size-resolved online chemical analysis of nanoaerosol particles: a thermal desorption differential mobility analyzer coupled to a chemical ionization time-of-flight mass spectrometer, Atmospheric Measurement Techniques, 11, 5489-5506, 2018.

Chemical composition of nanoparticles from α-pinene nucleation and the influence of isoprene and relative humidity at low temperature

Lucía Caudillo[1], Birte Rörup[2], Martin Heinritzi[1], Guillaume Marie[1], Mario Simon[1], Andrea C. Wagner[3], Tatjana Müller[1,4], Manuel Granzin[1], Antonio Amorim[5], Farnoush Ataei[6], Rima Baalbaki[2], Barbara Bertozzi[7], Zoé Brasseur[2], Randall Chiu[3], Biwu Chu[2], Lubna Dada[8], Jonathan Duplissy[2,9], Henning Finkenzeller[3], Loïc Gonzalez Carracedo[10], Xu-Cheng He[2], Victoria Hofbauer[11], Weimeng Kong[12,13], Houssni Lamkaddam[8], Chuan P. Lee[8], Brandon Lopez[11], Naser G. A. Mahfouz[11], Vladimir Makhmutov[14,26], Hanna E. Manninen[15], Ruby Marten[8], Dario Massabò[16], Roy L. Mauldin[17,11], Bernhard Mentler[18], Ugo Molteni[8,20,21], Antti Onnela[15], Joschka Pfeifer[15], Maxim Philippov[14], Ana A. Piedehierro[22], Meredith Schervish[11], Wiebke Scholz[18], Benjamin Schulze[12], Jiali Shen[2], Dominik Stolzenburg[2], Yuri Stozhkov[14], Mihnea Surdu[8], Christian Tauber[10], Yee Jun Tham[2], Ping Tian[23], António Tomé[24], Steffen Vogt[7], Mingyi Wang[11], Dongyu S. Wang[8], Stefan K. Weber[15], André Welti[22], Wang Yonghong[2], Wu Yusheng[2], Marcel Zauner-Wieczorek[1], Urs Baltensperger[8], Imad El Haddad[8], Richard C. Flagan[12], Armin Hansel[18,19], Kristina Höhler[7], Jasper Kirkby[1,15], Markku Kulmala[2,9,25], Katrianne Lehtipalo[2,22], Ottmar Möhler[7], Harald Saathoff[7], Rainer Volkamer[3], Paul M. Winkler[10], Neil M. Donahue[11], Andreas Kürten[1], Joachim Curtius[1].

[1]Institute for Atmospheric and Environmental Sciences, Goethe University Frankfurt, 60438 Frankfurt am Main, Germany
[2]Institute for Atmospheric and Earth System Research (INAR) / Physics, Faculty of Science, University of Helsinki, 00014 Helsinki, Finland
[3]Department of Chemistry & CIRES, University of Colorado Boulder, Boulder, CO, 80309-0215, USA
[4]Max Planck Institute for Chemistry, Mainz, 55128, Germany
[5]CENTRA and FCUL, University of Lisbon, 1749-016 Lisbon, Portugal
[6]Leibniz Institute for Tropospheric Research, Leipzig, 04318, Germany
[7]Institute of Meteorology and Climate Research, Karlsruhe Institute of Technology, 76344 Eggenstein-Leopoldshafen, Germany
[8]Laboratory of Atmospheric Chemistry, Paul Scherrer Institute, 5232 Villigen, Switzerland
[9]Helsinki Institute of Physics, University of Helsinki, 00014 Helsinki, Finland
[10]Faculty of Physics, University of Vienna, 1090 Vienna, Austria
[11]Center for Atmospheric Particle Studies, Carnegie Mellon University, Pittsburgh, PA, 15213, USA
[12]Division of Chemistry and Chemical Engineering, California Institute of Technology, Pasadena, CA 91125, USA
[13]California Air Resources Board, Sacramento, CA 95814, USA
[14]Lebedev Physical Institute, Russian Academy of Sciences, 119991, Moscow, Russia
[15]CERN, 1211 Geneva, Switzerland
[16]Dipartimento di Fisica, Università di Genova and INFN, 16146 Genova, Italy
[17]Department of Atmospheric and Oceanic Sciences, University of Colorado Boulder, Boulder, CO 80309, USA
[18]Institute for Ion and Applied Physics, University of Innsbruck, 6020 Innsbruck, Austria
[19]Ionicon Analytik GmbH, 6020 Innsbruck, Austria
[20]Forest Dynamics, Swiss Federal Institute for Forest, Snow and Landscape Research, 8903 Birmensdorf, Switzerland
[21]Department of Chemistry, University of California, Irvine, Irvine, CA 92697, USA
[22]Finnish Meteorological Institute, 00560 Helsinki, Finland
[23]Beijing Weather Modification Office, China
[24]IDL, Universidade da Beira Interior, R. Marquês de Ávila e Bolama, Covilhã, 6201-001, Portugal

[25]Aerosol and Haze Laboratory, Beijing Advanced Innovation Center for Soft Matter Science and Engineering, Beijing University of Chemical Technology, Beijing, 100029, P.R. China
[26]Moscow Institute of Physics and Technology (National Research University), 117303, Moscow, Russia

Correspondence to: Lucía Caudillo (lucia.caudillo@iau.uni-frankfurt.de) and Joachim Curtius (curtius@iau.uni-frankfurt.de)

Abstract. New Particle Formation (NPF) from biogenic organic precursors is an important atmospheric process. One of the major species is α-pinene, which upon oxidation, can form a suite of products covering a wide range of volatilities. A fraction of the oxidation products is termed Highly Oxygenated Organic Molecules (HOM). These play a crucial role for nucleation and the formation of Secondary Organic Aerosol (SOA). However, measuring the composition of newly formed particles is challenging due to their very small mass. Here, we present results on the gas and particle phase chemical composition for a system where α-pinene was oxidized by ozone, and for a mixed system of α-pinene and isoprene, respectively. The measurements took place at the CERN Cosmics Leaving Outdoor Droplets (CLOUD) chamber at temperatures between -50 °C and -30 °C and at low and high relative humidity (20 % and 60 ~~to 100 %~~ RH). These conditions were chosen to simulate pure biogenic new particle formation in the upper free troposphere. The particle chemical composition was analyzed by the Thermal Desorption-Differential Mobility Analyzer (TD-DMA) coupled to a nitrate chemical ionization time-of-flight mass spectrometer. This instrument can be used for particle and gas phase measurements using the same ionization and detection scheme. Our measurements revealed the presence of $C_{8\text{-}10}$ monomers and $C_{18\text{-}20}$ dimers as the major compounds in the particles (diameter up to ~ 100 nm). Particularly, for the system with isoprene added, C_5 ($C_5H_{10}O_{5\text{-}7}$) and C_{15} compounds ($C_{15}H_{24}O_{5\text{-}10}$) are detected. This observation is consistent with the previously observed formation of such compounds in the gas phase. However, although the C_5 and C_{15} compounds do not easily nucleate, our measurements indicate that they can still contribute to the particle growth at free tropospheric conditions. For the experiments reported here, most likely isoprene oxidation products~~might~~ enhance the growth of~~at~~ particles ~~sizes~~ larger than 15 nm. Additionally, ~~Besides the chemical information regarding the HOM formation for the α pinene (plus isoprene) system,~~ we report on the nucleation rates measured at 1.7 nm ($J_{1.7nm}$) and compared with previous studies, we found ~~that~~ lower $J_{1.7nm}$ values, ~~the lower $J_{1.7nm}$ values compared with previous studies are~~ very likely due to the higher α-pinene and ozone mixing ratios used in the present study.

1 Introduction

Approximately half of the global Cloud Condensation Nuclei (CCN) are produced by nucleation (Merikanto et al., 2009; Gordon et al., 2017). In particular, biogenic emissions of Volatile Organic Compounds (VOCs) play an important role in the formation of aerosol particles. The chemical reactions involving VOCs can lead to the formation of Highly Oxygenated Organic Molecules (HOM), which can be described as a class of organic compounds that are formed under atmospherically relevant conditions by gas phase autoxidation involving peroxy radicals (Ehn et al., 2014; Bianchi et al., 2019). These

compounds possess low saturation vapor pressures and are thus relevant for New Particle Formation (NPF) and Secondary Organic Aerosol (SOA) formation due to gas-to-particle conversion.

One of the most prominent biogenic precursors for the formation of particulate material is α-pinene ($C_{10}H_{16}$). It is known that α-pinene oxidation forms HOM that have the ability to nucleate on their own under atmospheric conditions, without the involvement of other trace gases, e. g., sulfuric acid (Kirkby et al., 2016; Tröstl et al., 2016). Stolzenburg et al. (2018) showed that the rapid growth of organic particles produced by α-pinene dark ozonolysis at +25 °C, +5 °C, and -25 °C is determined by the lower extent of autoxidation at reduced temperatures and the decrease in volatility of all oxidized molecules. Furthermore, Simon et al. (2020), extended the study of α-pinene gaseous oxidation products to even lower temperatures from +25 °C to -50 °C, showing that the oxygen to carbon ratio (O:C) and the yield for HOM formation decrease as the temperature decreases, whereas the reduction of volatility compensates this effect by increasing the nucleation rates at lower temperatures.

Isoprene (C_5H_8) is the biogenic vapor with the highest global emission rate. Its estimated emissions are between 500 to 600 Tg per year (Guenther et al., 2006; Sindelarova et al., 2014) and there are many studies that indicate the global importance of isoprene in terms of SOA formation (Surratt et al., 2006; Surratt et al., 2007; Surratt et al., 2010; Paulot et al., 2009; Lin et al., 2012; Riva et al., 2016). Kiendler-Scharr et al. (2009) presented observations at 15 ºC of a significant decrease in particle number and volume concentration by the presence of isoprene in an experiment under plant-emitted VOCs conditions. Subsequently, McFiggans et al. (2019) showed that isoprene, carbon monoxide, and methane can each suppress aerosol mass and the yield from monoterpenes in mixtures of atmospheric vapors.

Recently, a study by Heinritzi et al. (2020) revealed that the presence of isoprene in the α-pinene system suppresses new particle formation by altering the peroxy-radical termination reactions and inhibiting the formation of those molecules needed for the first steps of cluster and particle formation (species with 19 to 20 carbon atoms). For these biogenic systems, α-pinene and α-pinene + isoprene, the mechanisms behind the formation of HOM in the gas phase have been studied over a wide temperature range. However, the particle phase has not been characterized to the same extent because of the difficulties in measuring the nanoparticle chemical composition due to their very small mass. Despite that, there have been several efforts for designing and improving techniques to face this problem.

Some particle phase studies exist that report the chemical composition of newly formed nanoparticles. For instance, Kristensen et al. (2017), measuring at 293 K and 258 K, showed an increased contribution of less oxygenated species to α-pinene SOA particles formed from ozonolysis at sub-zero temperatures. Ye et al. (2019) measured the particle phase chemical composition from α-pinene oxidation between -50 °C and +25 °C with the FIGAERO (Lopez-Hilfiker et al., 2014). They found that during new particle formation from α-pinene oxidation, gas phase chemistry directly determines the composition of the condensed phase. Highly Oxygenated Organic Molecules are much more abundant in particles formed at higher temperatures, shifting the compounds towards higher O:C and lower volatilities. Additionally, some studies addressing the chemical composition, volatility, and viscosity of organic molecules have provided important insights into their influence on the climate (Huang et al., 2018; Reid et al., 2018; Champion et al., 2019).

Here, we present the results from gas and particle phase chemical composition measurements for a system where α-pinene was oxidized to simulate pure biogenic new particle formation at free tropospheric conditions in a range from -50 °C to -30 °C. The data are further compared to the mixed system of α-pinene and isoprene in order to better understand the partitioning processes. The particle chemical composition was analyzed by the Thermal Desorption-Differential Mobility Analyzer (TD-DMA) (Wagner et al., 2018), coupled to a nitrate chemical ionization time-of-flight mass spectrometer. This technique allows a direct comparison between gas and particle phase as both measurements are using the identical chemical ionization source and detector.

2. Methods

2.1 The CLOUD chamber at CERN and the experiments

The measurements took place in the Cosmics Leaving Outdoor Droplets (CLOUD) chamber at the European Organization for Nuclear Research (CERN) during the CLOUD14 campaign (Sep - Nov 2019). The CLOUD chamber is a stainless-steel cylinder, with a volume of 26.1 m^3, which has been built to the highest technical standards of cleanliness (Kirkby et al., 2011; Duplissy et al., 2016). By precisely controlling several parameters such as, gas concentrations, temperature, relative humidity, ultraviolet light intensity and internal mixing, specific atmospheric systems can be recreated in order to study the nucleation and growth processes of aerosols at atmospheric conditions. The biogenic gas concentrations, here α-pinene and isoprene, can be regulated by using individual evaporator supplies, in which dry nitrogen passes through the evaporator containing the precursors in a liquid form, at controlled temperature. In this way, the precursors are evaporated and diluted with clean air to achieve the desired concentration in the chamber. Ozone is introduced via a separate gas line. The chamber is continuously stirred by two magnetically coupled stainless-steel fans placed at the top and at the bottom of the chamber to provide a homogeneously mixed system (Voigtländer et al., 2012). In order to promote particle production from ions, Galactic Cosmic Rays conditions (GCR) can be achieved by turning off the high voltage field (30 kV m^{-1}). The equilibrium ion-pair concentration in the chamber due to GCR is around 700 cm^{-3} (Kirkby et al., 2016).

The experiments relevant for this work were done under GCR conditions and in a flow-through mode with continuous addition of the reactants, ~~and~~ performed at -50 °C and -30 °C, ~~and~~ at low and high relative humidity to simulate pure biogenic new particle formation at a range of free tropospheric conditions. Isoprene and α-pinene precursor gases were oxidized with O_3 and $^{\cdot}OH$ (produced from O_3 photolysis in the presence of H_2O and UV light) to induce both dark ozonolysis and photochemistry oxidation reactions. The α-pinene level was between 1 and 8 ppbv, the isoprene level up to 30 ppbv, and O_3 approximately 100 ppbv. The ozonolysis of α-pinene was performed at -50 °C and -30 °C, while the α-pinene + isoprene experiment was performed at -30 °C only. The experimental overview is discussed in more detail in Sect. 3.1.

2.2 TD-DMA

The particle chemical composition was analyzed by the Thermal Desorption-Differential Mobility Analyzer (TD-DMA) coupled to a nitrate chemical ionization time-of-flight mass spectrometer. The TD-DMA design and characterization have been described in detail by Wagner et al. (2018). This instrument allows the direct comparison between gas and particle phase chemical composition as both measurements use the same ionization scheme and mass spectrometer (the detection technique will be described in Sect. 2.3).

The TD-DMA uses an online and semi-continuous principle for the detection of the chemical composition of nanoparticles. The particles are sampled from the chamber, charged with an X-ray source, a specific size can be selected and immediately afterwards they are electrostatically collected on a filament. Heating the filament after a defined collection time evaporates the particles into a stream of clean carrier gas (N_2). The particle vapor is analyzed by the nitrate CI-APi-TOF mass spectrometer (Kürten et al., 2014). In order to estimate the instrumental background, two heating profiles are recorded: the first heating cycle evaporates all the particulate material collected; a second heating cycle constrains the background due to the heating of the inlet line. All reported particle phase signals are corrected based on this background measurement.

For the experiments that are reported in this work, a filament of platinum/rhodium (90:10) was used, and an integral, non-size —selective mode of operation was chosen in order to maximize the mass of collected particles. For desorbing the sample, an electric current was applied to the filament and ramped linearly over a duration of approximately 1 minute. Due to the very low experimental temperatures, cold sheath flows and isolated inlet lines were installed in order to avoid drastic temperature changes between the CLOUD chamber and the instrument. Evaporation of particulate material before the active heating ~~analysis~~ should therefore not be substantial.

2.3 Nitrate CI-APi-TOF mass spectrometer

The gas phase and the evaporated particulate material were measured using a nitrate chemical ionization atmospheric-pressure-interface time-of-flight (CI-APi-TOF) mass spectrometer, which has three major components: an atmospheric pressure ion-molecule reactor where the chemical ionization takes place; an atmospheric pressure interface for transporting the charged ions into the mass classifier; and a time-of-flight mass classifier where the ions are accelerated, separated according to their mass-to-charge ratio and detected with a microchannel plate (Jokinen et al., 2012; Kürten et al., 2014). The nitrate CI-APi-TOF mass spectrometer uses nitrate reagent ions $(HNO_3)_n\ NO_3^-$ with n = 0-2, which are created by an ion source using a corona discharge needle (Kürten et al., 2011). With this nitrate chemical ionization technique, sulfuric acid, iodic acid, dimethylamine and HOM can be detected (Kürten et al., 2014; Simon et al., 2016; Kirkby et al., 2016; He et al., 2021). HOM are detected because of the presence of functional groups such as hydroperoxy (-OOH) or hydroxy (-OH), which provide the hydrogen bonds required for clustering with the reagent ions.

Here the nitrate CI-APi-TOF mass spectrometer data for gas and particle phase have been corrected for background signals and the mass-dependent transmission efficiency in the mass classifier (Heinritzi et al., 2016). The data analysis and

processing were performed using IGOR Pro 7 (WaveMetrics, Inc., USA), Tofware (Version 3.2, Aerodyne Inc., USA) and MATLAB R2019b (MathWorks, Inc., USA).

2.4 Nucleation ~~Formation~~ rates

The particle number size distribution between ~ 1 nm and 1 μm is measured using a suite of particle counters namely a particle size magnifier, PSM (Vanhanen et al., 2011), a condensational particle counter (CPC 3776, TSI), a nano scanning mobility particle sizer (nano-SMPS 3982, TSI), and a home-built long scanning mobility particle sizer (long-SMPS). The PSM measures the size distribution between ~1 and 3 nm as well as the total particle number concentration above a defined cutoff, 1.7 nm in this study. The CPC on the other hand is used to measure the total particle number concentration above 2.5 nm. The nano-SMPS and long-SMPS together cover the particle number size distribution between 6 nm and 1 μm. The same set-up has been used in previous CLOUD experiments, see for example Lehtipalo et al. (2018) and Heinritzi et al. (2020).

The nucleation ~~particle formation~~ rate (J_{dp}), which is defined as the flux of particles of a certain size ~~as a function of time~~, is calculated using the method proposed by Dada et al. (2020), see equation (9) therein. For this study, the formation of particles with a diameter ≥ 1.7 nm is calculated ($J_{1.7}$) using the derivative of the total concentration of particles measured with the PSM while accounting for size-dependent losses to the chamber wall, by coagulation or via dilution. The error on $J_{1.7}$ is 30% based on run-to-run repeatability (Dada et al., 2020).

3. Results and discussion

3.1 Experimental overview

An overview of the experiments performed at -30 °C and -50 °C at low and high relative humidity is shown in **Fig. 1**. The mixing ratio of ozone was stable at ~ 100 ppbv for all of the experiments reported in this work (not shown). In order to represent pure biogenic new particle formation events, no other trace gases were added to the chamber and the levels of SO_2, NO_x, and other trace gases were monitored to remain always below the detection limits of the respective measurement devices. By using the TD-DMA, particles were collected in every NPF system (without resolving the particle size), the shaded area in **Fig. 1** refers to the period where the particle collection took place.

The upper panel of **Fig. 1** displays the size distribution measured by the Scanning Mobility Particle Sizer (SMPS). Four different experiments can be categorized as follows:

1. α-pinene + isoprene at -30 °C and 20 % RH (*αIP-30,20*);
2. α-pinene at -30 °C and 20 % RH (*α-30,20*);
3. α-pinene at -50 °C and 20 % RH (*α-50,20*); and,
4. α-pinene at -50 °C and 60 ~~to 100~~ % RH (*α-50,60~~-100~~*).

The color scale in the upper panel of **Fig. 1** indicates that the newly-formed particles appear in the smallest size channels of the SMPS soon after the concentration of α-pinene in the chamber is increased. The experiments were performed such that

the particles grew rapidly to reach sizes of approximately 100 nm, where they could potentially act as Cloud Condensation Nuclei (CCN) or Ice Nucleating Particle (INP) and were used for further CCN and INP studies.

The second panel of **Fig. 1** shows the particle number concentration measured by the Condensation Particle Counter ($CPC_{2.5nm}$) and by the Particle Size Magnifier (PSM) with a cut-off diameter of 1.7 nm. A higher particle number concentration can be observed for the experiments *α-50,20* and *α-50,60~~-100~~* at -50 °C, reaching ~ 2 x 10^5 cm^{-3}. By comparing the experiments at -30 °C, *α-30,20* and *αIP-30,20* a lower particle concentration is observed for the system where isoprene is present. The reduction is approximately a factor of 3; this can be attributed to the suppression of the new particle formation by isoprene oxidation. This is in line with ~~confirms~~ the results of Kiendler-Scharr et al. (2009), who first reported the decrease in particle number of the nucleated particles. The effect of isoprene in terms of total HOM concentration in the gas phase and on the measured nucleation ~~new particle formation~~ rates will be discussed in more detail in Sect. 3.4.2.

The third panel of **Fig. 1** shows the α-pinene and isoprene mixing ratios. For all of the systems, α-pinene was between 1 and 8 ppbv, while isoprene was only present during experiment *αIP-30,20* up to 30 ppbv. The precursor gases were measured by using a proton transfer reaction time-of-flight (PTR-TOF) mass spectrometer (Graus et al., 2010; Breitenlechner et al., 2017), which is capable of measuring VOCs.

The bottom panel of **Fig. 1** shows the total HOM concentration in the gas phase. Here, the total HOM is defined as the sum of C_5, C_{10}, C_{15} and C_{20} carbon classes; these classes consider compounds with C_2 - C_5, C_6 - C_{10}, C_{11} - C_{15} and C_{16} - C_{20}, respectively and considered as a HOM such compounds with five or more oxygen atoms as suggested in Bianchi et al. (2019). The total HOM was measured with a calibrated nitrate CI-APi-TOF mass spectrometer (Kürten et al., 2012). Additionally, a temperature dependent sampling loss correction factor is applied. From the evolution of these traces, it can be observed that, C_5 and C_{15} carbon classes have higher concentrations (approximately by a factor of 2.5) in experiment *αIP-30,20* compared with *α-30,20*, which can be explained by the presence of isoprene. However, possible fragmentation in the α-pinene ozonolysis systems also can lead to some C_5 and C_{15} compounds produced without the presence of isoprene.

3.2 Gas and particle phase chemical composition

Figure 2 shows the carbon distribution as an overview of the compounds detected in gas and particle phase for a system where only α-pinene was oxidized (*α-30,20*). $C_{8\text{-}10}$ monomers (**Fig. 2a**) and $C_{18\text{-}20}$ (**Fig. 2b**) dimers are observed in the gas as well as in the particle phase. For instance, some of the signals with the highest intensity correspond to $C_{10}H_{16}O_{3\text{-}9}$, and $C_{20}H_{32}O_{5\text{-}13}$, especially $C_{10}H_{16}O_6$ and $C_{10}H_{16}O_7$ have an important presence in both phases. Overall, most of the compounds that are present in the gas phase are detected as well in the particle phase, although their relative contribution to the total signal can differ between the phases. The corresponding carbon distribution for the other systems can be found in Figures S1 and S2 in the supplement.

3.2.1 Influence of isoprene on α-pinene system at -30 °C and 20 % RH

Figure 3 shows mass defect plots of gas and particle phase and the intensity difference between each phase~~them for the experiments~~ at -30 °C. **Figure 3a** and **Fig. 3d** display the gas and particle composition ~~of α-pinene at -30 °C and 20 % RH~~of ~~(~~*α-30,20*~~).~~ ~~w~~While the gas and particle composition of ~~of α-pinene + isoprene at -30 °C and 20 % RH (~~*αIP-30,20*~~)~~ are shown in **Fig. 3b** and **Fig. 3e**, respectively. As both phases were measured with the same instrument, they can be directly inter-compared.

The intensity difference is calculated based on the normalized signal (each single signal divided by the total signal for each system and phase). Essentially, the normalized signal can be understood as a measure of the fraction or contribution of every compound in the entire system. By looking at the intensity difference in the gas phase (**Fig. 3c**), it can be observed that some C_5 and C_{15} contribute significantly more in the system with isoprene added (*αIP-30,20*) that are not as pronounced in the system where only α-pinene was oxidized (*α-30,20*). This observation can be attributed to the presence of isoprene in the system. As described by Heinritzi et al. (2020), C_{15} dimers are formed in the gas phase when C_{10} RO_2· radicals from α-pinene ozonolysis undergo terminating reactions with C_5 RO_2· radicals from the isoprene oxidation with ·OH. Additionally, C_{19} and C_{20} dimers contribute more in the system where only α-pinene was oxidized (*α-30,20*).

Fig. 3f shows the intensity difference in the particle phase. In contrast with what is observed in the gas phase, the particle phase effects seem more diverse. There is an increase in the intensity difference for several species in the system with isoprene (*αIP-30,20*), such as $C_{4\text{-}5}$, $C_{13\text{-}16}$ and some $C_{17\text{-}19}$ (see **Fig. S1** in the supplement). Especially, a distinct group of C_{15} compounds $C_{15}H_{24}O_{5\text{-}10}$ and $C_5H_{10}O_{5\text{-}7}$ can be identified in the particle and in the gas phase. ~~This indicates that there is an enhancement of $C_{4\text{-}5}$ and $C_{13\text{-}16}$ compounds in the system with isoprene (*αIP-30,20*). There is especially a group of C_{15} compounds $C_{15}H_{24}O_{5\text{-}10}$ (see **Fig. S1** in the supplement) with significant signal in the particle phase.~~ A previous study has shown that isoprene can enhance particle growth rates despite its negative effect on nucleation ~~Since the particles collected reached sizes up to ~ 100 nm, and it has been shown in previous studies~~ (Heinritzi et al., 2020). The identification of ~~that~~ C_{15} dimers in nanometer-sized particles in the present study confirms this with a direct measurement. The suppressing effect of isoprene on nucleation will further be discussed ~~do contribute to the growth, this observation confirms the existence of these species in the condensed material. Certainly, isoprene can suppress new particle formation (it will be discussed~~ in Section 3.4.2~~)~~. However, isoprene can still contribute to the growth of particles by C_5 or by C_{15} compounds. Additionally, these species ~~Thus, these species~~ can be an important fingerprint to identify SOA formation from a mixture of biogenic vapors containing isoprene.

For the experiments presented in this study, we report in **Table 1** the particle growth rates (GR) determined from the nSEMS size distributions. The growth rates in 3.2-8 nm and 5-15 nm were calculated using the 50% appearance time method described in Stolzenburg et al. (2018). From the calculated values in **Table 1**, we observe that $GR_{3.2\text{-}8\ nm}$ for the α-pinene + isoprene system (*αIP-30,20*) at the first concentration stage is around 18 nm h^{-1} compared to ~ 77 nm h^{-1} for the α-pinene only system (*α-30,20*). This is a factor of ~ 4 difference~~.~~ ~~w~~While $GR_{5\text{-}15\ nm}$ represents a factor of 2 to 3 difference

between *αIP-30,20* compared to *α-30,20*. From these values, one would conclude that isoprene does not contribute to the growth in the size range reported here. Nevertheless, by looking at the aerosol mass concentration (see **Fig. S3** in the supplement), the mass reached during the experiment *αIP-30,20* is identical in the presence and absence of isoprene at -30 ºC and 20 % RH. Reaching the same mass with a lower number of particles for the experiment with isoprene (*αIP-30,20*) compared to *α-30,20*, means that the growth rates at larger sizes (> 15 nm) are higher in the presence of isoprene. This is consistent with the fact that the particle size reached in the presence of isoprene is higher. Most likely, isoprene might enhance growth at larger ~~higher~~ sizes (> 15 nm) in the present~~this~~ study.

3.2.2 Influence of relative humidity on α-pinene system at -50 °C

Figure 4 shows mass defect plots for the pure α-pinene experiments at -50 °C at low and high relative humidity: the gas and particle phase of α-pinene at -50 °C, 20 % RH (**Fig. 4a** and **Fig. 4d**); and the gas and particle phase of α-pinene at -50 °C, 60 ~~to 100~~ % RH (**Fig. 4b** and **4e**). In both gas and particle phase at high and low RH, we detected $C_{8\text{-}10}$ monomers and $C_{18\text{-}20}$ dimers. $C_{10}H_{16}O_{4\text{-}7}$ and $C_{20}H_{32}O_{5\text{-}11}$ are the most prominent signals (see **Fig. S2** in the supplement).

The relative humidity change from 20 % to 60 ~~100~~ % does not have a significant influence on the gas phase composition at temperatures of -50 °C (**Fig. 4c**), meaning that most of the gaseous compounds detected contribute practically equal to the total signal when the humidity changes over the reported range. In contrast, there are changes in the particle phase signal. Although, the intensity difference (**Fig. 4f**) does not show a clear humidity effect on the particle chemical composition; however, this comparison is based on the normalized signal (contribution of every compound to the total intensity). When looking only at the total intensity in the particle phase, we do observe an increase by a factor of ~ 3 in the total signal for the system at high RH (*α-50,60~~-100~~*) compared with the system at low RH (*α-50,20*). This observation can ~~be~~ likely be attributed to a~~the~~ change ~~o~~in the particle mass size distribution (see **Fig. S3** in the supplement), which indicates that at similar α-pinene and ozone mixing ratio, and the same temperature, the particle mass concentration increases possibly due to the effect of the relative humidity in the system. Besides, a possible impact of relative humidity on particle viscosity can influence particle mass formed, studies by Grayson et al. (2016) and Galeazzo et al. (2021) have reported lower viscosity with higher SOA mass concentration along with RH-dependence of viscosity for organic particles.

Our findings are consistent with previous experiments. Saathoff et al. (2009) observed that humidity has a significant influence on α-pinene SOA yields for lower temperatures. Cocker III et al. (2001) reported that the yield of SOA at higher RH for α-pinene ozonolysis (relative to the system at dry conditions) increases possibly due to the uptake of water. One explanation for this observation could be that the rate constant value of the α-pinene ozonolysis can be affected by the RH (Zhang et al., 2018). Nevertheless, our semi-continuous particle phase measurements do not allow to draw any conclusions on the magnitude of the rate constants. Continuous particle phase measurements under different RH conditions are required in order to better understand the RH effect on the SOA formation.

In general, for the experiments presented in this work, most of the compounds that are present in the gas phase are detected as well in the particle phase, although the relative contributions to the total signal can vary depending on the phase.

The more oxygenated material in the gas phase, specifically for C_{20} dimers with $n_O > 13$ is not observed in the particle phase. This is probably because of their very low concentrations and the difficulty to distinguish between real particle signal and background. We conjecture that especially at low temperatures this issue might be related to the fact that at lower temperatures, the auto~~o~~xidation process to form HOM is slower, therefore, the oxygen content and O:C decrease (Stolzenburg et al., 2018; Ye et al., 2019; Simon et al., 2020). The low contribution of these compounds in the gas phase might be reflected in the particle phase. Additionally, the heating cycle that evaporates all the particulate material collected on the filament can potentially result in the thermal decomposition of some of the larger molecular weight compounds. Therefore, it is possible that a break-up of some molecules occurs.

3.3 Volatility distribution of particle phase compounds

Figure 5 shows the volatility distribution of the oxidation products in the particle phase measured by the TD-DMA for the experiments reported in this work (in linear scale **Fig. S4** in the supplement). The volatility calculation was done by using the parametrization introduced by Donahue et al. (2011), and modified by Stolzenburg et al. (2018) and Simon et al. (2020). It is expressed as the logarithm of the saturation mass concentration, $\log_{10} c_i^*$ in µg m^{-3}, from the number of carbon and oxygen atoms in the specific molecules. This approximation parameterizes the volatility of a molecule based on its functional groups and, a free parameter to distinguish between monomers and dimers.

In **Fig. 5** each volatility bin contains the summed intensity of the oxidation products measured in the particle phase and it is normalized by the total signal. Most of the classes are distributed over the range of the volatility values that are displayed and at lower temperatures, lower volatilities are observed (experiments *α-50,20* and *α-50,60~~-100~~*). This observation is due to the fact of the strong dependency between saturation concentration and temperature. Essentially, there are no significant differences between the experiments at -30 °C (*α-30,20* compared with *αIP-30,20*) or between the experiments at -50 °C (*α-50,20* compared with *α-50,60~~-100~~*), which indicates that temperature is the main parameter affecting the volatility distribution for the experiments reported here.

We classified the volatility bins a~~A~~ccording to the ~~volatility~~ regimes proposed by Donahue et al. (2012) and Schervish and Donahue (2020), and calculated the corresponding fractions (Table 2). Overall, the particle phase detected compounds correspond mainly to Low Volatility Organic Compounds (LVOC) and Extremely Low Volatility Compounds (ELVOC) by explaining more than 80 % of the signals, while ~~and~~ Ultralow Volatility Organic Compounds (ULVOC) represent only a small fraction (between 6 and 17 %). With this parametrization we are able to approximate the saturation mass concentration for the particle phase compounds measured using the TD-DMA in the CLOUD chamber. For this parametrization we assume that the elemental composition is one of the main parameters to take into account.

3.4 Nucleation rates as a function of the total HOM

Previous CLOUD studies have reported nucleation rates ($J_{1.7nm}$) as a function of the total HOM concentration from α-pinene oxidation for different temperatures and gas mixtures (Kirkby et al., 2016; Heinritzi et al., 2020; Simon et al., 2020). For the

experiments discussed in the present study the nucleation ~~new particle formation~~ rates have not been reported yet. For this reason, **Table 1** gives an overview of the experimental conditions for the experiments *α-30,20*, *αIP-30,20*, *α-50,20* and *α-50,60* ~~*100*~~; it further includes the HOM total concentration and derived $J_{1.7nm}$ from the PSM data (see method description in Section 2.4).

3.4.1 New Particle formation on pure α-pinene experiments

Figure 6 displays pure biogenic $J_{1.7nm}$ vs total HOM concentration at different temperatures for pure α-pinene (Simon et al., 2020), in which can be seen that the total HOM concentration and their nucleation rates have a strong dependence on the temperature. As the temperature decreases, the nucleation rates increase strongly for a given HOM concentration. In other terms, the total HOM concentration needed to reach the same nucleation rate can be up to 2 orders of magnitude higher for +25 °C compared to -50 °C. As described by Simon et al. (2020) this can be attributed to the reduction in volatility with decreasing temperature. In other words, at low temperatures, molecules with less oxygen content can lead to the same nucleation rate as more highly oxygenated molecules at higher temperatures. Additionally, **Fig. 6** includes the data points at -30 °C and -50 °C from pure α-pinene experiments reported in this study (*α-30,20*, *α-50,20* and *α-50,60* ~~*100*~~). However, it can be observed that they do not follow the trend at their corresponding temperature.

For the pure α-pinene systems (*α-30,20*, *α-50,20* and *α-50,60* ~~*100*~~) and complementary pure α-pinene experiments at +5 °C and at -10 °C, we have calculated the HOM yield as described in Simon et al. (2020) and found that the resulting values are higher than previously reported (see **Fig. S5** in the supplement). In order to investigate a possible reason for this finding, we have chosen two representative experiments at -10 °C and 80 to 90 % RH with different levels of α-pinene and ozone. **Fig. 7** shows the mass defect plots for the gas phase chemical composition of the oxidation products. In one experiment (**Fig. 7a**) α-pinene and the ozone mixing ratio were between 0.2 to 0.8 ppbv and 40 to 50 ppbv, respectively, while for the second experiment (**Fig. 7b**) the mixing ratios were 2 to 3 ppbv and 100 ppbv, respectively. From **Fig. 7c** it can be concluded that the formation of HOM with low oxygen content is favored when the α-pinene and ozone mixing ratio are higher (relative to the system at low levels of precursor gases). An explanation for this is that the high concentration of RO_2 enhances the terminating reactions before the autoxidation can lead to high oxygen content for the products. As the compounds with low oxygen content tend to have higher saturation vapor pressures, they do not contribute efficiently to new particle formation. For this reason, a given total HOM concentration is not unambiguously tied to a nucleation ~~new particle formation~~ rate (even at constant temperature). The magnitude of the precursor gas mixing ratio (more specifically the full volatility distribution of the products and not just the simple measure of total HOM) also needs to be taken into account (see **Fig.S6** in the supplement). In summary, the lower $J_{1.7nm}$ values compared with previous studies are very likely due to the higher α-pinene and ozone mixing ratios used in the present study. There are several compounds with low oxygen content that contribute to the total HOM concentration in the gas phase while these do not contribute to the formation of new particles.

3.4.2 The influence of isoprene on new particle formation

In order to make the present study comparable with other studies that reported a suppression effect of isoprene on biogenic new particle formation, the values of the isoprene-to-monoterpene carbon ratio (*R*) are also provided in Table 1, here and in previous studies *R* is essentially the ratio between isoprene and α-pinene; for experiment *αIP-30,20*, R equals to 14.4 and 6.1 (for two steady-state periods in *αIP-30,20*).

Fig. 8 shows pure biogenic nucleation rates at 1.7 nm against total HOM concentration at different temperatures for the α-pinene and α-pinene + isoprene systems (Kirkby et al., 2016; Heinritzi et al., 2020; Simon et al., 2020). How rapidly particles are formed in a pure biogenic system depends strongly on the temperature and on the ion conditions. In general, we observe increasing nucleation rates at lower temperatures and at GCR conditions. The presence of isoprene lowers the nucleation rate (relative to the pure α-pinene system at similar conditions); this is known as isoprene suppression of new particle formation. In this regard, there is a suppression on the new particle formation caused by adding isoprene on an α-pinene system at -30 ºC and 20 % RH. However, it has been reported that the suppression effect is stronger when α-pinene is lower (and *R* is higher, see **Fig. S7** in the supplement). For instance, in ~~for~~ a plant chamber experiment ~~that~~ R = 19.5 resulted in no significant new particle formation (Kiendler-Scharr et al., 2009). Additionally, in the Michigan forest with R = 26.4, NPF events did not occur frequently (Kanawade et al., 2011). Lee et al. (2016) reported observations of NPF suppression in a rural forest in Alabama where R = 2.0.- However~~In spite of that~~, one has to consider that the suppression effect at a given value of *R* likely decreases as temperature decreases and so does the saturation vapor pressure of the oxidation products.

4 Conclusions

In this study, we showed the capability of the Thermal Desorption-Differential Mobility Analyzer (TD-DMA) coupled to a chemical ionization time-of-flight mass spectrometer for measuring HOMs in newly formed nano aerosol particles. Together with the nitrate CI-APi-TOF mass spectrometer, this set up is capable of measuring gas and particle phase, allowing a direct comparison as both measurements use the identical chemical ionization and detector.

For the pure biogenic NPF experiments performed at -50 °C and -30 °C in the CLOUD chamber at CERN, we detected in the particle phase (diameter up to ~ 100 nm) compounds such as $C_{10}H_{16}O_{3\text{-}9}$, and $C_{20}H_{32}O_{5\text{-}13}$. Especially for the system with isoprene added, C_5 ($C_5H_{10}O_{5\text{-}7}$) and C_{15} compounds ($C_{15}H_{24}O_{5\text{-}10}$) can be an important fingerprint to identify secondary organic aerosol from this biogenic source. Based on the elemental composition, we calculated the saturation mass concentration, and according to the volatility regimes, the particle phase compounds correspond mainly to Low Volatility Organic Compounds (LVOC) and Extremely Low Volatility Compounds (ELVOC) and Ultralow Volatility Organic Compounds (ULVOC).

We also showed that at -30 °C and an isoprene-to-monoterpene carbon ratio R = 14.4 and 6.1, there is a reduction of the nucleation rate (compared to the pure α-pinene system at similar conditions). In this way, isoprene suppresses NPF at -30 °C. Nevertheless, this suppression effect can be stronger at higher temperatures and at high *R*.

Lastly, the lower $J_{1.7}$ values compared with previous studies are very likely due to the higher α-pinene and ozone mixing ratios used in the present study. There are several compounds with low oxygen content that contribute to the total HOM concentration in the gas phase while these do not contribute to the formation of new particles. For this reason, a given total HOM concentration is not unambiguously tied to a nucleation ~~new particle formation~~ rate (even at constant temperature). The magnitude of the precursor gas mixing ratio, and thus the full volatility distribution, also needs to be taken into account.

Data availability. Data related to this article are available upon request to the corresponding authors.

Supplement. The supplement related to this article is available online at:

Author contributions. L. C., B. R., G. M., M. Sim., A. C. W., T. M., M. G., F. A., R. B., B. B., Z. B., R. C., B. C., J. Du., H. F., L. G. C., X.-C. H., V. H., W. K., H. L., C. P. L., B. L., N. G. A. M., V. M., H. E. M., R. M., R. L. M., B. M., U. M., A. O., J. P., M. P., A. A. P., W. S., B. S., J. S., D. S., Y. S., M. S., Y. J. T., P. T., A. T., S.V., M. W., D. S. W., S. K. W., A. W., W. Y., W. Y., M. Z.-W., U. B., I. E.-H., R. C. F., K. H., J. Kir., M. K., K. L., O. M., R. V., P. M. W., A. K., and J. Cu. prepared the CLOUD facility and measurement instruments. L. C., B. R., G. M., A. C. W., T. M., M. G., A. A., F. A., R. B., B. B., J. Du., L. G. C., V. H., H. L., C. P. L., N. G. A. M., V. M., R. M., D. M., R. L. M., B. M., U. M., W. S., B. S., D. S., M. S., C. T., Y. J. T., A. T., D. S. W., S. K. W., M. Z.-W., I. E.-H., J. Kir., R. V., and P. M. W. collected the data. L. C., B. R., M. H., G. M., F. A., L. D., R. L. M., U. M., W. S., B. S., S. K. W., and R. C. F. analyzed the data. L. C., M. H., M. Sim., A. C. W., T. M., M. G., L. D., R. L. M., U. M., M. S., W. S., D. S., U. B., I. E.-H., R. C. F., A. H., K. H., J. Kir., M. K., O. M., H. S., N. M. D., A. K., and J. Cu. contributed to the scientific discussion and interpretation of the results. L. C., M. H., A. C. W., L. D., U. B., R. C. F., H. S., N. M. D., A. K., and J. Cu. contributed to writing the manuscript.

Competing interests. The authors declare that they have no conflict of interest.

Acknowledgments. We thank CERN for providing the CLOUD facility to perform the experiments and the CLOUD community for supporting this study. We especially would like to thank Katja Ivanova, Timo Keber, Frank Malkemper, Robert Sitals, Hanna Elina Manninen, Antti Onnela, and Robert Kristic for their contributions to the experiment.

Financial support. This work has received funding from the European Union's Horizon 2020 research and innovation programme under the Marie Skłodowska-Curie grant agreement No 764991.~~This work was supported by Innovative Training Networks – ITN (CLOUD-Motion H2020-MSCA-ITN-2017 no. 764991)~~ and by the German Ministry of Science and Education (CLOUD-16, 01LK1601A). US National Science Foundation Award (AGS-1801280, AGS-1801574, AGS-1801897). Swiss National Science Foundation (20020_172602, BSSGI0_155846).

References

Bianchi, F., Kurtén, T., Riva, M., Mohr, C., Rissanen, M. P., Roldin, P., Berndt, T., Crounse, J. D., Wennberg, P. O., and Mentel, T. F.: Highly oxygenated organic molecules (HOM) from gas-phase autoxidation involving peroxy radicals: A key contributor to atmospheric aerosol, Chemical reviews, 119, 3472-3509, 2019.

Breitenlechner, M., Fischer, L., Hainer, M., Heinritzi, M., Curtius, J., and Hansel, A.: PTR3: An Instrument for Studying the Lifecycle of Reactive Organic Carbon in the Atmosphere, Analytical Chemistry, 89, 5824-5831, 10.1021/acs.analchem.6b05110, 2017.

Champion, W. M., Rothfuss, N. E., Petters, M. D., and Grieshop, A. P.: Volatility and Viscosity Are Correlated in Terpene Secondary Organic Aerosol Formed in a Flow Reactor, Environmental Science & Technology Letters, 6, 513-519, 10.1021/acs.estlett.9b00412, 2019.

Cocker III, D. R., Clegg, S. L., Flagan, R. C., and Seinfeld, J. H.: The effect of water on gas–particle partitioning of secondary organic aerosol. Part I: α-pinene/ozone system, Atmospheric Environment, 35, 6049-6072, 10.1016/j.jes.2017.10.011, 2001.

Dada, L., Lehtipalo, K., Kontkanen, J., Nieminen, T., Baalbaki, R., Ahonen, L., Duplissy, J., Yan, C., Chu, B., Petäjä, T., Lehtinen, K., Kerminen, V.-M., Kulmala, M., and Kangasluoma, J.: Formation and growth of sub-3-nm aerosol particles in experimental chambers, Nature Protocols, 15, 1013-1040, 10.1038/s41596-019-0274-z, 2020.

Donahue, N. M., Epstein, S., Pandis, S. N., and Robinson, A. L.: A two-dimensional volatility basis set: 1. organic-aerosol mixing thermodynamics, Atmospheric Chemistry and Physics, 11, 3303-3318, 2011.

Donahue, N. M., Kroll, J., Pandis, S. N., and Robinson, A. L.: A two-dimensional volatility basis set–Part 2: Diagnostics of organic-aerosol evolution, Atmospheric Chemistry and Physics, 12, 615-634, 2012.

Duplissy, J., Merikanto, J., Franchin, A., Tsagkogeorgas, G., Kangasluoma, J., Wimmer, D., Vuollekoski, H., Schobesberger, S., Lehtipalo, K., Flagan, R. C., Brus, D., Donahue, N. M., Vehkamäki, H., Almeida, J., Amorim, A., Barmet, P., Bianchi, F., Breitenlechner, M., Dunne, E. M., Guida, R., Henschel, H., Junninen, H., Kirkby, J., Kürten, A., Kupc, A., Määttänen, A., Makhmutov, V., Mathot, S., Nieminen, T., Onnela, A., Praplan, A. P., Riccobono, F., Rondo, L., Steiner, G., Tome, A., Walther, H., Baltensperger, U., Carslaw, K. S., Dommen, J., Hansel, A., Petäjä, T., Sipilä, M., Stratmann, F., Vrtala, A., Wagner, P. E., Worsnop, D. R., Curtius, J., and Kulmala, M.: Effect of ions on sulfuric acid-water binary particle formation: 2. Experimental data and comparison with QC-normalized classical nucleation theory, Journal of Geophysical Research: Atmospheres, 121, 1752-1775, 10.1002/2015JD023539, 2016.

Ehn, M., Thornton, J. A., Kleist, E., Sipila, M., Junninen, H., Pullinen, I., Springer, M., Rubach, F., Tillmann, R., Lee, B., Lopez-Hilfiker, F., Andres, S., Acir, I.-H., Rissanen, M., Jokinen, T., Schobesberger, S., Kangasluoma, J., Kontkanen, J., Nieminen, T., Kurten, T., Nielsen, L. B., Jorgensen, S., Kjaergaard, H. G., Canagaratna, M., Maso, M. D., Berndt, T., Petaja, T., Wahner, A., Kerminen, V.-M., Kulmala, M., Worsnop, D. R., Wildt, J., and Mentel, T. F.: A large source of low-volatility secondary organic aerosol, Nature, 506, 476-479, 10.1038/nature13032, 2014.

Galeazzo, T., Valorso, R., Li, Y., Camredon, M., Aumont, B., and Shiraiwa, M.: Estimation of Secondary Organic Aerosol Viscosity from Explicit Modeling of Gas-Phase Oxidation of Isoprene and α-pinene, Atmos. Chem. Phys. Discuss., 2021, 1-23, 10.5194/acp-2021-17, 2021.

Gordon, H., Kirkby, J., Baltensperger, U., Bianchi, F., Breitenlechner, M., Curtius, J., Dias, A., Dommen, J., Donahue, N. M., Dunne, E. M., Duplissy, J., Ehrhart, S., Flagan, R. C., Frege, C., Fuchs, C., Hansel, A., Hoyle, C. R., Kulmala, M., Kürten, A., Lehtipalo, K., Makhmutov, V., Molteni, U., Rissanen, M. P., Stozkhov, Y., Tröstl, J., Tsagkogeorgas, G., Wagner, R., Williamson, C., Wimmer, D., Winkler, P. M., Yan, C., and Carslaw, K. S.: Causes and importance of new particle formation in the present-day and preindustrial atmospheres, Journal of Geophysical Research: Atmospheres, 122, 8739-8760, 10.1002/2017jd026844, 2017.

Graus, M., Müller, M., and Hansel, A.: High resolution PTR-TOF: Quantification and formula confirmation of VOC in real time, Journal of the American Society for Mass Spectrometry, 21, 1037-1044, 10.1016/j.jasms.2010.02.006, 2010.

Grayson, J. W., Zhang, Y., Mutzel, A., Renbaum-Wolff, L., Böge, O., Kamal, S., Herrmann, H., Martin, S. T., and Bertram, A. K.: Effect of varying experimental conditions on the viscosity of α-pinene derived secondary organic material, Atmos. Chem. Phys., 16, 6027-6040, 10.5194/acp-16-6027-2016, 2016.

Guenther, A., Karl, T., Harley, P., Wiedinmyer, C., Palmer, P. I., and Geron, C.: Estimates of global terrestrial isoprene emissions using MEGAN (Model of Emissions of Gases and Aerosols from Nature), Atmos. Chem. Phys., 6, 3181-3210, 10.5194/acp-6-3181-2006, 2006.

He, X.-C., Tham, Y. J., Dada, L., Wang, M., Finkenzeller, H., Stolzenburg, D., Iyer, S., Simon, M., Kürten, A., Shen, J., Rörup, B., Rissanen, M., Schobesberger, S., Baalbaki, R., Wang, D. S., Koenig, T. K., Jokinen, T., Sarnela, N., Beck, L. J., Almeida, J., Amanatidis, S., Amorim, A., Ataei, F., Baccarini, A., Bertozzi, B., Bianchi, F., Brilke, S., Caudillo, L., Chen, D., Chiu, R., Chu, B., Dias, A., Ding, A., Dommen, J., Duplissy, J., El Haddad, I., Gonzalez Carracedo, L., Granzin, M., Hansel, A., Heinritzi, M., Hofbauer, V., Junninen, H., Kangasluoma, J., Kemppainen, D., Kim, C., Kong, W., Krechmer, J. E., Kvashin, A., Laitinen, T., Lamkaddam, H., Lee, C. P., Lehtipalo, K., Leiminger, M., Li, Z., Makhmutov, V., Manninen, H. E., Marie, G., Marten, R., Mathot, S., Mauldin, R. L., Mentler, B., Möhler, O., Müller, T., Nie, W., Onnela, A., Petäjä, T., Pfeifer, J., Philippov, M., Ranjithkumar, A., Saiz-Lopez, A., Salma, I., Scholz, W., Schuchmann, S., Schulze, B., Steiner, G., Stozhkov, Y., Tauber, C., Tomé, A., Thakur, R. C., Väisänen, O., Vazquez-Pufleau, M., Wagner, A. C., Wang, Y., Weber, S. K., Winkler, P. M., Wu, Y., Xiao, M., Yan, C., Ye, Q., Ylisirniö, A., Zauner-Wieczorek, M., Zha, Q., Zhou, P., Flagan, R. C., Curtius, J., Baltensperger, U., Kulmala, M., Kerminen, V.-M., Kurtén, T., Donahue, N. M., Volkamer, R., Kirkby, J., Worsnop, D. R., and Sipilä, M.: Role of iodine oxoacids in atmospheric aerosol nucleation, Science, 371, 589-595, 10.1126/science.abe0298, 2021.

Heinritzi, M., Simon, M., Steiner, G., Wagner, A. C., Kürten, A., Hansel, A., and Curtius, J.: Characterization of the mass-dependent transmission efficiency of a CIMS, Atmos. Meas. Tech., 9, 1449-1460, 10.5194/amt-9-1449-2016, 2016.

Heinritzi, M., Dada, L., Simon, M., Stolzenburg, D., Wagner, A. C., Fischer, L., Ahonen, L. R., Amanatidis, S., Baalbaki, R., Baccarini, A., Bauer, P. S., Baumgartner, B., Bianchi, F., Brilke, S., Chen, D., Chiu, R., Dias, A., Dommen, J., Duplissy, J., Finkenzeller, H., Frege, C., Fuchs, C., Garmash, O., Gordon, H., Granzin, M., El Haddad, I., He, X., Helm, J., Hofbauer, V., Hoyle, C. R., Kangasluoma, J., Keber, T., Kim, C., Kürten, A., Lamkaddam, H., Laurila, T. M., Lampilahti, J., Lee, C. P., Lehtipalo, K., Leiminger, M., Mai, H., Makhmutov, V., Manninen, H. E., Marten, R., Mathot, S., Mauldin, R. L., Mentler, B., Molteni, U., Müller, T., Nie, W., Nieminen, T., Onnela, A., Partoll, E., Passananti, M., Petäjä, T., Pfeifer, J., Pospisilova, V., Quéléver, L. L. J., Rissanen, M. P., Rose, C., Schobesberger, S., Scholz, W., Scholze, K., Sipilä, M., Steiner, G., Stozhkov, Y., Tauber, C., Tham, Y. J., Vazquez-Pufleau, M., Virtanen, A., Vogel, A. L., Volkamer, R., Wagner, R., Wang, M., Weitz, L., Wimmer, D., Xiao, M., Yan, C., Ye, P., Zha, Q., Zhou, X., Amorim, A., Baltensperger, U., Hansel, A., Kulmala, M., Tomé, A., Winkler, P. M., Worsnop, D. R., Donahue, N. M., Kirkby, J., and Curtius, J.: Molecular understanding of the suppression of new-particle formation by isoprene, Atmos. Chem. Phys., 20, 11809-11821, 10.5194/acp-20-11809-2020, 2020.

Huang, W., Saathoff, H., Pajunoja, A., Shen, X., Naumann, K. H., Wagner, R., Virtanen, A., Leisner, T., and Mohr, C.: α-Pinene secondary organic aerosol at low temperature: chemical composition and implications for particle viscosity, Atmos. Chem. Phys., 18, 2883-2898, 10.5194/acp-18-2883-2018, 2018.

Jokinen, T., Sipilä, M., Junninen, H., Ehn, M., Lönn, G., Hakala, J., Petäjä, T., Mauldin Iii, R. L., Kulmala, M., and Worsnop, D. R.: Atmospheric sulphuric acid and neutral cluster measurements using CI-APi-TOF, Atmos. Chem. Phys., 12, 4117-4125, 10.5194/acp-12-4117-2012, 2012.

Kanawade, V. P., Jobson, B. T., Guenther, A. B., Erupe, M. E., Pressley, S. N., Tripathi, S. N., and Lee, S. H.: Isoprene suppression of new particle formation in a mixed deciduous forest, Atmos. Chem. Phys., 11, 6013-6027, 10.5194/acp-11-6013-2011, 2011.

Kiendler-Scharr, A., Wildt, J., Maso, M. D., Hohaus, T., Kleist, E., Mentel, T. F., Tillmann, R., Uerlings, R., Schurr, U., and Wahner, A.: New particle formation in forests inhibited by isoprene emissions, Nature, 461, 381-384, 2009.

Kirkby, J., Curtius, J., Almeida, J., Dunne, E., Duplissy, J., Ehrhart, S., Franchin, A., Gagné, S., Ickes, L., Kürten, A., Kupc, A., Metzger, A., Riccobono, F., Rondo, L., Schobesberger, S., Tsagkogeorgas, G., Wimmer, D., Amorim, A., Bianchi, F., Breitenlechner, M., David, A., Dommen, J., Downard, A., Ehn, M., Flagan, R. C., Haider, S., Hansel, A., Hauser, D., Jud, W., Junninen, H., Kreissl, F., Kvashin, A., Laaksonen, A., Lehtipalo, K., Lima, J., Lovejoy, E. R., Makhmutov, V., Mathot, S., Mikkilä, J., Minginette, P., Mogo, S., Nieminen, T., Onnela, A., Pereira, P., Petäjä, T., Schnitzhofer, R., Seinfeld, J. H., Sipilä, M., Stozhkov, Y., Stratmann, F., Tomé, A., Vanhanen, J., Viisanen, Y., Vrtala, A., Wagner, P. E., Walther, H., Weingartner, E., Wex, H., Winkler, P. M., Carslaw, K. S., Worsnop, D. R., Baltensperger, U., and Kulmala, M.: Role of sulphuric acid, ammonia and galactic cosmic rays in atmospheric aerosol nucleation, Nature, 476, 429-433, 10.1038/nature10343, 2011.

Kirkby, J., Duplissy, J., Sengupta, K., Frege, C., Gordon, H., Williamson, C., Heinritzi, M., Simon, M., Yan, C., Almeida, J., Tröstl, J., Nieminen, T., Ortega, I. K., Wagner, R., Adamov, A., Amorim, A., Bernhammer, A.-K., Bianchi, F., Breitenlechner, M., Brilke, S., Chen, X., Craven, J., Dias, A., Ehrhart, S., Flagan, R. C., Franchin, A., Fuchs, C., Guida, R., Hakala, J., Hoyle, C. R., Jokinen, T., Junninen, H., Kangasluoma, J., Kim, J., Krapf, M., Kürten, A., Laaksonen, A., Lehtipalo, K., Makhmutov, V., Mathot, S., Molteni, U., Onnela, A., Peräkylä, O., Piel, F., Petäjä, T., Praplan, A. P., Pringle, K., Rap, A., Richards, N. A. D., Riipinen, I., Rissanen, M. P., Rondo, L., Sarnela, N., Schobesberger, S., Scott, C. E., Seinfeld, J. H., Sipilä, M., Steiner, G., Stozhkov, Y., Stratmann, F., Tomé, A., Virtanen, A., Vogel, A. L., Wagner, A. C., Wagner, P. E., Weingartner, E., Wimmer, D., Winkler, P. M., Ye, P., Zhang, X., Hansel, A., Dommen, J., Donahue, N. M., Worsnop, D. R., Baltensperger, U., Kulmala, M., Carslaw, K. S., and Curtius, J.: Ion-induced nucleation of pure biogenic particles, Nature, 533, 521-526, 10.1038/nature17953, 2016.

Kristensen, K., Jensen, L., Glasius, M., and Bilde, M.: The effect of sub-zero temperature on the formation and composition of secondary organic aerosol from ozonolysis of alpha-pinene, Environmental Science: Processes & Impacts, 19, 1220-1234, 2017.

Kürten, A., Rondo, L., Ehrhart, S., and Curtius, J.: Performance of a corona ion source for measurement of sulfuric acid by chemical ionization mass spectrometry, Atmos. Meas. Tech., 4, 437-443, 10.5194/amt-4-437-2011, 2011.

Kürten, A., Rondo, L., Ehrhart, S., and Curtius, J.: Calibration of a Chemical Ionization Mass Spectrometer for the Measurement of Gaseous Sulfuric Acid, The Journal of Physical Chemistry A, 116, 6375-6386, 10.1021/jp212123n, 2012.

Kürten, A., Jokinen, T., Simon, M., Sipilä, M., Sarnela, N., Junninen, H., Adamov, A., Almeida, J., Amorim, A., Bianchi, F., Breitenlechner, M., Dommen, J., Donahue, N. M., Duplissy, J., Ehrhart, S., Flagan, R. C., Franchin, A., Hakala, J., Hansel, A., Heinritzi, M., Hutterli, M., Kangasluoma, J., Kirkby, J., Laaksonen, A., Lehtipalo, K., Leiminger, M., Makhmutov, V., Mathot, S., Onnela, A., Petäjä, T., Praplan, A. P., Riccobono, F., Rissanen, M. P., Rondo, L., Schobesberger, S., Seinfeld, J. H., Steiner, G., Tomé, A., Tröstl, J., Winkler, P. M., Williamson, C., Wimmer, D., Ye, P., Baltensperger, U., Carslaw, K. S., Kulmala, M., Worsnop, D. R., and Curtius, J.: Neutral molecular cluster formation of sulfuric acid–dimethylamine observed in real time under atmospheric conditions, Proceedings of the National Academy of Sciences, 111, 15019-15024, 10.1073/pnas.1404853111, 2014.

Lee, S.-H., Uin, J., Guenther, A. B., de Gouw, J. A., Yu, F., Nadykto, A. B., Herb, J., Ng, N. L., Koss, A., Brune, W. H., Baumann, K., Kanawade, V. P., Keutsch, F. N., Nenes, A., Olsen, K., Goldstein, A., and Ouyang, Q.: Isoprene suppression of new particle formation: Potential mechanisms and implications, Journal of Geophysical Research: Atmospheres, 121, 14,621-614,635, 10.1002/2016JD024844, 2016.

Lehtipalo, K., Yan, C., Dada, L., Bianchi, F., Xiao, M., Wagner, R., Stolzenburg, D., Ahonen, L. R., Amorim, A., Baccarini, A., Bauer, P. S., Baumgartner, B., Bergen, A., Bernhammer, A.-K., Breitenlechner, M., Brilke, S., Buchholz, A., Mazon, S. B., Chen, D., Chen, X., Dias, A., Dommen, J., Draper, D. C., Duplissy, J., Ehn, M., Finkenzeller, H., Fischer, L., Frege, C., Fuchs, C., Garmash, O., Gordon, H., Hakala, J., He, X., Heikkinen, L., Heinritzi, M., Helm, J. C., Hofbauer, V., Hoyle, C. R., Jokinen, T., Kangasluoma, J., Kerminen, V.-M., Kim, C., Kirkby, J., Kontkanen, J., Kürten, A., Lawler, M. J., Mai, H., Mathot, S., Mauldin, R. L., Molteni, U., Nichman, L., Nie, W., Nieminen, T., Ojdanic, A., Onnela, A., Passananti, M., Petäjä, T., Piel, F., Pospisilova, V., Quéléver, L. L. J., Rissanen, M. P., Rose, C.,

Sarnela, N., Schallhart, S., Schuchmann, S., Sengupta, K., Simon, M., Sipilä, M., Tauber, C., Tomé, A., Tröstl, J., Väisänen, O., Vogel, A. L., Volkamer, R., Wagner, A. C., Wang, M., Weitz, L., Wimmer, D., Ye, P., Ylisirniö, A., Zha, Q., Carslaw, K. S., Curtius, J., Donahue, N. M., Flagan, R. C., Hansel, A., Riipinen, I., Virtanen, A., Winkler, P. M., Baltensperger, U., Kulmala, M., and Worsnop, D. R.: Multicomponent new particle formation from sulfuric acid, ammonia, and biogenic vapors, Science Advances, 4, eaau5363, 10.1126/sciadv.aau5363, 2018.

Lin, Y.-H., Zhang, Z., Docherty, K. S., Zhang, H., Budisulistiorini, S. H., Rubitschun, C. L., Shaw, S. L., Knipping, E. M., Edgerton, E. S., Kleindienst, T. E., Gold, A., and Surratt, J. D.: Isoprene Epoxydiols as Precursors to Secondary Organic Aerosol Formation: Acid-Catalyzed Reactive Uptake Studies with Authentic Compounds, Environmental Science & Technology, 46, 250-258, 10.1021/es202554c, 2012.

Lopez-Hilfiker, F. D., Mohr, C., Ehn, M., Rubach, F., Kleist, E., Wildt, J., Mentel, T. F., Lutz, A., Hallquist, M., Worsnop, D., and Thornton, J. A.: A novel method for online analysis of gas and particle composition: description and evaluation of a Filter Inlet for Gases and AEROsols (FIGAERO), Atmos. Meas. Tech., 7, 983-1001, 10.5194/amt-7-983-2014, 2014.

McFiggans, G., Mentel, T. F., Wildt, J., Pullinen, I., Kang, S., Kleist, E., Schmitt, S., Springer, M., Tillmann, R., Wu, C., Zhao, D., Hallquist, M., Faxon, C., Le Breton, M., Hallquist, Å. M., Simpson, D., Bergström, R., Jenkin, M. E., Ehn, M., Thornton, J. A., Alfarra, M. R., Bannan, T. J., Percival, C. J., Priestley, M., Topping, D., and Kiendler-Scharr, A.: Secondary organic aerosol reduced by mixture of atmospheric vapours, Nature, 565, 587-593, 10.1038/s41586-018-0871-y, 2019.

Merikanto, J., Spracklen, D. V., Mann, G. W., Pickering, S. J., and Carslaw, K. S.: Impact of nucleation on global CCN, Atmos. Chem. Phys., 9, 8601-8616, 10.5194/acp-9-8601-2009, 2009.

Paulot, F., Crounse, J. D., Kjaergaard, H. G., Kürten, A., Clair, J. M. S., Seinfeld, J. H., and Wennberg, P. O.: Unexpected epoxide formation in the gas-phase photooxidation of isoprene, Science, 325, 730-733, 2009.

Reid, J. P., Bertram, A. K., Topping, D. O., Laskin, A., Martin, S. T., Petters, M. D., Pope, F. D., and Rovelli, G.: The viscosity of atmospherically relevant organic particles, Nature Communications, 9, 956, 10.1038/s41467-018-03027-z, 2018.

Riva, M., Budisulistiorini, S. H., Zhang, Z., Gold, A., and Surratt, J. D.: Chemical characterization of secondary organic aerosol constituents from isoprene ozonolysis in the presence of acidic aerosol, Atmospheric Environment, 130, 5-13, https://doi.org/10.1016/j.atmosenv.2015.06.027, 2016.

Saathoff, H., Naumann, K. H., Möhler, O., Jonsson, Å. M., Hallquist, M., Kiendler-Scharr, A., Mentel, T. F., Tillmann, R., and Schurath, U.: Temperature dependence of yields of secondary organic aerosols from the ozonolysis of α-pinene and limonene, Atmos. Chem. Phys., 9, 1551-1577, 10.5194/acp-9-1551-2009, 2009.

Schervish, M., and Donahue, N. M.: Peroxy radical chemistry and the volatility basis set, Atmos. Chem. Phys., 20, 1183-1199, 10.5194/acp-20-1183-2020, 2020.

Simon, M., Heinritzi, M., Herzog, S., Leiminger, M., Bianchi, F., Praplan, A., Dommen, J., Curtius, J., and Kürten, A.: Detection of dimethylamine in the low pptv range using nitrate chemical ionization atmospheric pressure interface time-of-flight (CI-APi-TOF) mass spectrometry, Atmos. Meas. Tech., 9, 2135-2145, 10.5194/amt-9-2135-2016, 2016.

Simon, M., Dada, L., Heinritzi, M., Scholz, W., Stolzenburg, D., Fischer, L., Wagner, A. C., Kürten, A., Rörup, B., He, X. C., Almeida, J., Baalbaki, R., Baccarini, A., Bauer, P. S., Beck, L., Bergen, A., Bianchi, F., Bräkling, S., Brilke, S., Caudillo, L., Chen, D., Chu, B., Dias, A., Draper, D. C., Duplissy, J., El-Haddad, I., Finkenzeller, H., Frege, C., Gonzalez-Carracedo, L., Gordon, H., Granzin, M., Hakala, J., Hofbauer, V., Hoyle, C. R., Kim, C., Kong, W., Lamkaddam, H., Lee, C. P., Lehtipalo, K., Leiminger, M., Mai, H., Manninen, H. E.,

Marie, G., Marten, R., Mentler, B., Molteni, U., Nichman, L., Nie, W., Ojdanic, A., Onnela, A., Partoll, E., Petäjä, T., Pfeifer, J., Philippov, M., Quéléver, L. L. J., Ranjithkumar, A., Rissanen, M. P., Schallhart, S., Schobesberger, S., Schuchmann, S., Shen, J., Sipilä, M., Steiner, G., Stozhkov, Y., Tauber, C., Tham, Y. J., Tomé, A. R., Vazquez-Pufleau, M., Vogel, A. L., Wagner, R., Wang, M., Wang, D. S., Wang, Y., Weber, S. K., Wu, Y., Xiao, M., Yan, C., Ye, P., Ye, Q., Zauner-Wieczorek, M., Zhou, X., Baltensperger, U., Dommen, J., Flagan, R. C., Hansel, A., Kulmala, M., Volkamer, R., Winkler, P. M., Worsnop, D. R., Donahue, N. M., Kirkby, J., and Curtius, J.: Molecular understanding of new-particle formation from α-pinene between −50 and +25 °C, Atmos. Chem. Phys., 20, 9183-9207, 10.5194/acp-20-9183-2020, 2020.

Sindelarova, K., Granier, C., Bouarar, I., Guenther, A., Tilmes, S., Stavrakou, T., Müller, J. F., Kuhn, U., Stefani, P., and Knorr, W.: Global data set of biogenic VOC emissions calculated by the MEGAN model over the last 30 years, Atmos. Chem. Phys., 14, 9317-9341, 10.5194/acp-14-9317-2014, 2014.

Stolzenburg, D., Fischer, L., Vogel, A. L., Heinritzi, M., Schervish, M., Simon, M., Wagner, A. C., Dada, L., Ahonen, L. R., Amorim, A., Baccarini, A., Bauer, P. S., Baumgartner, B., Bergen, A., Bianchi, F., Breitenlechner, M., Brilke, S., Buenrostro Mazon, S., Chen, D., Dias, A., Draper, D. C., Duplissy, J., El Haddad, I., Finkenzeller, H., Frege, C., Fuchs, C., Garmash, O., Gordon, H., He, X., Helm, J., Hofbauer, V., Hoyle, C. R., Kim, C., Kirkby, J., Kontkanen, J., Kürten, A., Lampilahti, J., Lawler, M., Lehtipalo, K., Leiminger, M., Mai, H., Mathot, S., Mentler, B., Molteni, U., Nie, W., Nieminen, T., Nowak, J. B., Ojdanic, A., Onnela, A., Passananti, M., Petäjä, T., Quéléver, L. L. J., Rissanen, M. P., Sarnela, N., Schallhart, S., Tauber, C., Tomé, A., Wagner, R., Wang, M., Weitz, L., Wimmer, D., Xiao, M., Yan, C., Ye, P., Zha, Q., Baltensperger, U., Curtius, J., Dommen, J., Flagan, R. C., Kulmala, M., Smith, J. N., Worsnop, D. R., Hansel, A., Donahue, N. M., and Winkler, P. M.: Rapid growth of organic aerosol nanoparticles over a wide tropospheric temperature range, Proceedings of the National Academy of Sciences, 115, 9122-9127, 10.1073/pnas.1807604115, 2018.

Surratt, J. D., Murphy, S. M., Kroll, J. H., Ng, N. L., Hildebrandt, L., Sorooshian, A., Szmigielski, R., Vermeylen, R., Maenhaut, W., Claeys, M., Flagan, R. C., and Seinfeld, J. H.: Chemical Composition of Secondary Organic Aerosol Formed from the Photooxidation of Isoprene, The Journal of Physical Chemistry A, 110, 9665-9690, 10.1021/jp061734m, 2006.

Surratt, J. D., Lewandowski, M., Offenberg, J. H., Jaoui, M., Kleindienst, T. E., Edney, E. O., and Seinfeld, J. H.: Effect of Acidity on Secondary Organic Aerosol Formation from Isoprene, Environmental Science & Technology, 41, 5363-5369, 10.1021/es0704176, 2007.

Surratt, J. D., Chan, A. W., Eddingsaas, N. C., Chan, M., Loza, C. L., Kwan, A. J., Hersey, S. P., Flagan, R. C., Wennberg, P. O., and Seinfeld, J. H.: Reactive intermediates revealed in secondary organic aerosol formation from isoprene, Proceedings of the National Academy of Sciences, 107, 6640-6645, 2010.

Tröstl, J., Chuang, W. K., Gordon, H., Heinritzi, M., Yan, C., Molteni, U., Ahlm, L., Frege, C., Bianchi, F., Wagner, R., Simon, M., Lehtipalo, K., Williamson, C., Craven, J. S., Duplissy, J., Adamov, A., Almeida, J., Bernhammer, A.-K., Breitenlechner, M., Brilke, S., Dias, A., Ehrhart, S., Flagan, R. C., Franchin, A., Fuchs, C., Guida, R., Gysel, M., Hansel, A., Hoyle, C. R., Jokinen, T., Junninen, H., Kangasluoma, J., Keskinen, H., Kim, J., Krapf, M., Kürten, A., Laaksonen, A., Lawler, M., Leiminger, M., Mathot, S., Möhler, O., Nieminen, T., Onnela, A., Petäjä, T., Piel, F. M., Miettinen, P., Rissanen, M. P., Rondo, L., Sarnela, N., Schobesberger, S., Sengupta, K., Sipilä, M., Smith, J. N., Steiner, G., Tomè, A., Virtanen, A., Wagner, A. C., Weingartner, E., Wimmer, D., Winkler, P. M., Ye, P., Carslaw, K. S., Curtius, J., Dommen, J., Kirkby, J., Kulmala, M., Riipinen, I., Worsnop, D. R., Donahue, N. M., and Baltensperger, U.: The role of low-volatility organic compounds in initial particle growth in the atmosphere, Nature, 533, 527, 10.1038/nature18271, 2016.

Vanhanen, J., Mikkilä, J., Lehtipalo, K., Sipilä, M., Manninen, H. E., Siivola, E., Petäjä, T., and Kulmala, M.: Particle Size Magnifier for Nano-CN Detection, Aerosol Science and Technology, 45, 533-542, 10.1080/02786826.2010.547889, 2011.

Voigtländer, J., Duplissy, J., Rondo, L., Kürten, A., and Stratmann, F.: Numerical simulations of mixing conditions and aerosol dynamics in the CERN CLOUD chamber, Atmos. Chem. Phys., 12, 2205-2214, 10.5194/acp-12-2205-2012, 2012.

Wagner, A. C., Bergen, A., Brilke, S., Fuchs, C., Ernst, M., Hoker, J., Heinritzi, M., Simon, M., Bühner, B., and Curtius, J.: Size-resolved online chemical analysis of nanoaerosol particles: a thermal desorption differential mobility analyzer coupled to a chemical ionization time-of-flight mass spectrometer, Atmospheric Measurement Techniques, 11, 5489-5506, 2018.

Ye, Q., Wang, M., Hofbauer, V., Stolzenburg, D., Chen, D., Schervish, M., Vogel, A. L., Mauldin, R. L., Baalbaki, R., Brilke, S., Dada, L., Dias, A., Duplissy, J., El Haddad, I., Finkenzeller, H., Fischer, L., He, X., Kim, C., Kürten, A., Lamkaddam, H., Lee, C. P., Lehtipalo, K., Leiminger, M., Manninen, H. E., Marten, R., Mentler, B., Partoll, E., Petäjä, T., Rissanen, M. P., Schobesberger, S., Schuchmann, S., Simon, M., Tham, Y. J., Vazquez-Pufleau, M., Wagner, A. C., Wang, Y., Wu, Y., Xiao, M., Baltensperger, U., Curtius, J., Flagan, R., Kirkby, j., Kulmala, M., Volkamer, R., Winkler, P. M., Worsnop, D. R., and Donahue, N. M.: Molecular Composition and Volatility of Nucleated Particles from α-Pinene Oxidation between -50 °C and +25 °C, Environmental Science & Technology, 10.1021/acs.est.9b03265, 2019.

Zhang, G., Fu, H., and Chen, J.: Effect of relative humidity and the presence of aerosol particles on the α-pinene ozonolysis, Journal of Environmental Sciences, 71, 99-107, 10.1016/j.jes.2017.10.011, 2018.

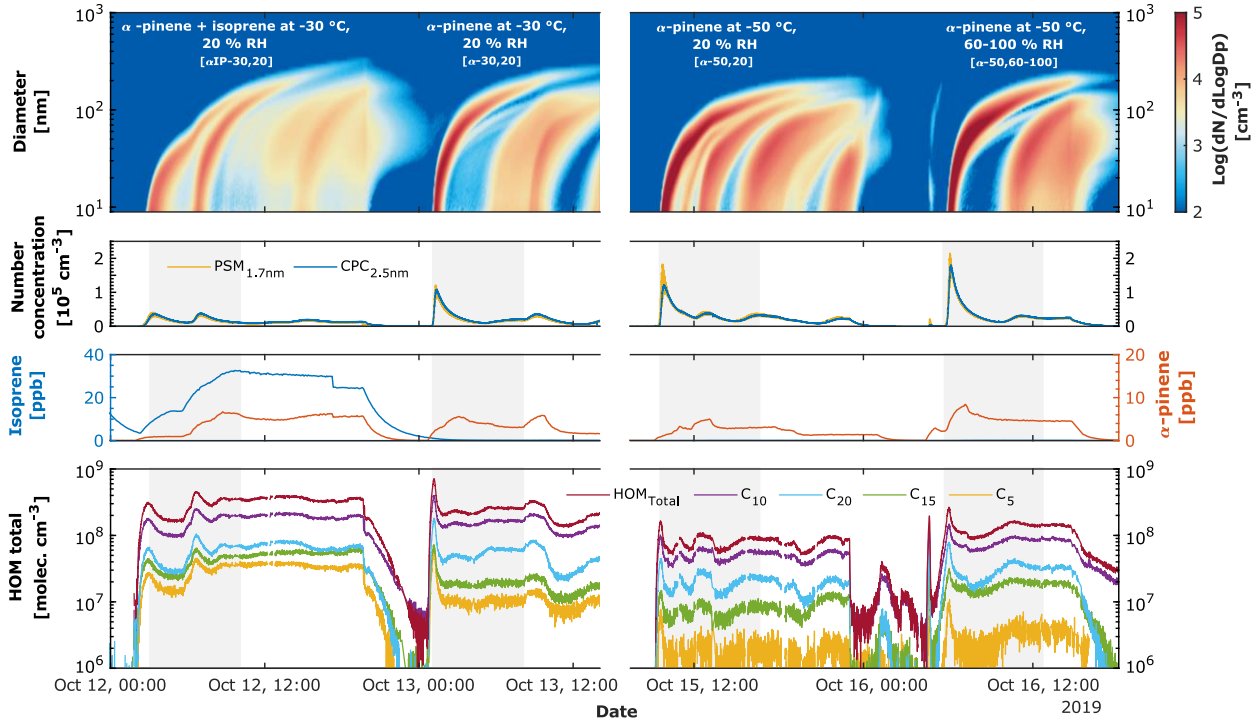
α -pinene + isoprene at -30 °C, 20 % RH [αIP-30,20]
α-pinene at -30 °C, 20 % RH [α-30,20]
α-pinene at -50 °C, 20 % RH [α-50,20]
α-pinene at -50 °C, 60-100 % RH [α-50,60-100]
Diameter [nm]
Log(dN/dLogDp) [cm-3]
Number concentration [10^5 cm-3]
PSM1.7nm
CPC2.5nm
Isoprene [ppb]
α-pinene [ppb]
HOM total [molec. cm-3]
HOMTotal
C10
C20
C15
C5
Oct 12, 00:00
Oct 12, 12:00
Oct 13, 00:00
Oct 13, 12:00
Oct 15, 12:00
Oct 16, 00:00
Oct 16, 12:00
2019
Date

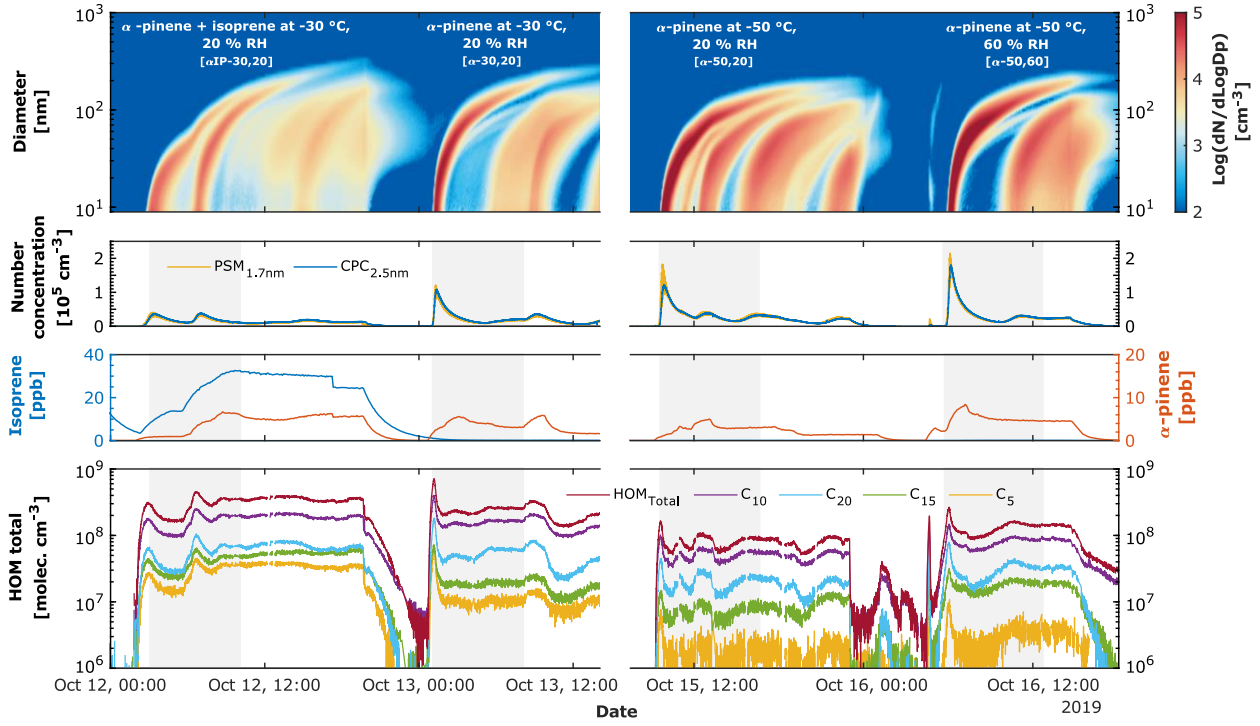

Figure 1. Experimental overview for pure biogenic new particle formation. First panel: particle size distribution for four different experiments: α-pinene + isoprene at -30 °C and 20 % RH (αIP-30,20); α-pinene at -30 °C and 20 % RH (α-30,20); α-pinene at -50 °C and 20 % RH (α-50,20) and α-pinene at -50 °C and 60~~-100~~ % RH (α-50,60~~-100~~). The color scale represents the log 10 of the normalized particle concentration in cm^{-3}. Second panel: Particle number concentration in cm^{-3} measured by the PSM with a cut-off diameter of 1.7 nm and CPC 2.5 nm. Third panel: Mixing ratio in ppbv for the biogenic precursor gases, isoprene and α-pinene. Fourth panel: Evolution of total HOM concentration in molec. cm^{-3}, measured in the gas phase by the Nitrate CI-APi-TOF mass spectrometer. HOM total is defined as the sum of C_5, C_{10}, C_{15} and C_{20} carbon classes which are shown as well. Ozone level is not shown, though remains stable over the whole period ~ 100 ppbv. The shaded areas refer to the time where the particles were collected using the TD-DMA.

Table 1. Summary of the main parameters for four pure biogenic new particle formation experiments.

Experiment	Isoprene [ppb]	α-pinene [ppb]	Isoprene-to-monoterpene carbon ratio (*R*)	Ozone [ppb]	T [°C]	RH [%]	HOM total* [molec. cm^{-3}]	$J_{1.7}$* [cm^{-3} s^{-1}]	Growth rate 3.2-8 nm [nm h^{-1}]	Growth rate 5-15 nm [nm h^{-1}]	Mass $_{<15\ nm}$ /Mass $_{>15\ nm}$** [%]
αIP-30,20	13.71	0.95	14.4	98.58	-30	20	1.50e8	7.29	18.0	22.8	0.29 / 99.7
	31.38	5.12	6.1	101.56	-30	20	3.04e8	10.10	NA	39.0	
α-30,20	~ 0	3.35	NA	102.10	-30	20	2.20e8	23.76	76.9	77.1	0.11 / 99.9
α-50,20	~ 0	3.04	NA	100.55	-50	20	6.72e7	51.24	41.1	42.0	0.26 / 99.7
α-50,60 ~~100~~	~ 0	7.72	NA	110.20	-50	60 ~~100~~	8.00e7	79.17	63.4	78.4	0.09 / 99.9

* Run-to-run experimental uncertainties of HOMs is ± 20 % and for $J_{1.7}$ is ± 30 %. NA, Not Applicable. **Mass fraction of particles collected on the filament during the TD-DMA collection time, calculation based on SMPS mass distributions.

715

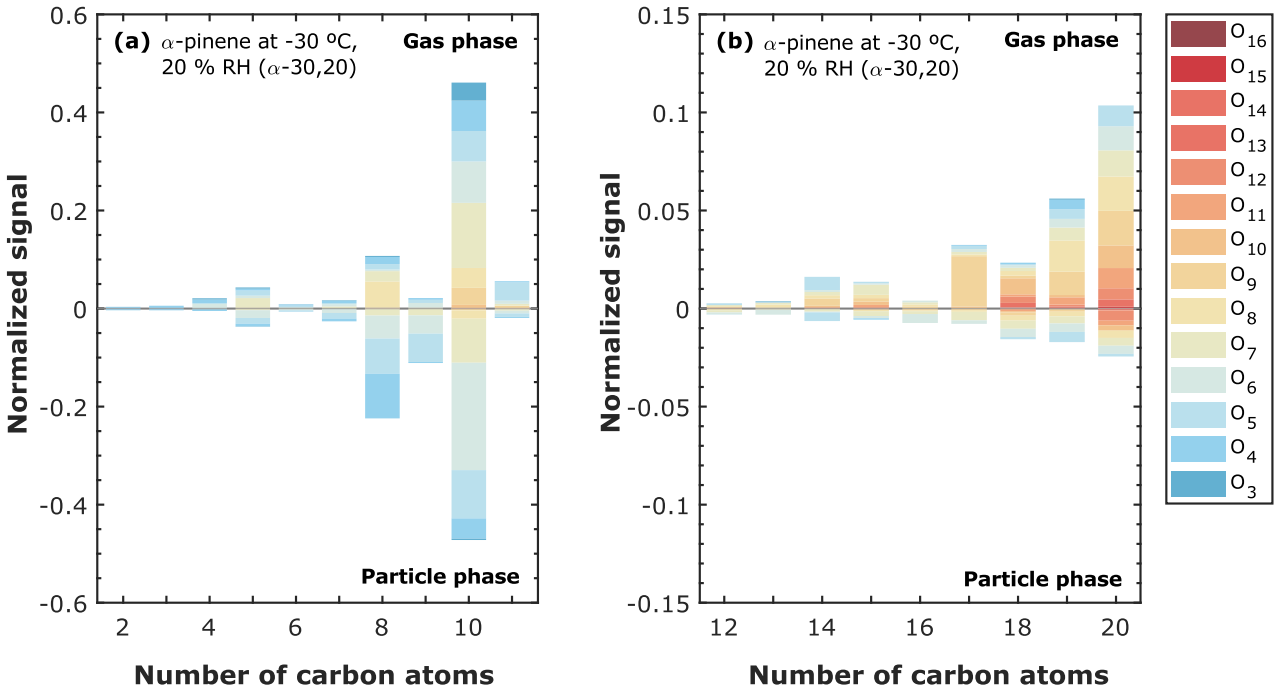

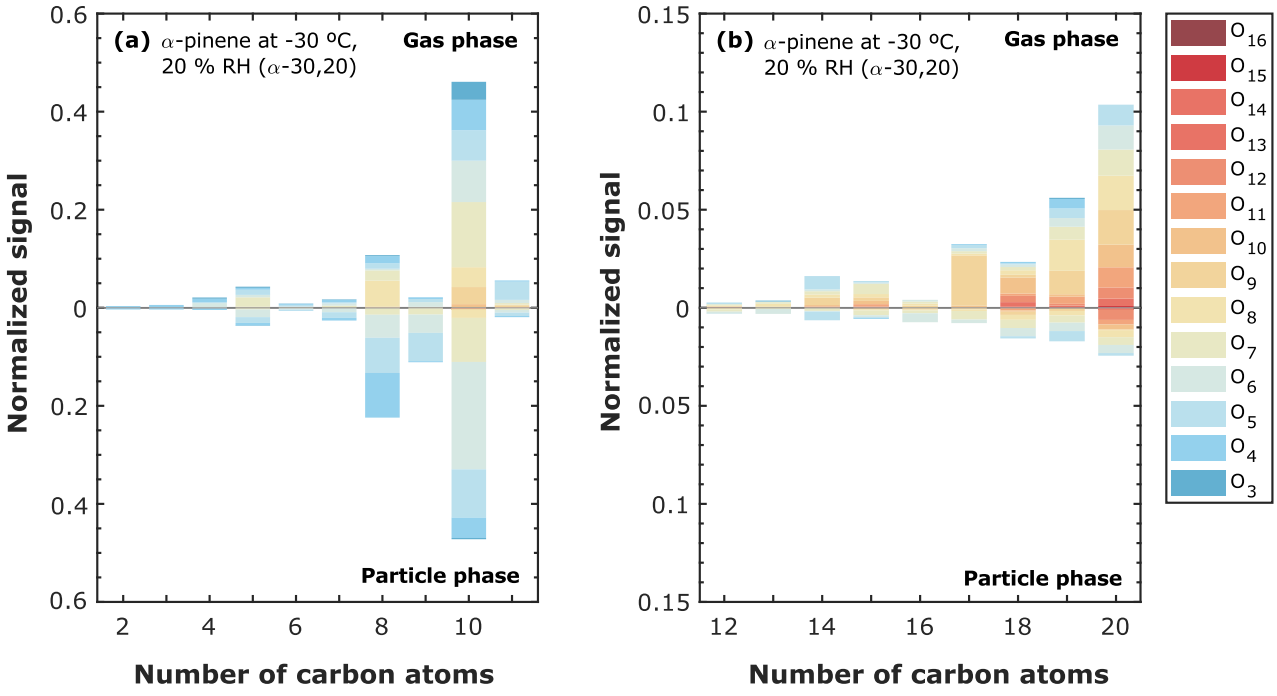

Figure 2. Carbon atom distribution and oxygen atom content in gas and particle phase molecules for α-pinene oxidation products at -30 °C and 20 % RH (α-30,20). Both phases are measured with a Nitrate CI-APi-TOF Mass Spectrometer, while the TD-DMA is coupled to it for particle phase measurements. (a) carbon atom distribution $C_{2\text{-}11}$ and (b) carbon atom distribution $C_{12\text{-}20}$. The level of α-pinene was between 1 and 8 ppbv and Ozone level was stable at ~ 100 ppbv. The intensities are normalized by the total signal in each system and phase. Each color represents a specific number of oxygen atoms in the range of 3 to 16.

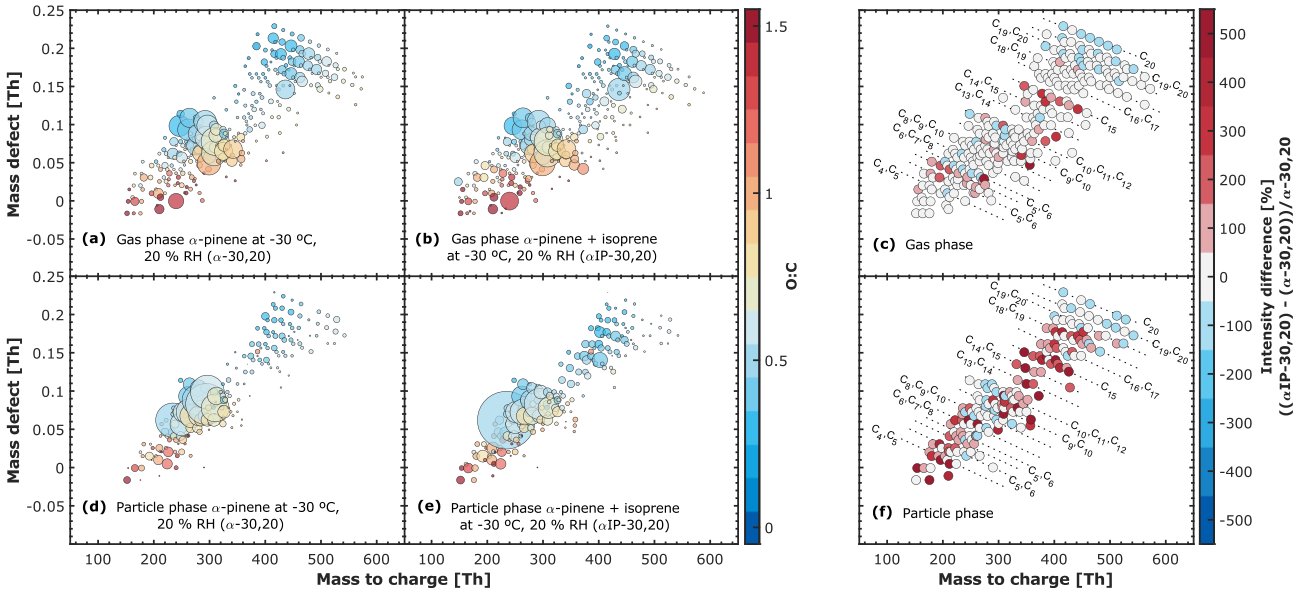

Figure 3. Mass defect plots of gas and particle phase and the intensity difference between each phase~~them~~. Both phases are measured with a Nitrate CI-APi-TOF Mass Spectrometer, while the TD-DMA is coupled to it for particle phase measurements. (a) gas and (d) particle for α-pinene oxidation products at -30 °C and 20 % RH (α-30,20). (b) gas and (e) particle for α-pinene + isoprene oxidation products at -30 °C and 20 % RH (αIP-30,20). The level of α-pinene was between 1 and 8 ppbv in both experiments, while isoprene was present only in experiment αIP-30,20 reaching up to 30 ppbv. Ozone levels were ~ 100 ppbv in both experiments. The symbol sizes in (a), (b), (d) and (e) are the intensities normalized by the total signal in each system. The intensity difference in gas (c) and in particle (f) is indicated as ((αIP-30,20) - (α-30,20))/ α-30,20. The color scale represents the difference in percent.

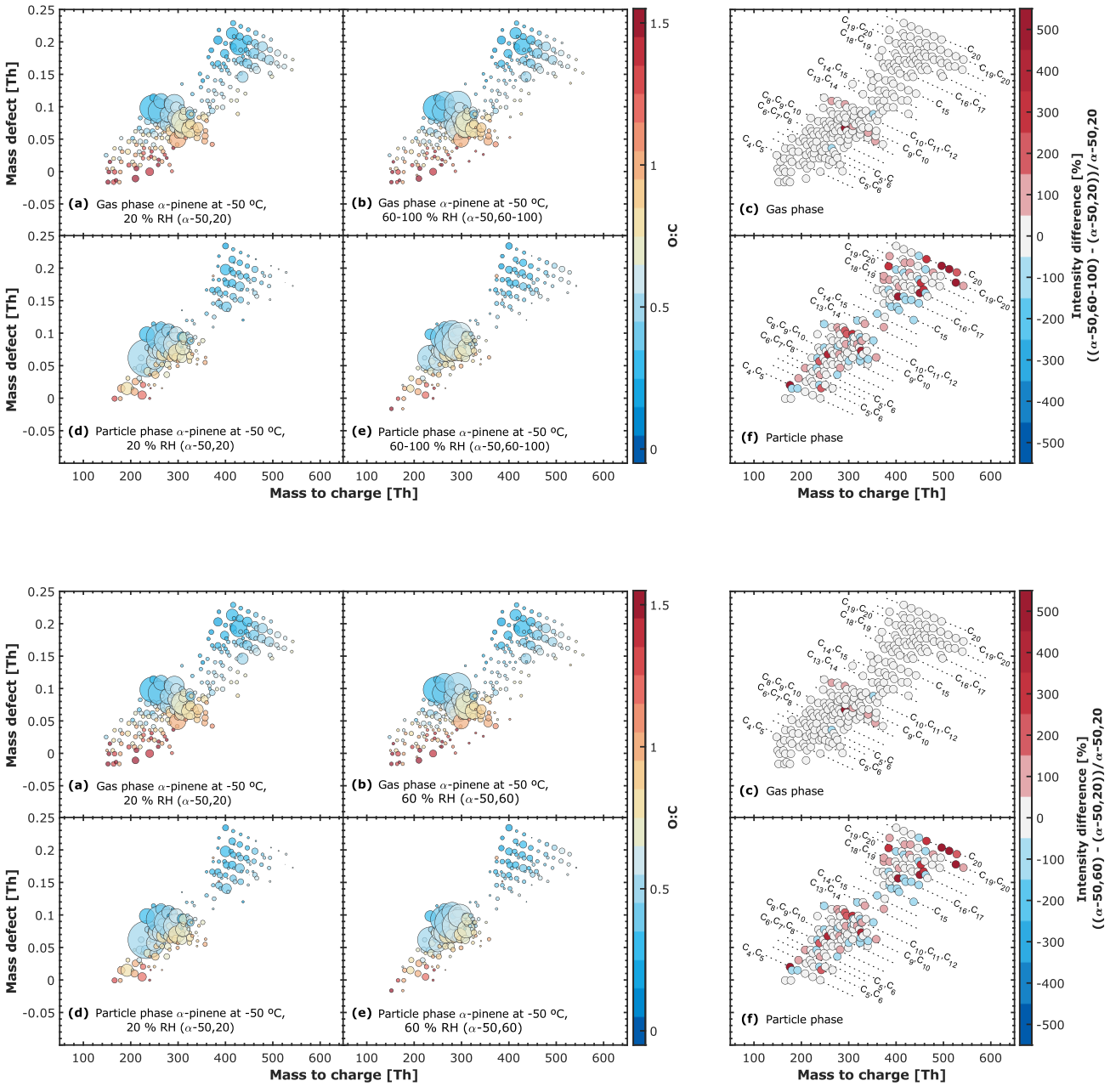

735

Figure 4. Mass defect plots of gas and particle phase and the intensity difference between each phase~~them~~. Both phases are measured with a Nitrate CI-APi-TOF Mass Spectrometer, while the TD-DMA is coupled to it for particle phase measurements. (a) gas and (d) particle for α-pinene oxidation products at -50 °C and 20 % RH (α-50,20). (b) gas and (e) particle for α-pinene 740 **oxidation products at -50 °C and 60 ~~to 100~~ % RH (α-50,60~~-100~~). The level of α-pinene was between 1 and 8 ppbv and Ozone levels were ~ 100 ppbv in both experiments. The symbol sizes in (a), (b), (d) and (e) are the intensities normalized by the total signal in**

each system. The intensity difference in gas (c) and in particle (f) is indicated as ((α-50,60~~-100~~) - (α-50,20))/ α-50,20. The color scale represents the difference in percent.

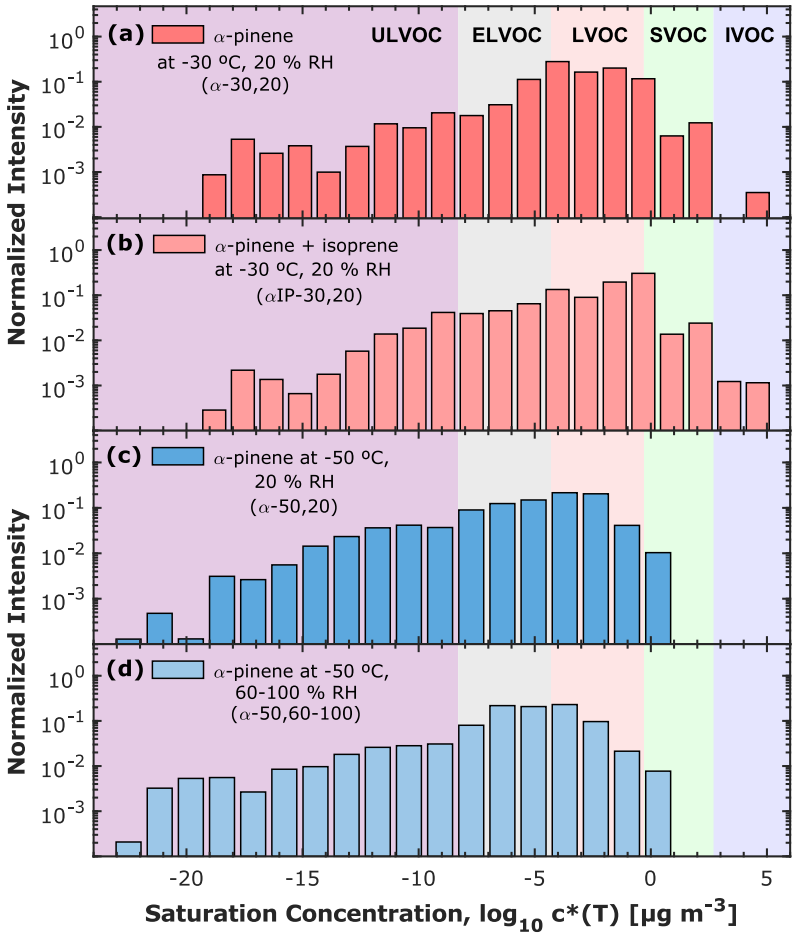
(a) α-pinene
at -30 ºC, 20 % RH
(α-30,20)
ULVOC
ELVOC
LVOC
SVOC
IVOC
(b) α-pinene + isoprene
at -30 ºC, 20 % RH
(αIP-30,20)
(c) α-pinene at -50 ºC,
20 % RH
(α-50,20)
(d) α-pinene at -50 ºC,
60-100 % RH
(α-50,60-100)
Normalized Intensity
Normalized Intensity
10^0
10^-1
10^-2
10^-3
-20
-15
-10
-5
0
5
Saturation Concentration, log10 c*(T) [µg m-3]

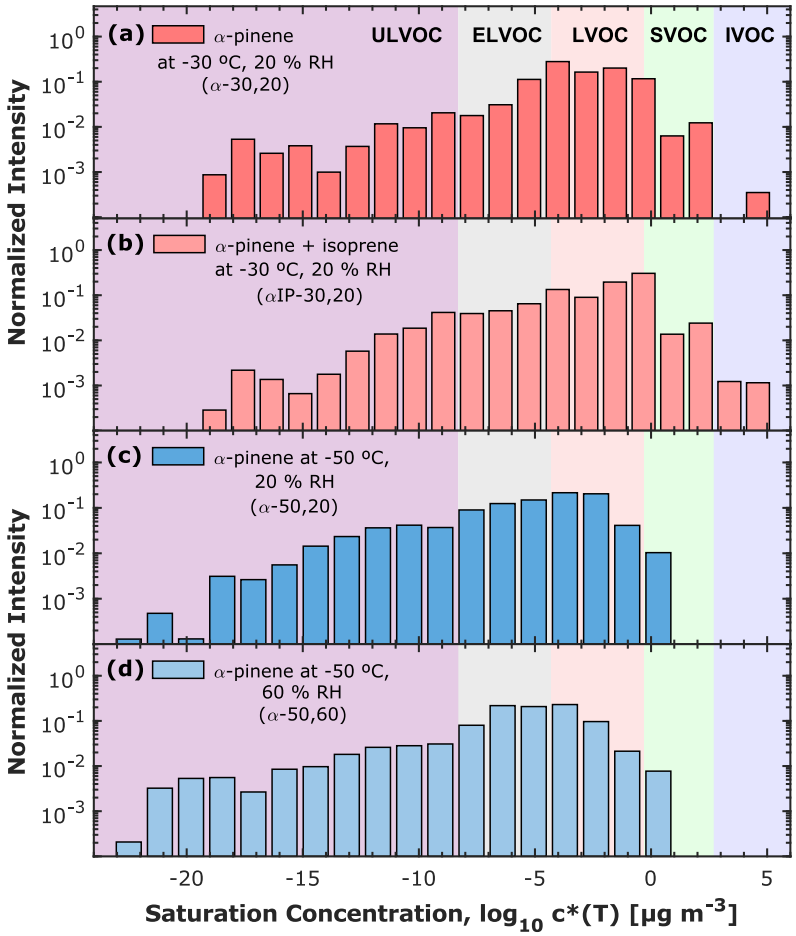

Figure 5. TD-DMA Volatility distribution of the measured oxidation products in the particle phase for four different experiments: (a) α-pinene at -30 °C and 20 % RH (α-30,20); (b) α-pinene + isoprene at -30 °C and 20 % RH (αIP-30,20); (c) α-pinene at -50 °C and 20 % RH (α-50,20) and (d) α-pinene at -50 °C and 60~~-100~~ % RH (α-50,60~~-100~~). Every individual volatility bin includes the sum of the intensity for the oxidation products normalized by the total signal in each system. Every individual volatility bin is defined at 300 K, shifted, and widened according to their corresponding temperature. The color bands in the background indicate the volatility regimes as in Donahue et al. (2012) and in Schervish and Donahue (2020). The normalized intensity is dimensionless. Nevertheless, it should be noted that the particle phase signal is given in normalized counts per second integrated over the evaporation time [ncps. s].

Table 2. Bin volatility fractions for the different experiments.

Experiment	T [°C]	RH [%]	ULVOC [%]	ELVOC [%]	LVOC [%]	SVOC [%]	IVOC [%]
αIP-30,20	-30	20	8.6	28.3	59.1	3.8	0.2
α-30,20	-30	20	5.9	44.1	48.1	1.9	0
α-50,20	-50	20	16.5	36.4	46.1	1.0	0
α-50,60	-50	60	13.8	50.6	34.8	0.8	0

775

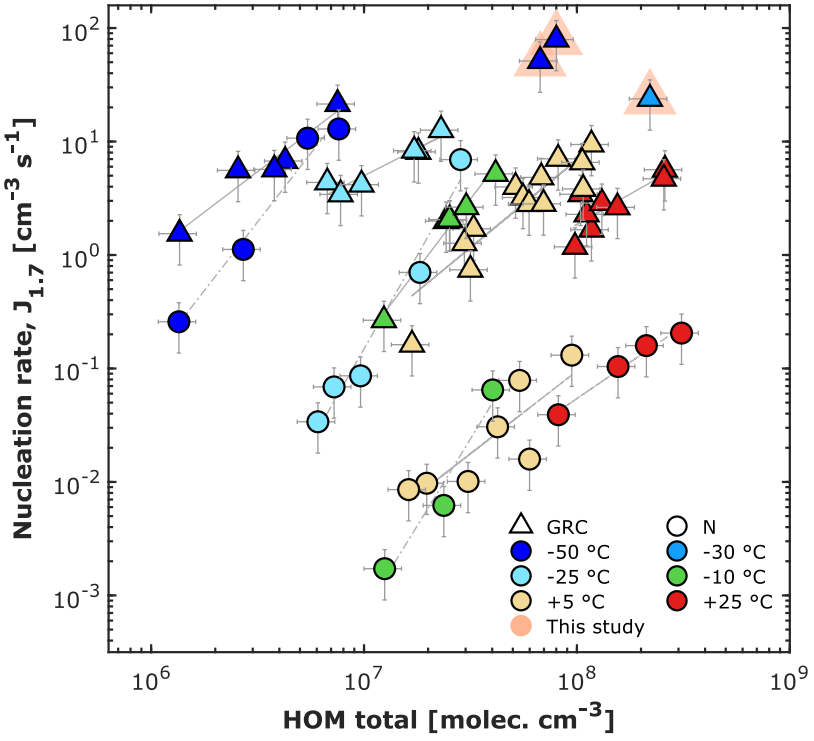

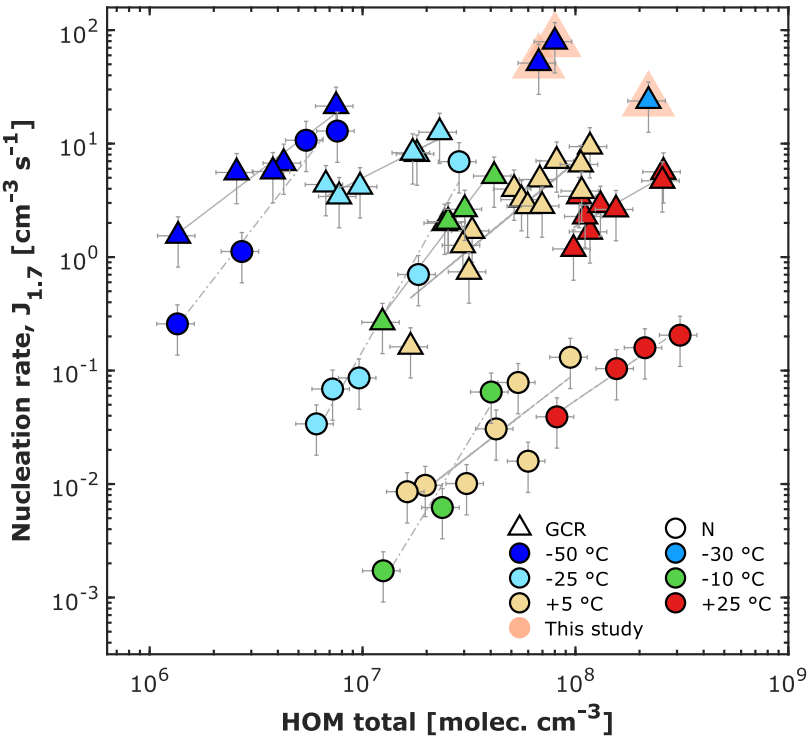

Figure 6. Pure biogenic nucleation rates of pure α-pinene at 1.7 nm diameter against total HOM concentration at different temperatures. HOM total is defined as the sum of C_5, C_{10}, C_{15} and C_{20} carbon classes. Triangles represent Gg~~g~~alactic C~~c~~osmic R~~r~~ays (GCR) conditions and circles represent Neutral conditions. Data points at -50 °C, -25 °C, -10 °C, +5 °C and +25 °C are from Simon et al. (2020). The points with orange marker on the background are the contribution of this study (experiments α-30,20, α-50,20 and α-50,60~~-100~~). Solid and dashed lines represent power-law fits to GCR and Neutral conditions. Bars indicate 1 σ~~α~~ run-to-run experimental uncertainty. The overall systematic scale uncertainty of HOM of +78 % and -68 % ~~and~~ is not shown.

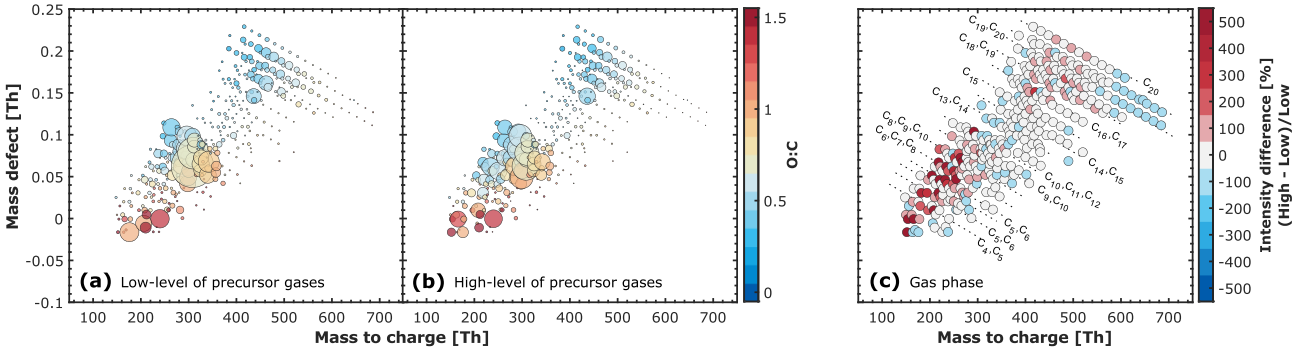

Figure 7. Mass defect plots of gas phase for two different systems and the normalized difference between them. Gas phase is measured with a Nitrate CI-APi-TOF Mass Spectrometer, (a) α-pinene oxidation products at -10 °C and 90 % RH at low-level of precursor gases, (b) α-pinene oxidation products at -10 °C and 80 % RH at high-level of precursor gases. α-pinene was 0.2 - 0.8 ppbv and Ozone ~ 40 - 50 ppbv in (a), and α-pinene was 2 - 3 ppbv and Ozone ~ 100 ppbv in (b). The symbol sizes and colors in (a) and (b) represent the intensities normalized by the total signal in each system. (c) The difference between the normalized signals shown in (a) and (b) is represented by the color scale.

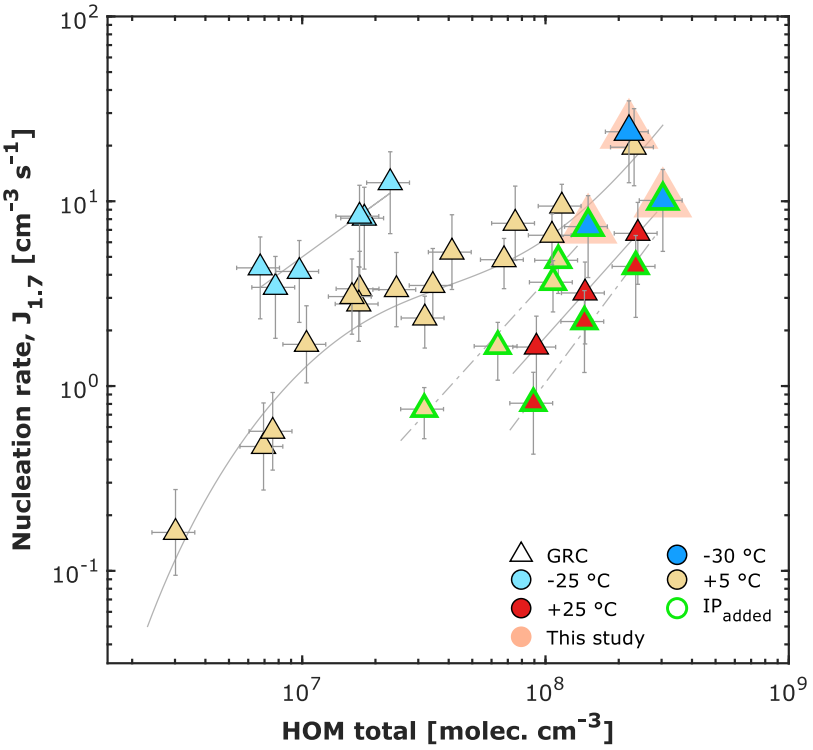
Nucleation rate, $J_{1.7}$ [cm^{-3} s^{-1}]
HOM total [molec. cm^{-3}]
GRC
-25 °C
+25 °C
This study
-30 °C
+5 °C
IP_{added}

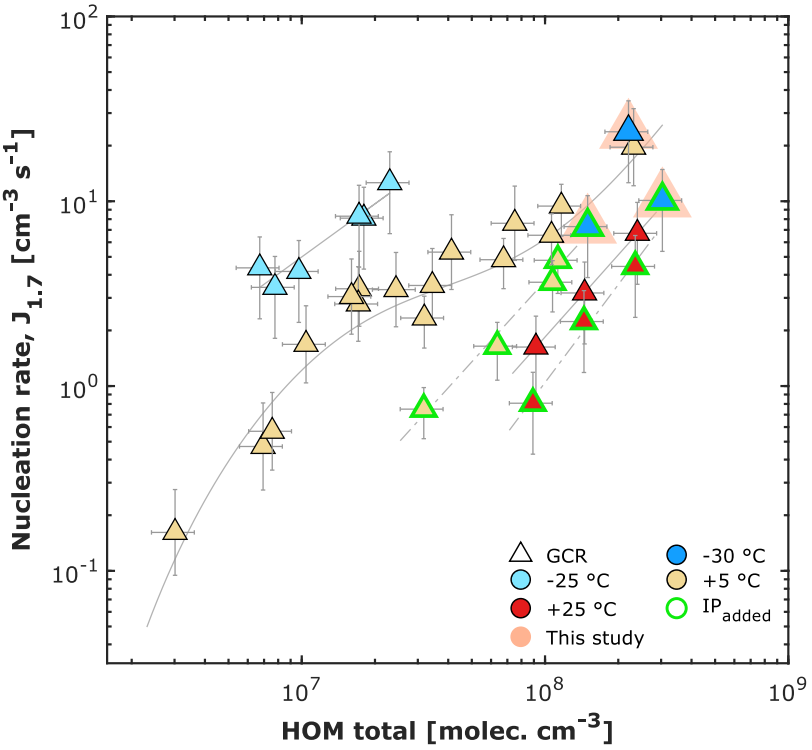

Figure 8. Pure biogenic nucleation rates at 1.7 nm diameter against total HOM concentration at different temperatures for α-pinene and α-pinene + isoprene systems. HOM total is defined as the sum of C_5, C_{10}, C_{15} and C_{20} carbon classes. Triangles represent Galactic Cosmic Rays (GCR) conditions. Data points at +5 °C and +25 °C are from Kirkby et al. (2016) and Heinritzi et al., (2020). Data points at -25 °C are from Simon et al., (2020). The value of isoprene-to-monoterpene carbon ratio (R) varies from 1.5 to 6.5 for Heinritzi et al., (2020), and R equals to 14.4 and 6.1 for this study. The points with orange marker on the background indicate the contribution of this work. Solid lines represent power-law fits to GCR conditions of the systems with α-pinene only and dashed lines are the power-law fits of the systems with isoprene added. Bars indicate 1 σ~~α~~ run-to-run experimental uncertainty. The overall systematic scale uncertainty of HOM of +78 % and -68 % ~~and~~ is not shown.

Chemical composition of nanoparticles from α-pinene nucleation and the influence of isoprene and relative humidity at low temperature

Lucía Caudillo[1], Birte Rörup[2], Martin Heinritzi[1], Guillaume Marie[1], Mario Simon[1], Andrea C. Wagner[3], Tatjana Müller[1,4], Manuel Granzin[1], Antonio Amorim[5], Farnoush Ataei[6], Rima Baalbaki[2], Barbara Bertozzi[7], Zoé Brasseur[2], Randall Chiu[3], Biwu Chu[2], Lubna Dada[8], Jonathan Duplissy[2,9], Henning Finkenzeller[3], Loïc Gonzalez Carracedo[10], Xu-Cheng He[2], Victoria Hofbauer[11], Weimeng Kong[12,13], Houssni Lamkaddam[8], Chuan P. Lee[8], Brandon Lopez[11], Naser G. A. Mahfouz[11], Vladimir Makhmutov[14,26], Hanna E. Manninen[15], Ruby Marten[8], Dario Massabò[16], Roy L. Mauldin[17,11], Bernhard Mentler[18], Ugo Molteni[8,20,21], Antti Onnela[15], Joschka Pfeifer[15], Maxim Philippov[14], Ana A. Piedehierro[22], Meredith Schervish[11], Wiebke Scholz[18], Benjamin Schulze[12], Jiali Shen[2], Dominik Stolzenburg[2], Yuri Stozhkov[14], Mihnea Surdu[8], Christian Tauber[10], Yee Jun Tham[2], Ping Tian[23], António Tomé[24], Steffen Vogt[7], Mingyi Wang[11], Dongyu S. Wang[8], Stefan K. Weber[15], André Welti[22], Wang Yonghong[2], Wu Yusheng[2], Marcel Zauner-Wieczorek[1], Urs Baltensperger[8], Imad El Haddad[8], Richard C. Flagan[12], Armin Hansel[18,19], Kristina Höhler[7], Jasper Kirkby[1,15], Markku Kulmala[2,9,25], Katrianne Lehtipalo[2,22], Ottmar Möhler[7], Harald Saathoff[7], Rainer Volkamer[3], Paul M. Winkler[10], Neil M. Donahue[11], Andreas Kürten[1], Joachim Curtius[1].

[1]Institute for Atmospheric and Environmental Sciences, Goethe University Frankfurt, 60438 Frankfurt am Main, Germany
[2]Institute for Atmospheric and Earth System Research (INAR) / Physics, Faculty of Science, University of Helsinki, 00014 Helsinki, Finland
[3]Department of Chemistry & CIRES, University of Colorado Boulder, Boulder, CO, 80309-0215, USA
[4]Max Planck Institute for Chemistry, Mainz, 55128, Germany
[5]CENTRA and FCUL, University of Lisbon, 1749-016 Lisbon, Portugal
[6]Leibniz Institute for Tropospheric Research, Leipzig, 04318, Germany
[7]Institute of Meteorology and Climate Research, Karlsruhe Institute of Technology, 76344 Eggenstein-Leopoldshafen, Germany
[8]Laboratory of Atmospheric Chemistry, Paul Scherrer Institute, 5232 Villigen, Switzerland
[9]Helsinki Institute of Physics, University of Helsinki, 00014 Helsinki, Finland
[10]Faculty of Physics, University of Vienna, 1090 Vienna, Austria
[11]Center for Atmospheric Particle Studies, Carnegie Mellon University, Pittsburgh, PA, 15213, USA
[12]Division of Chemistry and Chemical Engineering, California Institute of Technology, Pasadena, CA 91125, USA
[13]California Air Resources Board, Sacramento, CA 95814, USA
[14]Lebedev Physical Institute, Russian Academy of Sciences, 119991, Moscow, Russia
[15]CERN, 1211 Geneva, Switzerland
[16]Dipartimento di Fisica, Università di Genova and INFN, 16146 Genova, Italy
[17]Department of Atmospheric and Oceanic Sciences, University of Colorado Boulder, Boulder, CO 80309, USA
[18]Institute for Ion and Applied Physics, University of Innsbruck, 6020 Innsbruck, Austria
[19]Ionicon Analytik GmbH, 6020 Innsbruck, Austria
[20]Forest Dynamics, Swiss Federal Institute for Forest, Snow and Landscape Research, 8903 Birmensdorf, Switzerland
[21]Department of Chemistry, University of California, Irvine, Irvine, CA 92697, USA
[22]Finnish Meteorological Institute, 00560 Helsinki, Finland
[23]Beijing Weather Modification Office, China
[24]IDL, Universidade da Beira Interior, R. Marquês de Ávila e Bolama, Covilhã, 6201-001, Portugal

[25]Aerosol and Haze Laboratory, Beijing Advanced Innovation Center for Soft Matter Science and Engineering, Beijing University of Chemical Technology, Beijing, 100029, P.R. China
[26]Moscow Institute of Physics and Technology (National Research University), 117303, Moscow, Russia

Correspondence to: Lucía Caudillo (lucia.caudillo@iau.uni-frankfurt.de) and Joachim Curtius (curtius@iau.uni-frankfurt.de)

Supplementary Material

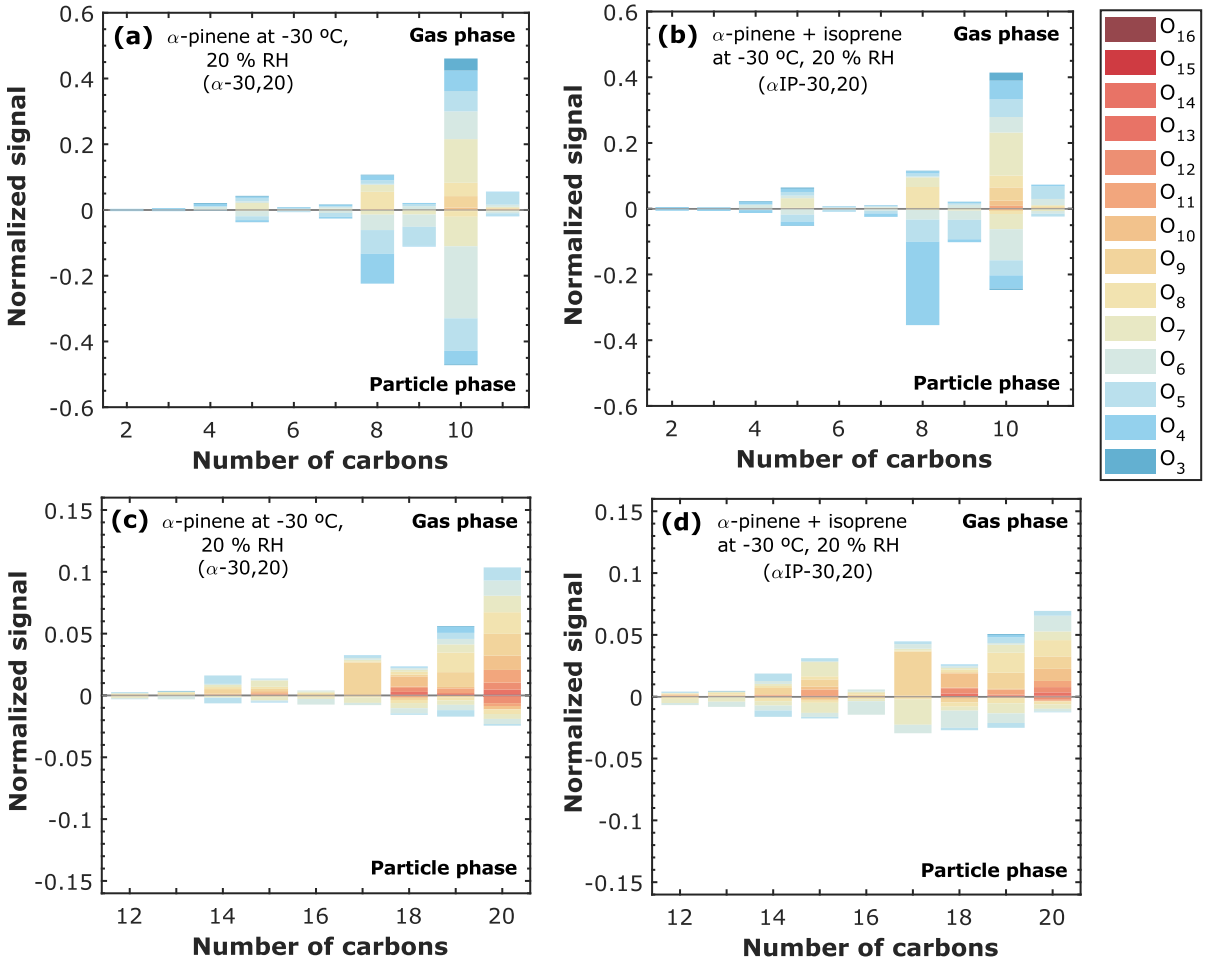

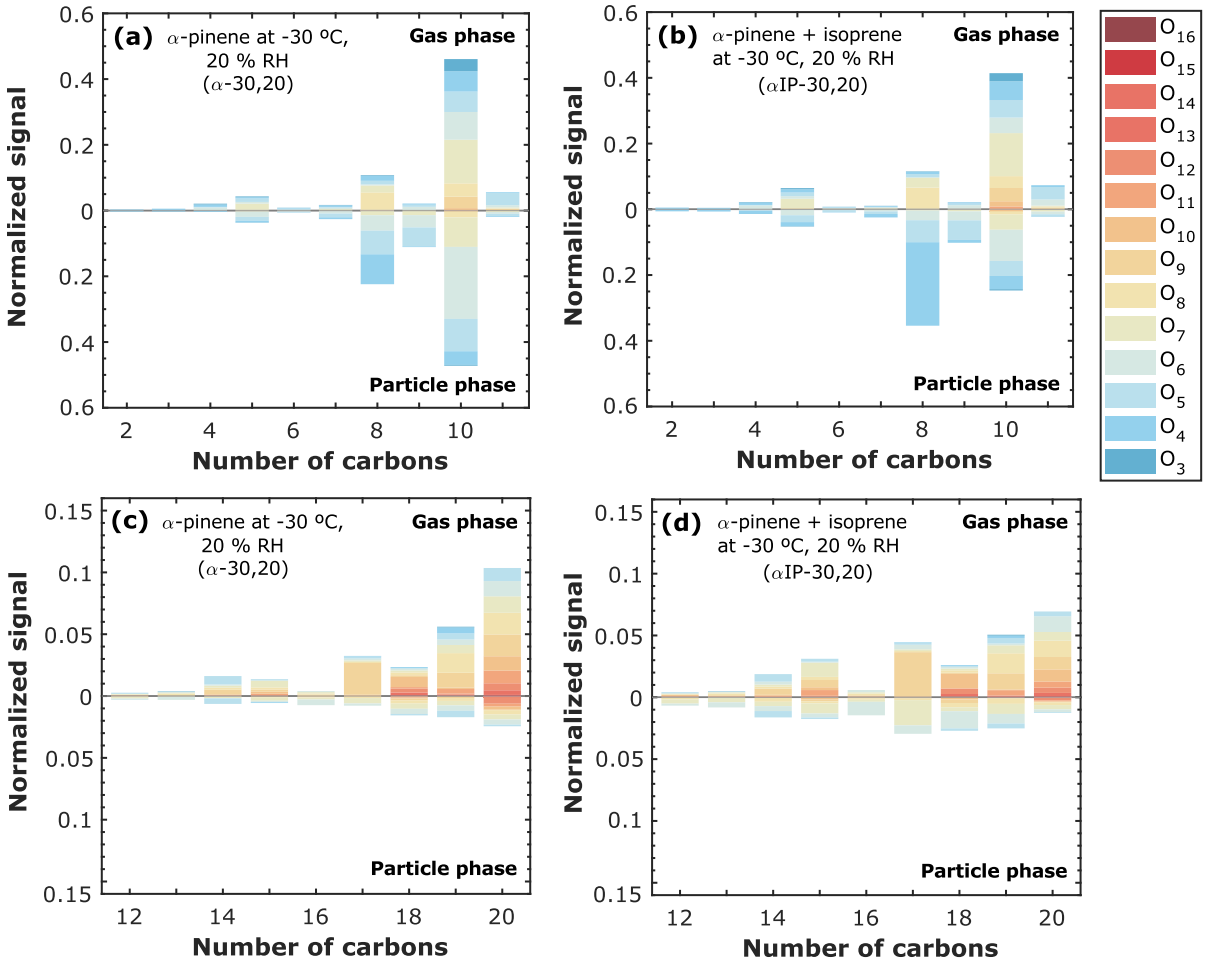

Figure S1. Carbon atom distribution $C_{2\text{-}11}$ and $C_{12\text{-}20}$ and oxygen atom content in gas and particle phase molecules. Both phases are measured with a Nitrate CI-APi-TOF Mass Spectrometer, while the TD-DMA is coupled to it for particle phase measurements. (a) and (c) α-pinene oxidation products at -30 °C and 20 % RH (α-30,20), (b) and (d) α-pinene + isoprene oxidation products at -30 °C and 20 % RH (αIP-30,20). The level of α-pinene was between 1 and 8 ppbv in (a) (b) (c) and (d), while isoprene level reached up to 30 ppbv in (b) and (d). Ozone level was stable at ~ 100 ppbv for all the experiments. The intensities are normalized by the total signal in each system and phase. Each color represents a specific number of oxygen atoms in the range of 3 to 16.

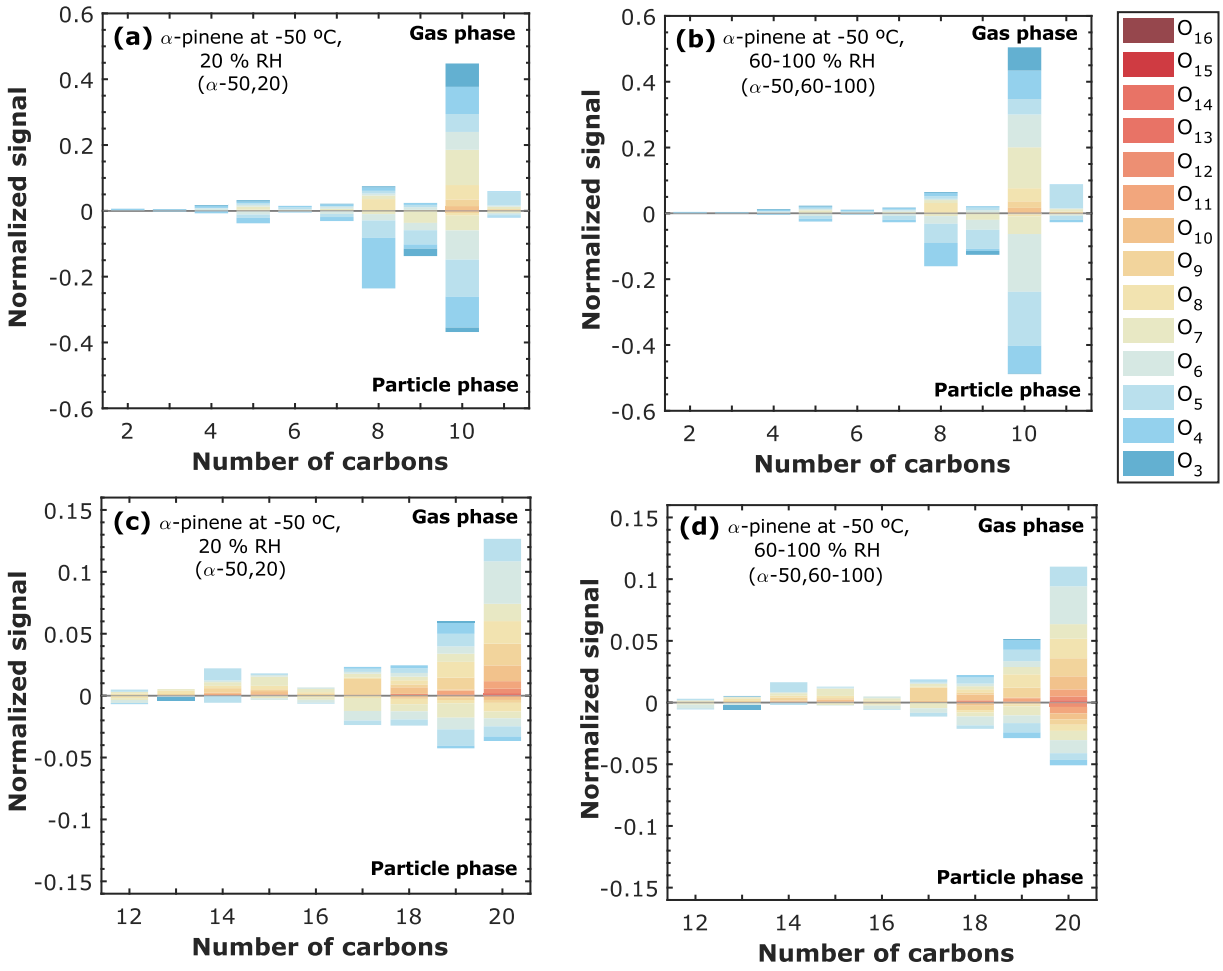
(a) α-pinene at -50 ºC, 20 % RH (α-50,20)
Gas phase
Particle phase
Normalized signal
Number of carbons
(b) α-pinene at -50 ºC, 60-100 % RH (α-50,60-100)
Gas phase
Particle phase
Normalized signal
Number of carbons
O16
O15
O14
O13
O12
O11
O10
O9
O8
O7
O6
O5
O4
O3
(c) α-pinene at -50 ºC, 20 % RH (α-50,20)
Gas phase
Particle phase
Normalized signal
Number of carbons
(d) α-pinene at -50 ºC, 60-100 % RH (α-50,60-100)
Gas phase
Particle phase
Normalized signal
Number of carbons

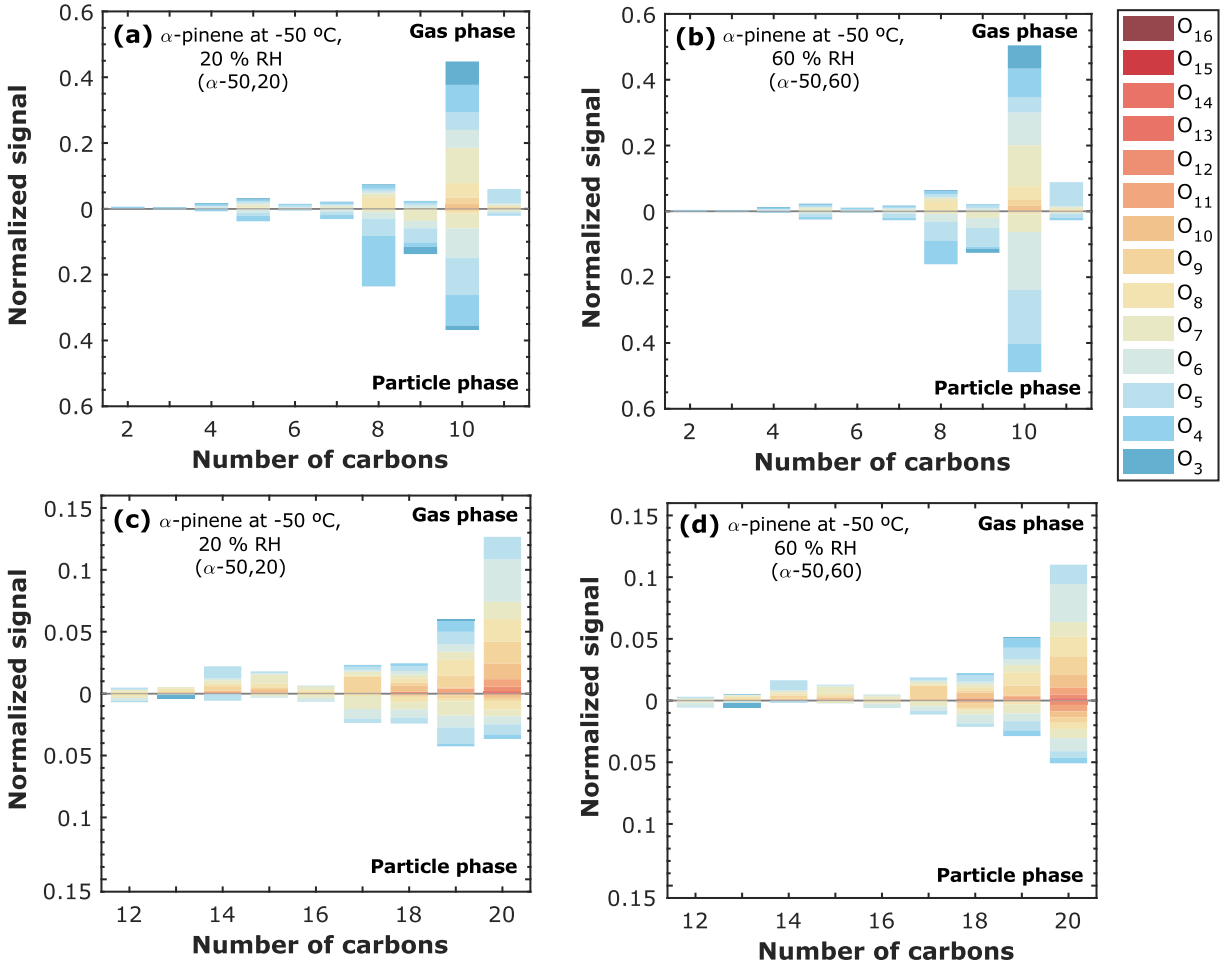

Figure S2. Carbon atom distribution $C_{2\text{-}11}$ and $C_{12\text{-}20}$ and oxygen atom content in gas and particle phase molecules. Both phases are measured with a Nitrate CI-APi-TOF Mass Spectrometer, while the TD-DMA is coupled to it for particle phase measurements. (a) and (c) α-pinene oxidation products at -50 °C and 20 % RH (α-50,20), (b) and (d) α-pinene oxidation products at -50 °C and 60~~–100~~ % RH (α-50,60~~–100~~). The level of α-pinene was between 1 and 8 ppbv and Ozone level was stable at ~ 100 ppbv for all the experiments. The intensities are normalized by the total signal in each system and phase. Each color represents a specific number of oxygen atoms in the range of 3 to 16.

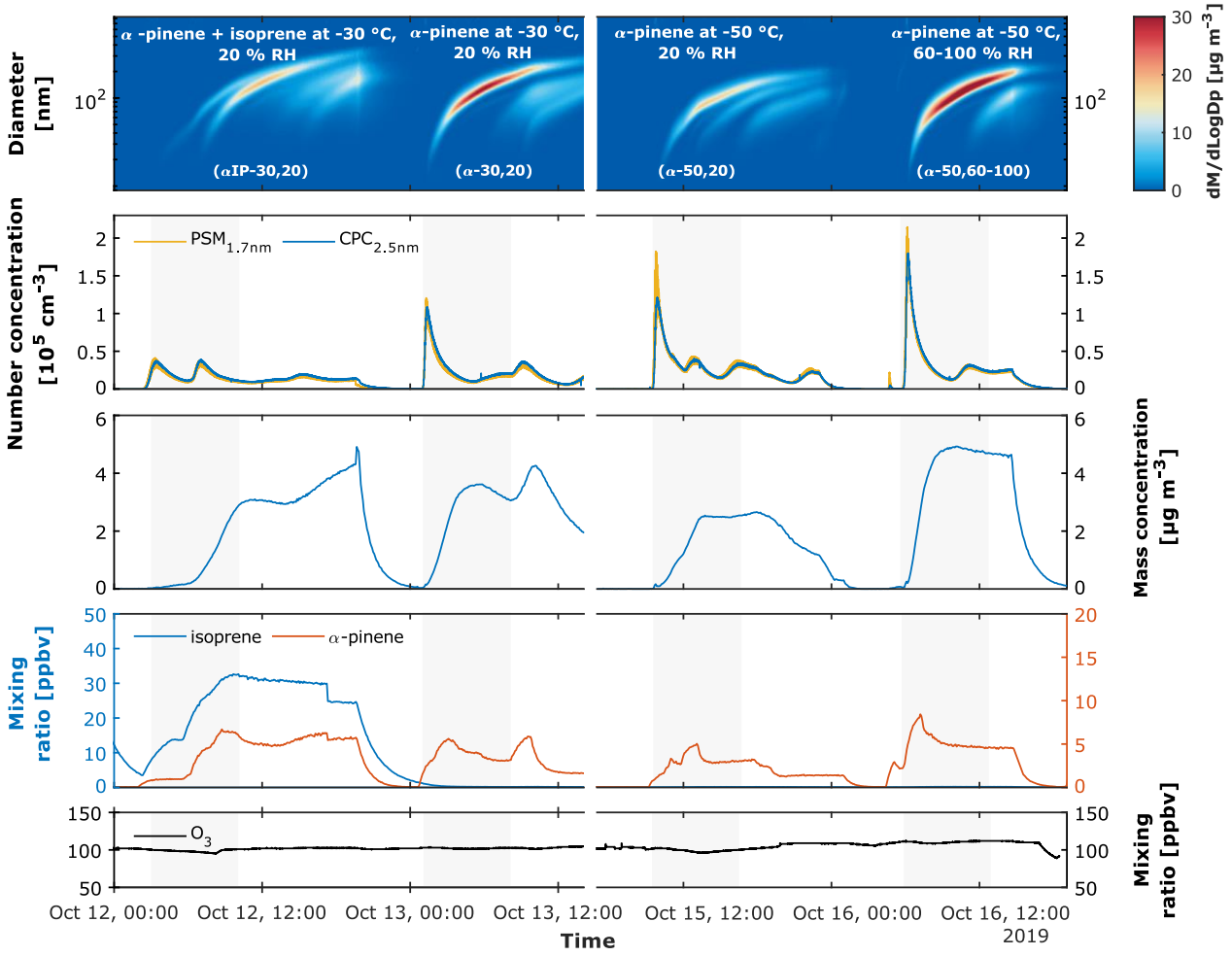

~~**Figure S3. Experimental overview for pure biogenic new particle formation. First panel: particle size distribution for four different experiments: α-pinene + isoprene at -30 °C and 20 % RH (αIP-30,20); α-pinene at -30 °C and 20 % RH (α-30,20); α-pinene at -50 °C and 20 % RH (α-50,20) and α-pinene at -50 °C and 60-100 % RH (α-50,60-100). The color scale represents the normalized mass concentration in µg m^{-3}. Second panel: Particle number concentration in cm^{-3} measured by the PSM with a cut-off diameter of 1.7 nm and CPC with a cut-off diameter of 2.5 nm. Third panel: Mass concentration in µg m^{-3} (obtained by integrating the normalized mass concentration from the SMPS). Fourth panel: Mixing ratio in ppbv for the biogenic precursor gases, isoprene and α-pinene. Fifth panel: Ozone mixing ratio in ppbv. The shaded areas refer to the time where the particles were collected using the TD-DMA.**~~

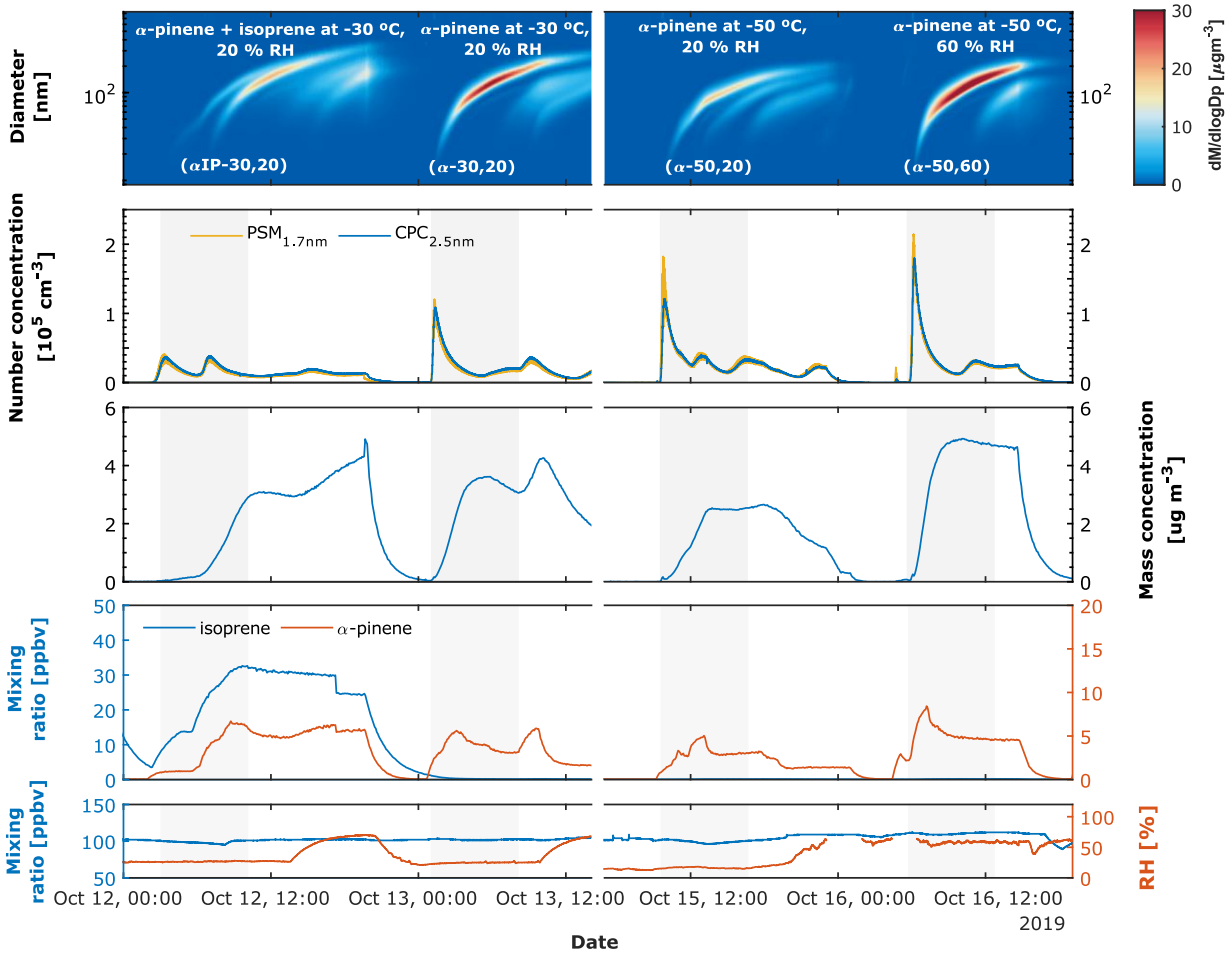

Figure S3. Experimental overview for pure biogenic new particle formation. First panel: particle size distribution for four different experiments: α-pinene + isoprene at -30 °C and 20 % RH (αIP-30,20); α-pinene at -30 °C and 20 % RH (α-30,20); α-pinene at -50 °C and 20 % RH (α-50,20) and α-pinene at -50 °C and 60~~-100~~ % RH (α-50,60~~-100~~). The color scale represents the normalized mass concentration in μg m^{-3}. Second panel: Particle number concentration in cm^{-3} measured by the PSM with a cut-off diameter of 1.7 nm and CPC with a cut-off diameter of 2.5 nm. Third panel: Mass concentration in μg m^{-3} (obtained by integrating the normalized mass concentration from the SMPS). Fourth panel: Mixing ratio in ppbv for the biogenic precursor gases, isoprene and α-pinene. Fifth panel: Ozone mixing ratio in ppbv and relative humidity in %. The shaded areas refer to the time where the particles were collected using the TD-DMA.

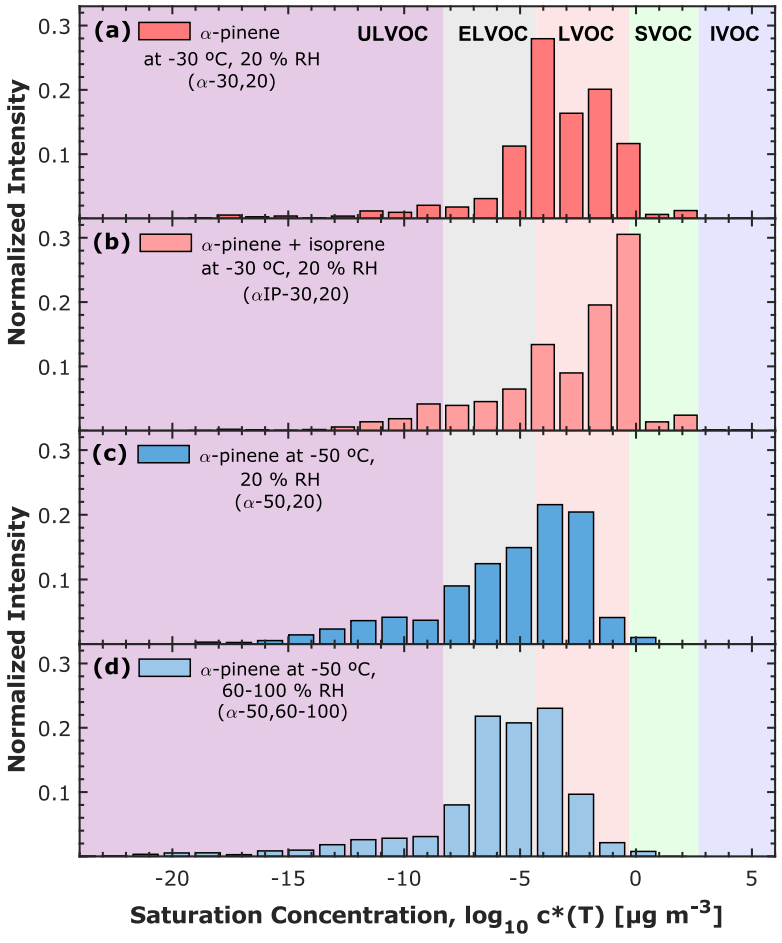
(a) α-pinene at -30 ºC, 20 % RH (α-30,20)
ULVOC
ELVOC
LVOC
SVOC
IVOC
(b) α-pinene + isoprene at -30 ºC, 20 % RH (αIP-30,20)
(c) α-pinene at -50 ºC, 20 % RH (α-50,20)
(d) α-pinene at -50 ºC, 60-100 % RH (α-50,60-100)
Normalized Intensity
0.3
0.2
0.1
-20
-15
-10
-5
0
5
Saturation Concentration, log10 c*(T) [µg m-3]

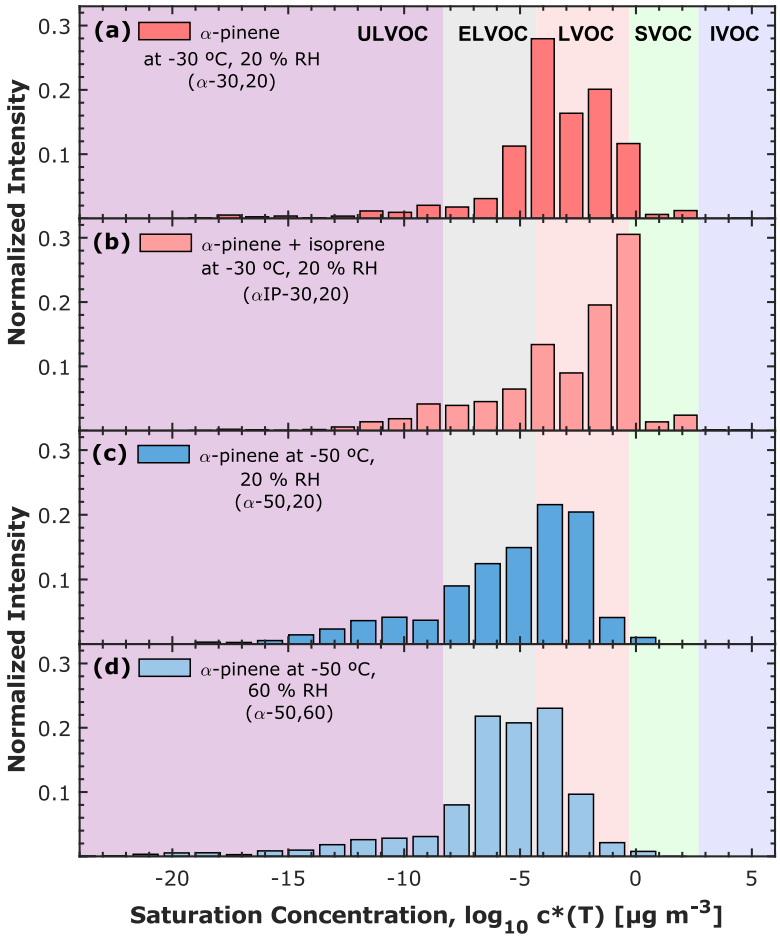

Figure S4. TD-DMA Volatility distribution of the measured oxidation products in the particle phase for four different experiments (Figure 5 in linear scale): (a) α-pinene at -30 °C and 20 % RH (α-30,20); (b) α-pinene + isoprene at -30 °C and 20 % RH (αIP-30,20); (c) α-pinene at -50 °C and 20 % RH (α-50,20) and (d) α-pinene at -50 °C and 60~~-100~~ % RH (α-50,60~~-100~~). Every individual volatility bin includes the sum of the intensity for the oxidation products normalized by the total signal in each system. Every individual volatility bin is defined at 300 K, shifted, and widened according to their corresponding temperature. The color bands in the background indicate the volatility regimes as in Donahue et al. (2012) and in Schervish and Donahue (2020). The normalized intensity is dimensionless. Nevertheless, it should be noted that the particle phase signal is given in normalized counts per second integrated over the evaporation time [ncps. s].

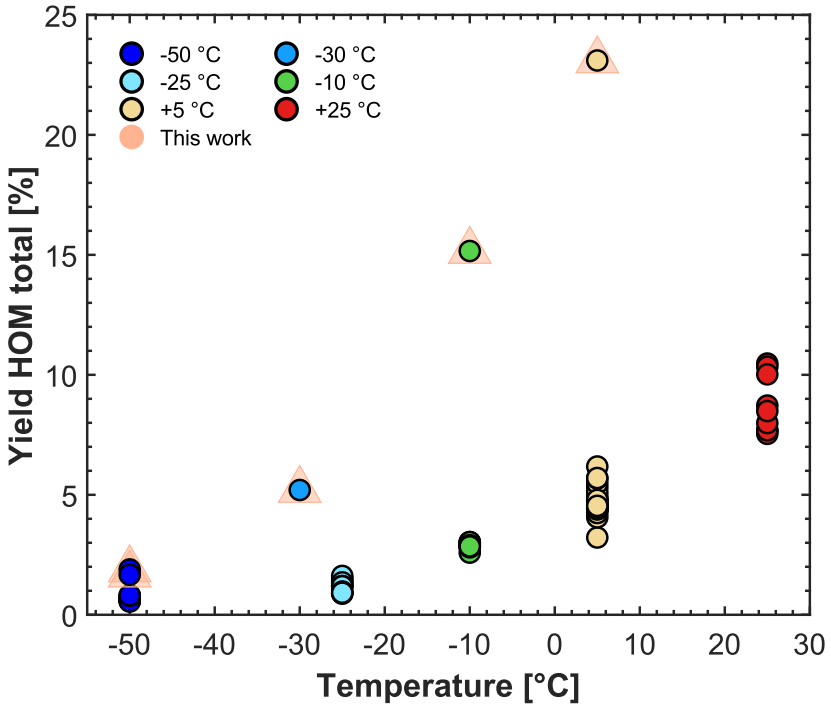
-50 °C
-25 °C
+5 °C
This work
-30 °C
-10 °C
+25 °C
Yield HOM total [%]
Temperature [°C]
0
5
10
15
20
25
-50
-40
-30
-20
-10
0
10
20
30

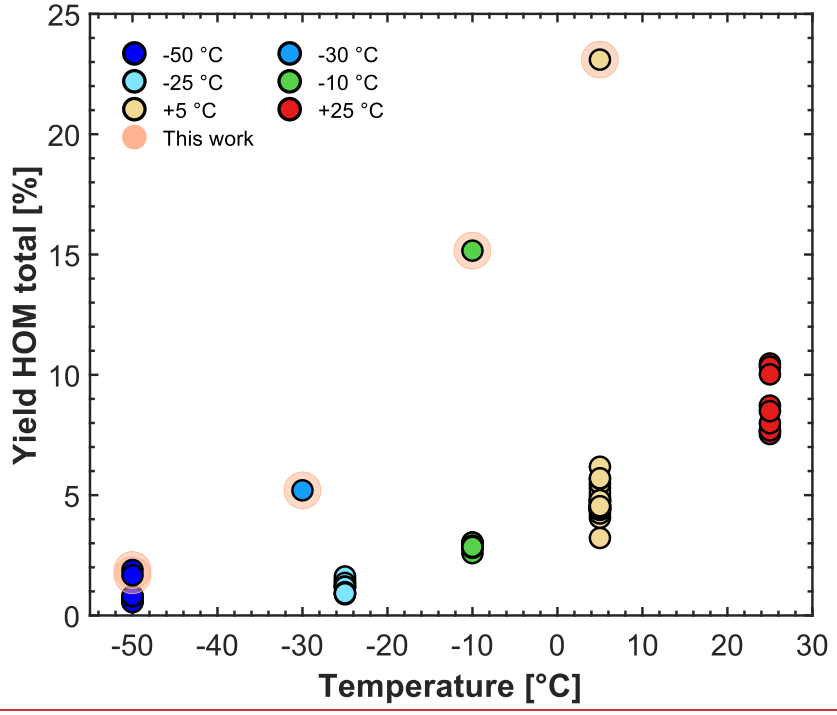
-50 °C
-25 °C
+5 °C
This work
-30 °C
-10 °C
+25 °C
Yield HOM total [%]
Temperature [°C]
0
5
10
15
20
25
-50
-40
-30
-20
-10
0
10
20
30

100

Figure S5. Yield of total HOM as a function of temperature for pure α-pinene systems. Data points at -50 °C, -25 °C, -10 °C, +5 °C and +25 °C are from Simon et al. (2020) and the data points with the orange shadows are the contribution of this study (α-30,20, α-50,20 and α-50,60~~-100~~ and complementary pure α-pinene experiments at +5 °C and at -10 °C). The level of precursor gases from Simon et al., (2020) were 0.2 to 0.8 ppbv for α-pinene and 40 to 50 ppbv for ozone, while for experiments reported here (shown with orange shadows), the mixing ratios were 1 to 8 ppbv for α-pinene and 100 ppbv for ozone.

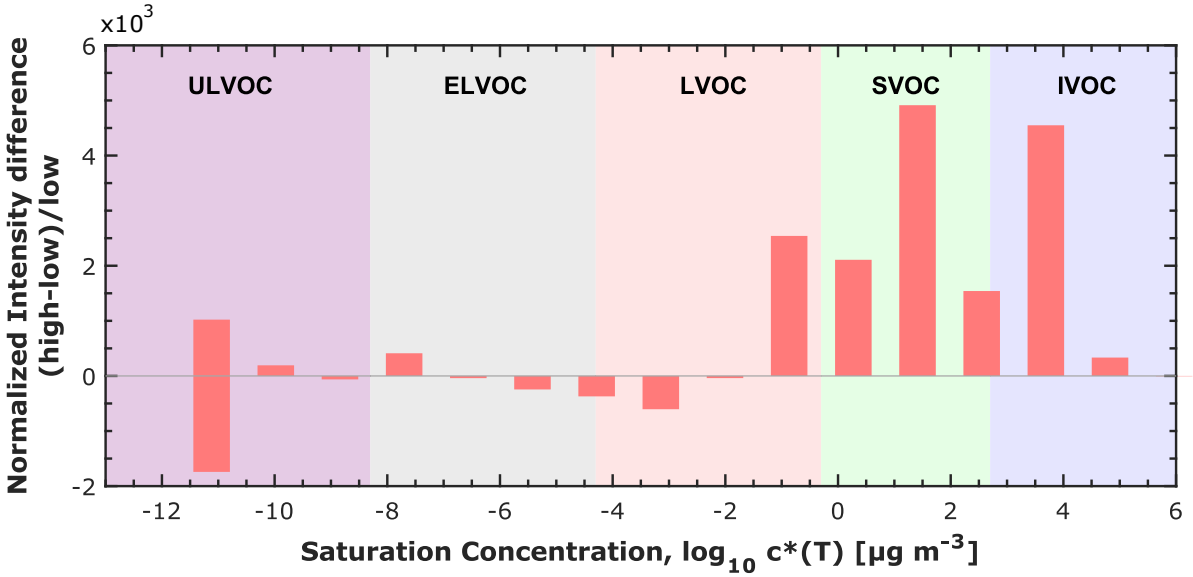

Figure S6. Volatility distribution of gas phase for two different systems and the normalized difference between them. Gas phase is measured with a Nitrate CI-APi-TOF Mass Spectrometer. Every individual volatility bin includes the normalized intensity difference (high-low)/low, which is calculated based on intensity of the system at high level of precursor gases (α-pinene was 2 - 3 ppbv and Ozone ~ 100 ppbv) and on the system at low level of precursor gases (α-pinene was 0.2 - 0.8 ppbv and Ozone ~ 40 - 50 ppbv). Every individual volatility bin is defined at 300 K, shifted, and widened according to their corresponding temperature. The lowest bin is an overflow bin (which contains the volatility bins with saturation concentration < -11 ug m^{-3}.). The color bands in the background indicate the volatility regimes as in Donahue et al. (2012) and in Schervish and Donahue (2020).

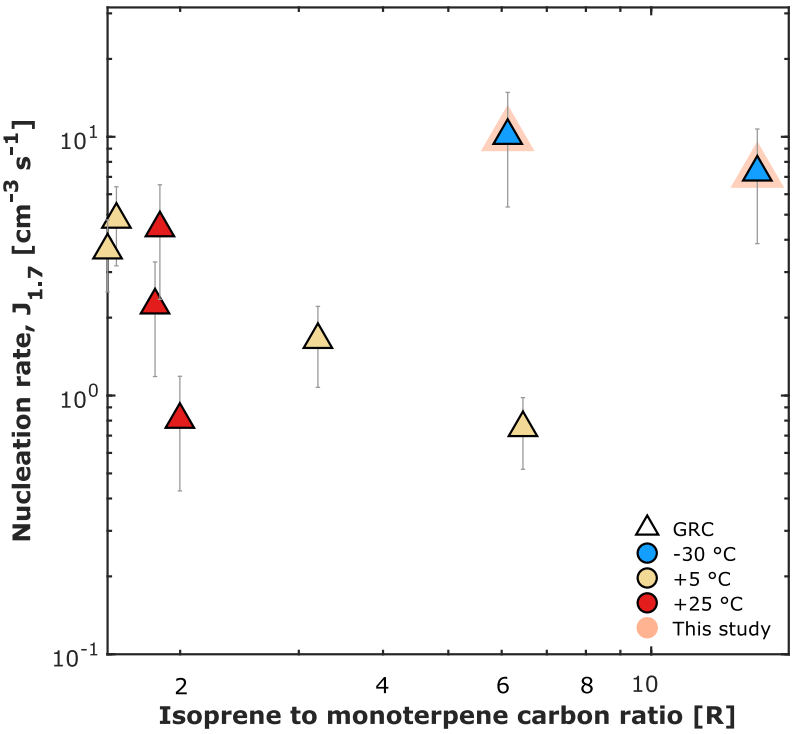

Figure S7. Pure biogenic nucleation rates at 1.7 nm diameter against isoprene-to-monoterpene carbon ratio (R) at different temperatures. Triangles represent Galactic Comic Rays (GCR) conditions. Data points at +5 °C and +25 °C are from Heinritzi et al., (2020). The points with the orange shadows are the experiments reported in this study for α-pinene + isoprene oxidation products at -30 °C and 20 % RH (αIP-30,20).